Novel fabrication techniques for the production of porous biphasic calcium phosphate ceramics for bone substitute application

Casey, Brian Paul

Award date:
2003

Awarding institution:
University of Bath

Novel Fabrication Techniques for the Production of Porous Biphasic Calcium Phosphate Ceramics for Bone Substitute Application

submitted by Brian Paul Casey

for the degree of Doctor of Philosophy

of the University of Bath

2003

ProQuest LLC
789 East Eisenhower Parkway
P.O. Box 1346
Ann Arbor, MI 48106-1346

Acknowledgements

I would like to thank the University of Bath for providing funding and support for this research studentship and Stryker Howmedica Osteonics for providing support to the project in the form of technical input, material supplies and financial contributions over the course of the studentship.

I would also like to thank my supervisors Dr. Irene Turner and Prof. Tony Miles for their tireless support and guidance throughout the course of this research.

I would also like to gratefully acknowledge the contribution of the Worshipful Company of Armourers and Brasiers who contributed to my expenses in attending and presenting at ESB 2001.

In addition to those mentioned above I would also like to thank Dr. A Perry, Mr. G Insley Mr. J Gittings, Yu-Shu Shui and Mr. B Grimm for not only their technical input but also for their encouragement and support throughout. I would also like to especially thank Mr. Frank Hammet who's assistance and experience proved invaluable.

Lastly I would like to thank Lisa, for being there.

Abstract

There is a growing requirement for the development of a synthetic bone substitute material due in some part to the pressure on current allograft stocks but also due to the increasing number of innovative orthopaedic reconstruction and corrective techniques being developed. The desired form factor for such a material would vary according to the desired application, with a granular material being useful in applications such as impaction grafting revision hip arthoplasty, and a bulk shaped component being useful in maxillofacial and orthopaedic reconstructive surgery.

The aim of the current work was to develop a mechanically robust material with a chemical composition and an interconnected pore structure that would be conducive to osseoconduction when implanted. The key method developed to achieve this goal was that of vacuum pressure impregnation of a reticulated foam. The method involves the impregnation of a reticulated organic foam with a highly loaded calcium phosphate slip. The impregnated foam is then dried to a green body and sintered between 1150°C and 1280°C. The burn out of the organic foam and sintering produces a biphasic calcium phosphate ceramic with a network of interconnected macroporosity.

X-ray diffraction analysis of the sintered materials demonstrated the composition to be a mix of hydroxyapatite, β-tricalcium phosphate and α-tricalcium phosphate. The mass fraction in which each of these components was present was determined by the mix of input powders and the temperature at which the materials were sintered. Image analysis of micrographs taken of the sintered materials found that the macropore size was dependent on the base foam structure. With the coarse foams a significant number of the resultant macropores were in the 150μm-500μm range deemed to be optimal for bone ingrowth. In addition to the macroporosity present, a high level of microporosity was found in all the slip based materials, this microporosity was found to be massively interconnected and to constitute 20% of the materials' volume. Compressive testing of the materials showed them to be mechanically robust with the well impregnated samples producing ultimate compressive strengths in excess of 20 MPa.

In conclusion, the current work presents a method for the production of a mechanically robust HA/TCP ceramic with interconnected macroporosity in a size range suitable for osseoconduction in which the macropore structure and ratio of HA:TCP can be tailored to a specific application. This ceramic bone substitute can be produced as a granule or as a shaped component. The material has a high degree of microporosity and hence a large surface area suggesting a potential for use as a drug delivery system.

Table of Contents

Illustration Index

Index of Tables

1 Introduction

1.1 Overview

At present a requirement exists for bone substitute materials to replace or restore bone tissue lost through various causes ranging from disease and trauma to reconstructive or corrective surgery. This requirement has been made more acute by the development of advanced surgical techniques which increasingly rely on bone graft or bone substitute materials for their successful use. The success of these techniques has greatly increased their popularity with the result that the more traditional approaches to bone grafting are reaching their limitations[1][2]. Due to these factors a large amount of work has been carried out in recent years to develop synthetic bone replacement materials that can provide an improvement over existing materials. Once the limitations of the traditional techniques and materials have been overcome, the development of new bone substitute materials combined with improved drug treatments and delivery methods will allow the creation of ever more sophisticated and successful orthopaedic techniques.

The current work focuses on the development of a ceramic material which possesses the chemical and physical characteristics required to allow its use as a bone substitute material. The ultimate aim of the project was to develop a bone substitute which could be used in a load bearing environment but still possess sufficient porosity to allow bone ingrowth and remodeling ultimately leading to the complete resorption of the implanted material.

The introduction attempts to place the use of bone substitutes and other orthopaedic implants in their historical context. The clinical requirements driving the development of bone substitute materials will be outlined in more detail. Examples will be given of the types of applications in which these materials could see use. In addition, the properties of bone which should be considered in the development of a bone substitute material will be outlined.

The state of the art as regards bone substitute materials will then be assessed with particular attention to the biological response to these material, their fabrication method, their physical structure and mechanical properties. The potential applications for these and the next generation of bone substitute materials will then be outlined with the possible advances in orthopaedic surgery resulting from these developments being discussed.

1.2 Historical Context

The early history of orthopaedic implants is a catalogue of failures with cases of sepsis, metal toxicity and rejection abounding. The earliest successful reported use of a synthetic ceramic as a bone substitute was the use of calcium sulphate in 1892 to fill the defects produced by TB infection[3]. Later this material was used during the Vietnam War to fill massively damaged bones and for craniofacial reconstruction[4][5]. This remained the only synthetic bone substitute material in use until the development of Bioglass by Hench *et al*[3][6]. In recent years ceramics based on calcium phosphate have become more commonly used and by and large represent the majority of the current generation of synthetic bone substitute materials[3].

1.3 Clinical Need for Synthetic Bone Material

As the aim of the project was to develop a synthetic bone substitute material to replace and ultimately extend the role of current bone graft materials, the first step in the design process was to assess the applications in which bone stock replacements are currently used. An outline of the types of applications in which a synthetic material could be employed is given below with examples of a number of key applications discussed.

To understand the clinical requirements of an implant material it is necessary to develop an understanding of the environment into which the material is to be implanted. Therefore the structure and properties of bone are examined and a brief description of the biological processes seen in normal bone and at a bone wound site in a healing situation follows below.

Understanding the effects that implanting a foreign material into the human body can have on these processes is also a necessity. Therefore some time is devoted to understanding the levels of biocompatability materials can possess and in particular the types of bone-implant interactions that can occur.

The primary applications of any bone graft or bone substitute material are to aid in the recovery of lost bone stock and to provide the facility to augment existing bone so as to facilitate corrective orthopaedic surgery. Bone stock can be lost for a number of reasons ranging from disease and trauma to surgical removal.

Current Applications

Orthopaedic Reconstruction

A dramatic example of the usefulness of bone graft and bone substitute use in a defect filling role is given by Hornicek et al [7] in their study of limb salvage with bone graft

material. The study looked at the use of wide excision as an alternative to limb amputation in the treatment of malignant bone tumours. The oncologic results have demonstrated that wide excision provides a viable alternative to amputation, however the salvage of the limb requires that the defect formed by this excision be filled with bone graft material to facilitate bone healing, in this case the graft material used was donated human bone. The study showed that, though many of the patients experienced complications, in 66% of the cases the the limb salvage was accomplished with good or excellent results without shortening the disease free period or compromising long term survivorship of the patient when compared with amputation.

On a smaller scale, graft and substitute materials have been successfully used in maxillofacial and cranialofacial reconstruction or alteration. In these applications repositioning of bones and augmentation of jaw length and chin size are common. In such cases the graft material is required both as a defect filler and as a scaffold on which to grow new bone[8].

In a similar vein corrective orthopaedic use of bone graft or bone substitute relies on incorporation of the graft or substitute into the bone at the implant thus altering its shape and effecting the correction. Ransford *et al*[9] describes a good example of this type of application, where a bone graft or a bone substitute material was used to effect fusion of the posterior spinal vertibrea for the correction of idiopathic scoliosis. In that particular study the the use of a synthetic bone substitute was compared to the use of bone grafted from another site on the patient. The classification and relative merits of these various substitute/graft materials is explored in some detail below.

Impaction Grafting

The use of bone graft in impaction grafting for arthoplasty and revision arthoplasty is an example of defect filling application that is worthy of specific note due to its increasing popularity and the growing sophistication of techniques which have evolved around its use. The technique has been successful in the replacement of various joints[10], but none so extensively as in the femoral and actebular revision of total hip arthoplasty. The use of impaction grafting for revision total hip arthoplasty (THA) allows extensive recovery of the bone stock lost due to osteolysis as a result wear, aseptic loosening and load shadowing [11][12], and loss due to the explant of the failed femoral or acetabular component.

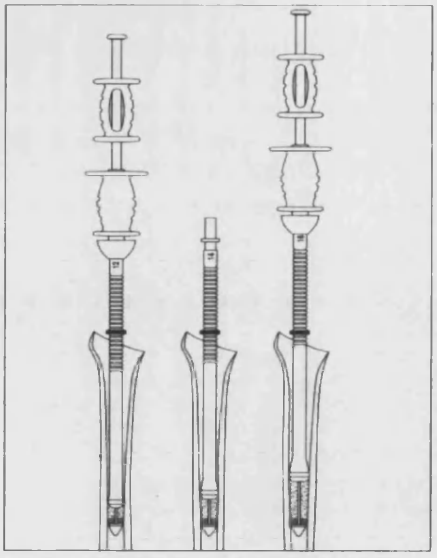

Figure 1 Distal occlusion and distal impaction [13]

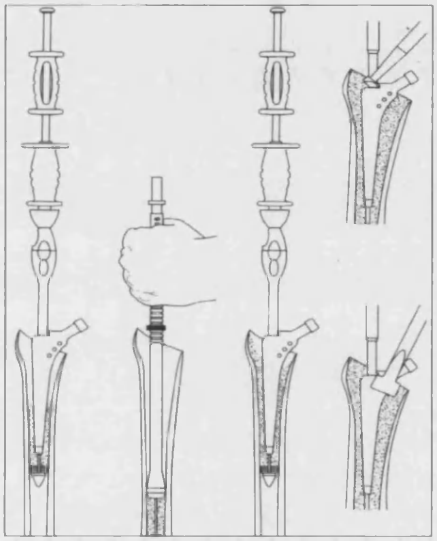

Figure 2 Proximal impaction with oversized stem [13]

A good example of a technique using this approach is the X-change system for revision of the femoral component of a failed hip implant as developed by Stryker Howmedica Osteonics[13]. In this technique the failed femoral component is removed and the femoral cavity reamed out until good bone stock is revealed. The distal end of the femoral cavity is then occluded, usually by the insertion of a threaded intermedullary plug. Ground bone graft sourced from donated bone stock is then placed in the distal cavity and compacted down by means of impaction (see Figure 1[13]). Further bone graft chips are introduced into the cavity and are impacted into shape using an over sized femoral stem known as the proximal impactor. The processes of introducing bone chips and impacting to shape is repeated until the entire femoral cavity has been lined with bone graft (see Figure 2[13]). A trial reduction is carried out to check the fit of the new stem before it is bonded into place

using bone cement. This technique has been demonstrated to be very successful at both promoting the recovery of lost bone stock [14][15] and at securely fixing the femoral stem in place [1][12].

Current Usage

In the case of impaction grafting for THA the number of procedures, and thus the required volume of bone graft material, is large. For example a study of THA revision in Scotland[2] demonstrated that the rate of THA revision procedures *per annum* to be approximately 29.5 per 100,000 population. Where impaction grafting is used, each procedure requires a volume of bone graft material the equivalent of two femoral heads. In a survey produced by the NHS R&D Health Technology Assessment Programme[16] the number of THA procedures carried out in the UK in 1998 was estimated at 40,000, with 13% of these procedures being revision THA. Though not all of these revision procedures involve the use of impaction grafting, it is clear from the figures the scale of the requirement for bone graft materials for this application alone.

Given the clear clinical need for bone graft and bone substitute materials the first step in developing new materials for this application is to develop some understanding of the structure and composition of bone, its mechanical properties and also an understanding of the biological activity in bone as a living tissue.

1.4 Structure of Bone

There are, broadly speaking, two distinct bone types. The highly dense cortical bone found in the outer region of long bones and the less dense spongy or cancellous bone found in endochrondal areas or interior of the long bones. Irrespective of its type and structure all bone is made of organic collagen fibres in a mineral matrix of hydroxyapatite ($Ca_{10}(PO_4)_6(OH)_2$) plus a small quantity of ground substance or cement consisting of polysaccharides[17].

Collagen

Collagen comprises three molecular chains twisted into a fibril 300nm by 1.5nm, these in turn are twisted together into a larger fibril 64nm in diameter. The collagen fibre itself consists of large numbers of these fibrils which are loosely crosslinked. When subjected to tensile load the fibres first respond by uncoiling some of the twist in their structure and only when this has occurred does the backbone of the collagen molecule become stretched and crosslinks between fibrils break. This property of collagen is key to its viscoelastic response and has a profound effect on the mechanical properties of bone, of which it is a key structural element.

Cortical Bone

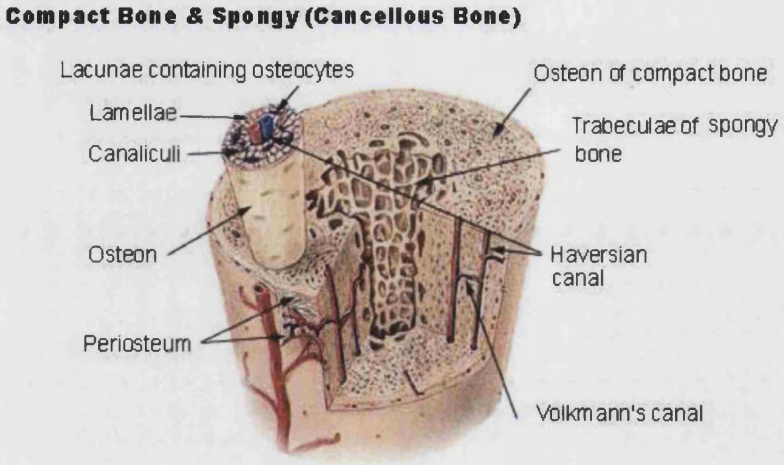

Figure 3 Cut away of bone, showing clearly the osteon structures in the compact cancellous bone[18]

Cortical bone is the dense bone typically associated with the exterior of long bones. The structure of this bone consists of densely packed collagen fibres encapsulated in hydroxyapatite. These densely packed structures are comprised of three to four micron thick lamellar sheets of hydroxyapatite between which collagen fibres run parallel to the plane of the sheet. These sheets are themselves bonded together by a thin layer of cement and disorganised collagen. Some of these lamellar are arranged into cylindrical structures running along the long axis of the bone called osteons, the most common of which is the concentric structure centred on the Haversian canals in the bone, see Figure 3[18]. These Haversian canals carry circulatory systems and nerve fibres through the bone. These structures can be several centimetres long but only 300-400 micron in diameter.

Cancellous Bone

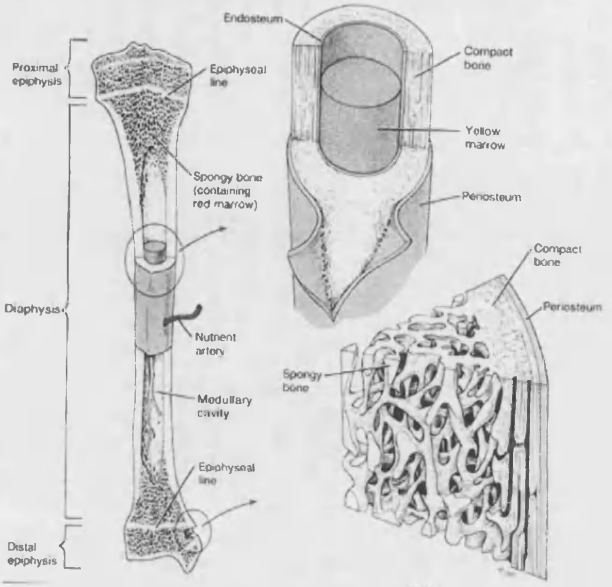

Figure 4 Cancellous bone structure. [19]

In contrast to the dense structure of corticle bone, cancellous bone is a low density structure made up of trabeculae of bone connected together to form an open network of bone (see Figure 4[19]). This open structure is filled by the highly cellular periostal membrane. Within the trabeculae the collagen fibres are aligned along the long axis of the strut. These trabeculae are themselves arranged in a organised cellular structure which is optimised for load bearing under normal load conditions.

Due to the highly orientated nature of both cancellous and cortical bone, both structures are highly anisotropic with respect to their mechanical properties[20] . For example the longitudinal to transverse stiffness in the cancellous bone of the human differing by as much as a factor of ten[21] .

The mechanical properties of cancellous bone has been shown to depend strongly on the th relative density of the material, where relative density is the density of the porous cancellous bone over the density of a theoretical 100% dense bone material. This dependency of mechanical properties on the relative density can be seen in a large number of cellular materials and foams. In the case on compressive strength, modelling techniques developed for generic foams can be used to predict the behaviour of cancellous bone. In the case where the relative density of the bone is low and compressive failure is dominated by elastic buckling of the trabeculae then compressive strength is proportional to the square of the relative density. At higher densities microfracture of the trabeculae

dominates the failure mode the compressive strength is proportional to the relative density raised to the power of three over two[21] .

Biological Function of Bone

Though providing other biological functions, bone's main function in the body is that of load bearing and protection of vital organs. During the normal body function bone is constantly undergoing a process of renewal. This renewal is a result of the conflicting actions of two cell types, osteoclasts which break down bone and osteoblasts which deposit new bone tissue. This action allows bone to be constantly remodelled to best accommodate the load environment in accordance with Wolff's Law[22]. This action of constant replacement and remodeling of bone plays a key role in the wound healing mechanism of damaged bone.

Upon initial fracture the bleeding from the bone quickly clots to fill the defect and surrounding region with blood clot. This clot becomes mineralised to form callus. The callus is invaded by osteoclast, osteoblast and fibroblast cells within two weeks of fracture. At six weeks post-fracture extensive remodelling of the callus structure will have occurred with extensive new bone and osteoid formation. At 12 weeks complete healing and repair of the cortical and cancellous bone structure will have occurred[23][24].

Any bone substitute or bone graft material must make accommodation for the type of bone it seeks to augment and must allow the biological process of wound healing and bone remodeling to occur in such a manner that the substitute material is either incorporated into new bone or resorbed by the body so that overall bone stock can be increased[25].

1.5 Biocompatability of Materials

The requirements for biocompatability and bioactivity in the implant materials are of great importance if the material is to perform well as a bone substitute material. In its broadest sense the biocompatability of a material can be seen as the ability of a material to be implanted into the body and provoke a minimal biological response. This type of definition however only deals with biocompatability in terms of rejection and possible toxicity issues with the material and makes no reference to the positive function of the implant. A more useful way of thinking of biocompatability in the current context is that the material implanted should supplement or take on the function of the tissue which it has replaced without provoking an adverse or rejection response[26]. This more focused approach to the function of a material in a specific application puts more of an emphasis on the positive function of the material and sets a more useful criteria for the design of new

materials. It is also worth pointing out that the biocompatability of a material must also take into account the positive or detrimental effects the actions of the body will have on the implanted material.

Therefore a closer look at the different spectrum of interactions between the body and implanted materials is required. At one end of the scale there are materials which are bioinert, which means that they provoke very little response from the body at the selected implant site. What little response these materials do provoke is usually characterised by a mild rejection response in which the material is surrounded by fibrous scar tissue and is thus isolated from further interaction with the body[27].

With more biocompatable materials the degree of biological tolerance for the material is increased allowing a more intimate contact between normal tissue and the implanted material to occur. At the other end of the spectrum from the bioinert materials are bioactive materials. These materials actively promote the growth of new tissue at their surface stimulating the body's healing response. These type of materials commonly undergo resorption by the body allowing complete recovery of normal tissue function[17].

Osteoconduction/Osteoinduction

When looking at bone implant materials, further distinctions can be made in terms of the growth behaviours of hard and soft tissue adjacent to the implant. As in the general case there are a number of materials which are well tolerated when implanted into bony tissue and many of these materials allow the formation of an intimate interface between the implant and the adjacent bone. There are also a small number of materials that have been shown to actively promote the growth of new bone tissue. This response of promotion of new bone growth is referred to as the osteogenic potential and can be further divided into an osteoconductive response and an osteoinductive response. Osteoconduction is the ability to promote the growth of new bone from adjacent bone tissue onto the material's surface, in these cases the implant material usually provides a stable scaffold onto which the tissue can grow and often provides some additional stimulus to promote this growth[28]. Osteoinductive materials by contrast initiate the growth of new bone without the requirement of intimate contact with bony tissue[28]. The mechanism and materials requirements for osteoconduction will be discussed later. The mechanisms of osteoinduction are somewhat beyond the scope of this project, however the issue of drug delivery is dealt with in this project as drugs, such as the osteogenic protein OP-1™ do exhibit a potential for osteoinduction. Therefore it is useful to outline this phenomena here.

1.6 Current Materials in Clinical Use

The next step in designing a new bone substitute material is to assess the state of the art in terms of the current range of materials used as bone grafts or bone substitutes. The materials currently being used in the type of applications discussed earlier can be broken down into four main groups these are autograft, allograft , xenograft and synthetic graft materials. These materials are discussed below.

Autograft

Autograft material is bone stock taken from elsewhere on the patient's body prior to implantation. This material is harvested at the time of the operation and typical harvest sites include tibia, distal radius and ribs, though the most common site is that of the iliac crest of pelvis[29]. This material offers several benefits, firstly it presents little or no rejection or cross infection risk as it is the patient's own tissue. Secondly as the time between explant and implant of the material is minimal, and it undergoes very little treatment, it retains much of its cell activity and therefore its osteogenic potential remains largely intact[28]. Finally, as the autograft material is the patient's own tissue and undergoes minimal manipulation and is for homologous use it is not subject to the regulatory restrictions associated with the implant of foreign materials[28]. This material does have some serious limitations and drawbacks. The key limitation of autograft is the limited volume of the material that can be safely harvested from the donor site and also the limitation on the form and shape of the harvested material imposed by extraction, precluding its use in applications requiring large shaped components. The graft harvesting procedure adds time and complication to the operation increasing blood loss and time under anesaethic and thereby patient risk. The chief drawback of autograft use however is the frequency of complications at the donor site. In one study on the complications at iliac crest donor sites[29] minor complications were reported in 10% of the cases, with major complications being reported in nearly 6% of cases. Minor complications included superficial infections and minor haematomas. Major complications however included vascular injuries, nerve damage, deep infections and deep haematoma, donor defect hernias and iliac wing fractures. Clearly these donor site complications represent a major drawback in the use of autograft material.

Allograft

Allograft is human bone stock that has been harvested from donors which is processed and stored in tissue banks prior to its use as a graft material. In Europe this material is acquired from live sources, for example, femoral heads recovered during procedures such as primary hip arthoplasty. In the US bone stock from cadaver donors can be used in this

role[28][30]. The material once harvested must be washed and then quickly frozen to avoid cell degradation. Samples of the donated material are then screened for infection[2]. Allograft has the benefit of being osteoconductive and can also be resorbed and remodeled by cellular action *in vivo*. Also as the bone has undergone little processing it retains much of its original structure and its viscoelastic mechanical response remains intact. As the material undergoes little processing post implant and is for homologous use in the US it is not subject to the regulatory restrictions associated with the implant of foreign materials and is dealt with in much the same manner as autograft[28]. As with autograft, allograft does have a number of serious drawbacks and limitations. The most serious drawback is the risk of cross infection due to transplant. Currently all allograft material is screened for bacteriological and viral infection. In the case of bacteriological infection the material can be treated so as to kill the infection and make the material suitable for use. This post treatment of infected tissue is carried out in 10% to 15% of all cases[2]. The screening and post treatment process adds additional cost to the already expensive storage of the donated bone.

Another drawback inherent in allograft material is the huge variability in the quality of the donated bone. As the main source for this material in Europe is from femoral heads removed during primary arthoplasty. Since a large number of the donor patients will be suffering from arthritis or other bone disorders, the quality of the donated bone is highly variable. For this reason and reasons of viral infection, up to 18% of donated material must be rejected[30]. This rejected material exascabates the problem of limited supplies of allograft. Much like autograft material the size and form of allograft is limited, allograft is generally used ground as a chip material. Finally, it has been shown that resorption behaviour of allograft is unpredictable. This can lead to grafts being substantially resorbed before viable bone ingrowth has been established[31].

Xenograft

Xenograft is material obtained from other, non-human, biological sources and used as a bone graft material. These materials generally utilise the similarities in the physical and chemical nature of the xenograft to that of human bone. Two of the most notable xenograft materials are sterilised coral and denatured bovine cancellous bone. In both cases the porosity of the material and the fact that they are composed primarily of calcium phosphate or calcium carbonate makes their usefulness as bone graft materials apparent. The preparation of both these materials involves the removal of organic material from the mineral structure.

Coralline Material

The successful use of coral derived xenograft material has been shown in studies using coral as a bone graft material. In the study by Guillemin *et al*[32] organic elements of the coral were removed by sun drying and then washing the coral in an ultrasonic bath. This denatured material was then sterilised by heating to 131°C in an autoclave for one hour. One of the benefits of using coral is that the organic content of the structure in its live state is typically 1% with the other 99% being made up of aragonite, a form of calcium carbonate. This low organic content allows the coral to be implanted with a minimum of preprocessing. The structure of the coral material is dependent on the species involved. Of the three species used in the study each had an overall open porosity between 46 and 48 %. The Goniopora species have an open pored structure with interconnected porosity similar to that of cancellous bone. The Favites and Lobophyllia species have a closed porous structure that resembles the structure of cortical bone.

Though the calcium carbonate structure of the coral differs from the HA structure of bone it has been shown that it has good osteoconductive properties and undergoes resorption under the action of osteoclasts[32][33]. The main drawback with the use of coral as a bone substitute material arises from availability issues with the coralline materials due to the fragile nature of the coralline ecosystem and the damage caused by the harvesting of the specific corals. For this reason coralline material is not widely used though coralline based products are commercially available.

Denatured Bovine Material

A more readily available source of hydroxyapatite material with the structure of cancellous bone is that of material harvested from the cancellous region of bovine bone[34]. This material is generally washed and sterilised prior to hydrothermal treatment to remove all trace of organic materials and to modify the crystalline structure of the HA in the material. An example of this type of material is Endobon®, which is produced by Biomet-Merck. This material comprises crystalline hydroxyapatite with an interconnecting network of pores in a structure not dissimilar to that found in human cancellous bone. This material has been demonstrated to be osteoconductive and to undergo remodelling in the body[35]. The drawbacks of these types of materials are mainly related to the difficulty and expense involved in harvesting the material and its treatment and the limitations in scale and structure imposed by its source. These limitations aside, this type of material has been used successfully in a number of applications though its popularity has been effected by recent fears over possible prion infection.

Synthetic Materials

The final group of materials are those derived from a purely synthetic source, and it is the development and characterisation of such a material that will be the key focus of this project. The synthetic graft materials currently in use primarily consist of glass or ceramic materials which are known to have positive interaction with bony tissue when implanted. These interactions were demonstrated in a number of *in vitro* and *in vivo* studies[27][36][37][38][23][39] that evaluated the biological response to implanted hydroxyapatite (HA), Bioglass®, alpha tricalcium phosphate (α-TCP), beta tricalcium phosphate (β-TCP) and a range of other calcium phosphate powders. Alumina, which is held to be bioinert, was used in a number of these studies to provide a control. The histological response to HA and TCP materials will be examined in more detail later. In many of these studies no attempt was made to introduce structure into the synthetic material.

1.7 Current Synthetic Materials

A wide range of materials are currently under development for use in bone substitute and bone healing applications. These include calcium phosphate filled collagen materials, calcium sulphate materials and a range of resorbable polymeric materials designed to carry bone morphogenic proteins[28]. The current work focuses on purely synthetic ceramic bone graft materials which have an introduced pore structure designed to promote bone ingrowth *in vivo*. These materials have been designed to have a porosity in a specific size range and consist of calcium phosphate ceramics, commonly hydroxyapatite (HA) or tricalcium phosphate (TCP). These materials have been produced by a number of means including burnt out polymer spheres method, blown foam method, coated reticulated foam route and by lost wax processes. Each of these processes will be discussed in detail later, outlining the advantages and the limitations of each approach. Animal and clinical trials on some of these materials have demonstrated their potential for bone graft and bone substitute use[40].

Synthetic materials offer the possibility of producing large volumes of disease free bone substitute materials in an inexpensive and reliable manner where the structure and composition of the material can be tailored to a specific application. These materials could also be produced as large shaped components, a task not easily achieved by the other graft sourced materials. The drawbacks associated with the current generation of synthetic materials are that either the porosity in the material is small and isolated or that the material is too fragile to fulfil any load bearing requirement. One of the aims of the project was to develop a material which overcame these limitations by combining the porosity

requirement for bone ingrowth (see section 1.8.2) with requirements for the material to be robust and capable of being machined pre-implantation.

1.8 Histological Response

As mentioned earlier one of the key steps in the development of a new bone substitute material is the development of an understanding of the factors affecting the interactions between the implanted material and the bone at the implant site. The chemical and phase composition of the implant material are an important factor in the biological response to the implant. The other key factor affecting the bone/implant interaction is the porosity of the implant material and the size and structure of this porosity.

In designing an implant material it is assumed that the optimum response is one wherein the growth of new bone is stimulated by the implant material and the mechanical interlock between the implant and the new bone is strong. Bone growth into any pore structure in the implant will obviously greatly improve the quality of this interlock. The ideal outcome is one in which the implant is either strongly incorporated into new bone or has undergone resorption or remodelling in such a manner as to allow the bone to return to its healthy structure[25].

As mentioned earlier the range of materials currently available is large and varied ranging from resorbable polymeric materials designed to release bone morphogenic proteins (BMP's) to calcium phosphate filled collagen. Many of these materials are beyond the scope of the current project which is focused on hard materials such as biocompatable glass and ceramic materials.

Effects of Phase Composition on Histological Response

The interactions between implanted glass or ceramic materials and bony tissue at an implant site have been the focus of a number of *in vitro*[36] and *in vivo* studies. One key study on these interactions was carried out by Oonishi *et al*[27] which looked at the *in vivo* response to Bioglass® and to various calcium phosphate materials when implanted into rabbit femurs. The implanted materials were HA, low crystallinity HA, α-TCP , β-TCP, tetracalcium phosphate [$Ca_4O(PO_4)_2$] and Bioglass®.

In the case of Bioglass® the material used was Bioglass® (45S5) which is composed of 45 wt% SiO_2 , 24.5 wt % CaO, 24.5% Na_2O, 6 wt % P_2O_5. This material was shown to promote rapid growth of new bone tissue along the surface of the implant with good contact and bonding between the new bone and the Bioglass® surface[41]. This rapid bone growth is attributed to the Bioglass® being surface bioactive material. This surface

bioactive effect arises from the interactions between the Bioglass® and the physoligical fluid forming a layer on the surface of the implant which is rich in calcium and phosphate[17]. The presence of these species in the layer is found to promote osteoblast activity and thus the formation of new bone.

The materials of greater relevance to this project were the calcium phosphate ceramics, and of these the HA and TCP materials are of key interest as they are the two calcium phosphate materials which have been most extensively used in clinical orthopaedic practice.

In the same study as above by Oonshi *et al*[27]the results for the high crystallinity HA showed there to be an osteoconductive effect resulting in growth of new bone onto the surface of the implanted HA and that this new bone was found to bond directly with the implanted material without the formation of a layer of interconnecting tissue. It has been demonstrated that a bioactive surface layer is also formed as the physiological fluid interacts with the HA implant[41]. This layer is detectable as an electron dense region which was found to contain high concentrations of calcium and phosphorus[37]. However it was found by the Oonishi study that the high crystallinity HA did not stimulate the growth of new bone to the same degree as the Bioglass® material. The HA material was however shown to slowly resorb. This was demonstrated by the smaller particles of HA being enveloped by trabecular bone and disappearing over time. The rate of this resorption was indicative of it being due to cell action on the HA material rather than dissolution, though another study[37] looking at implants in the middle ear found no detectable resorption suggesting that this effect may be dependent on implant site.

By contrast the behaviour of α-TCP and β-TCP *in vivo* was found to be characterised by dissolution of the implanted TCP material and subsequent growth of new bone into the space left by this dissolution process[38][27]. In the study by Oonishi *et al* the interface between the TCP and the adjacent bony tissue was found to be more defined than with the HA or Bioglass® implant indicating little or no attachment between the bone and the TCP implant. It has been shown however that a good mechanical interlock can develop between β-TCP and adjacent bone *in vivo* with no evidence of an intermediate layer of fibrous tissue[42].

Therefore it has been postulated that the dissolution of the TCP produces a region of high calcium and phosphate adjacent to the implant site. This calcium and phosphate rich region is thought to stimulate osteoblast activity in the region leading to the rapid growth and remodelling of new bone tissue at the bone implant interface. It was found in this and

other studies[38] that α-TCP dissolved more rapidly than the beta form. It was noted in the study by Klein *et al* that the density of bone formed adjacent to implanted HA material was greater than that found at the dissolution sites of α-TCP and β-TCP, leading to the conclusion that the ostegenic potential of the TCP was lower than that of the HA. It has been shown[38][23] that the dissolution rate of β-TCP *in vivo* is between 10 to 20 times higher than that of highly crystalline HA.

The dissolution or resorption of TCP *in vivo* can be both cell mediated and solution mediated[36][27], and it is likely that the actual mechanism is a combination of these two effects. The dissolution of TCP in distilled water occurs by the following mechanism.

$$3Ca\ (PO\ )_{-} + H\ O \rightarrow Ca\ (OH)(HPO\ )(P$$

The β-TCP was found to form an apatite in aqueous solution, which on redeposition formed a non-stoiciometric apatite with a high degree of lattice water associated with the structure[43].

It has been shown that the osteoconductive potential of biphasic calcium phosphate ceramic material comprising of HA and β-TCP are greater than that of single phase HA[23][44][45][46]. The mechanism of this enhanced response centres on the dissolution of the β-TCP and reprecipitation of a poorly crystallised apatite structure on the HA substrate. The deposited carbonatehydroxyapatite is analogous to the material occurring in human bone and has been found to encourage bone ingrowth. It has also been observed[37] that the presence of metal ions such as Al and Mg is a common feature in the interface between HA implants and new bone. These metal ions are thought to be trace impurities from the HA concentrated in the interface layer by cell action at the surface and it is thought that these may contribute to stimulating cell response.

Effects of Physical Structure on Histological Response

In addition to the effects of phase and chemical composition of the implanted material, the porosity and surface texture of the implanted material also have a strong effect on its interaction with the body and specifically on interaction between the implant and adjacent bony tissue. These porosity effects have been studied in HA and in modified xenograft and relationships between pore size and bone ingrowth into pores has been proposed.

Work by Hulbert *et al*[47] demonstrated that the ingrowth of tissue into a porous implant was determined largely by the pore size in the implant material. The findings from *in vivo* trials demonstrated there was a less adverse rejection response to porous implants of

largely inert ceramic (calcium aluminate) than to fully dense implants of the same material. More specifically in relation to bony tissue it was found that a pore size of greater than 200μm was required to allow osseoconduction into the pore. It was however found that this critical pore size was influenced by the osteogeneic potential of the implant material.

The exact size range of porosity to give optimal bone ingrowth into porous HA ceramic implants is the subject of some controversy as differing material fabrication techniques and implant methods have produced widely varying results. Comparisons between the various studies are difficult to make due to the differences in techniques.

A more recent study by Lu *et al*[39] investigated the effect of pore interconnection size on bone ingrowth into porous osteoconductive implants. In their study *in vivo* and *in vitro* trials of porous HA and β-TCP were carried out where the pore size and interconnections in the ceramic material were carefully controlled. From their correlated research it is suggested that a pore size of 1-10μm would allow ingrowth of cells into the implant . A pore size of 15-50μm would allow fibrous tissue to penetrate the implant and allow for vascularisation of the implant. A pore size of 150-300μm would allow ingrowth of bone into the implant, though findings in their own work revealed bone formation in interconnected pores as small as 50μm. Their findings also reveal that the size and density of the interconnection between larger pores is a vital factor governing the ingrowth of new bone with interconnection sizes of 20μm allowing cell transport between macropores, thus allowing osteoblast and fibroblast cell penetration into subsurface macropores. An interconnection size of 50μm was shown to allow mineralised bone formation in the connected macropores.

A further finding of their work was that the rate of bone ingrowth into the β-TCP material accelerated with time. This was deemed to be due to an increase in interconnection size with the dissolution of the β-TCP[39][46].

The effect of porosity on dissolution rate should also be taken into account as macroporosity and microporosity in an implant material will increase the specific surface area of the material allowing greater contact between the implant and physoligical fluid *in vivo*. Therefore given adequate diffusion or transport of dissolved material away from the surface, the surface area will have a strong effect on dissolution rate.

The microporosity of the material, and hence its surface area will also have a bearing on the materials effectiveness as a drug delivery system. This is particularly true in the case of bone morphogenic proteins (BMP's) as they are water soluble and in the absence of a carrier are quickly lost from the implant site, limiting their effectiveness. A study by Yuan

et al[48] has demonstrated that a high surface area calcium phosphate ceramic implant provides a highly effective delivery and release system for BMP's, increasing their effectiveness and reducing the sensitivity of the *in vivo* response of drug dosage.

1.9 Fabrication Techniques

Having established the requirements of a synthetic bone substitute material, the following section outlines the fabrication techniques currently being employed in the production of porous ceramic materials in general, and of calcium phosphate ceramics for bone graft applications in particular. The interest in ceramic materials with controlled large scale porosity extends far beyond the field of bioceramics, being employed in peizoeletric and filtration applications to name but two, and many of the techniques outlined below were developed to produce materials for these applications.

BurPS Technique

Early work by Shrout *et al*[49] pioneered the use of the burnt out polymeric spheres (BurPS) technique to generate controlled large scale porosity in ceramic components. This technique involves the blending of an organic filler of suitable size with a ceramic powder. This blend is then pressed to consolidate the particles into a green body which is subsequently fired to burn out the organic inclusions and sinter the ceramic powder.

The use of the BurPS method to produce a porous calcium phosphate ceramic with a controlled porosity for bone substitute applications has been demonstrated by Dean-Mo Liu[50]. This method involved the uni-axial pressing of hydroxyapatite powder and PVB sphere filler to produce a bulk green body and ultimately a macroporous sintered HA material.

In this study, a high purity hydroxyapatite power was produced by reacting reagent grade $Ca(OH)_2$ and H_3PO_4 solutions in a pH buffered solution (pH 9 by use of ammonia hydroxide) to produce a precipitate. This precipitate was dried in an oven at 200°C and spray dried to produce granules of a near spherical shape approximately 100 microns in diameter. The Ca/P ratio of this powder was found to be 1.67.

The polymer used to produce porosity in this material was polyvinyl butadiene (PVB). These particles were of three different size ranges 0.093mm, 0.188mm and 0.42mm.

Mixtures of hydroxyapatite granules and polymer powder were made up with a polymer powder content of 42-62% by volume. These mixtures were uni-axially pressed at pressures of 27MPa or 55MPa to form rectangular blocks. These blocks were heated to

500°C at a heating rate of 0.5°C min^{-1} to drive off the polymer particles and other volatile materials before sintering at 1200°C for between 2 and 48 hours for densification.

A noteworthy modification of the above technique[51] produced porous particles which were spherical, or near spherical in shape. The hydroxyapatite powder was produced in the same manner as above and was subsequently ball milled in deionised water using an alumina ball medium. The PVB particles were added to the resultant slurry. These particles were 0.95mm, 0.25mm and 0.4mm in size. The resultant slip was cast into plaster moulds with semi-spherical surface indents. When dried, the action of surface tension and the cavity geometry produced a spherical or near spherical particle. These green bodies were heated to 500°C to drive off the volatile materials prior to sintering at 1200°C for two hours. This resulted in a material that was porous and had a size range that could be controlled by the mould geometry and the amount of slip dispensed per mould cavity.

The characterisation of these materials focused mainly on optical and scanning electron microscopy of the micropore and macropore structure of these materials, and determination of pore size distribution and pore volume by Mercury porosimetry.

The material produced by Dean-Mo Lui[51] via the BurPS method had a porosity 10-12% higher than the volume fraction of PVB particles included in the green body prior to sintering. This additional porosity was found to be due to microporosity within the structure, and was constant for a given pressing pressure. As the pressing pressure was increased to 55 MPa the pore volume approached that of the volume of the polymeric inclusions. The resulting porosity was spherical and of the same size as the polymeric inclusions.

It was also shown in this study that prolonged sintering could also effectively eliminate the microporosity. Prolonged sintering also resulted in a reduction of macropore volume. Mercury porosimetry indicated that the macroporosity in this material was interconnected and in the range of 47-61% of the volume fraction.

The pressing pressure which can be employed to increase consolidation is limited in the case of uniaxial pressing. This limitation is due to the deformation of the polymeric spheres in the pressing process. This deformation causes the formation of elliptical or oblong pores which make the resultant material highly anisotropic, affecting mechanical strength[50].

In a similar study by the same author, a slip casting technique was employed to produce porous granules by the BurPS method. Though these granules were consolidated by prolonged sintering the resulting structure had an open porosity of 12-18% above the

volume fraction of the polymeric inclusions due to open microporosity. The macroporosity was of the same size and shape as the polymeric inclusions and was uniformly dispersed throughout the granules. Though the pore walls were highly pore interconnected the macropores themselves were not shown to be interconnected.

The surface morphology of these granules was found to be smooth with low porosity. At higher magnifications cracks were apparent on the granule's surface. This surface cracking was thought to be as a result of the burn-out of the organic filler material in the process.

In work by O'Kelly *et al*[52] a detailed comparison of the structure of denatured bovine bone and that of synthetic porous HA was made by image analysis. Using NIH Image 1.54 image analysis software, O'Kelly *et al* determined the mineral area fraction (MAF) and the mean plate distance (MPD) in the denatured bovine bone and the synthetic material. The MPD was measured by counting the number of mineral/void interfaces along a given line. The MAF was determined by measuring the size of the mineral area on the image. This image analysis showed that the pore architecture of the cancellous bone could to a large degree be successfully reproduced in the synthetic material by use of the BurPS method.

The basic limitation of the BurPS technique when applied to the production of bone substitute materials is that the macroporosity generated by the technique is inherently non -interconnecting, which has been shown to be non-ideal for bone ingrowth. This problem can be overcome by the use of high filler volumes so that the high pore volume generated results in pore impingement and thus interconnection. It will be shown later in this work that using such an approach to produce a HA material with an interconnected pore structure in the size range to allow bone ingrowth is highly problematic and results in a mechanically weak material.

A modification of the BurPS technique has been developed by Richart et al[53][54] in which a lattice of polymeric beads was pressed together and heated such that a significant degree of bonding between adjacent beads was achieved. This lattice was then impregnated with a ceramic slip and fired to produce a porous ceramic artefact with a level of interconnected porosity which would be difficult to achieve by the standard BurPS route.

Foamed Slip Method

Porous hydroxyapatite ceramics have also been successfully produced by the blown or foamed slip method. In this process a porous green body is produced by stabilising a foamed slip sufficiently to allow drying while preserving the foamed structure.

Binner and Reichert produced porous hydroxyapatite ceramics using foamed slips[55] that were not fully dispersed. The use of a non-dispersed slip has been shown to produce

clusters during sintering which leads to an increase in surface area due to pore formation. In this paper, foamed slips were produced with and without the aid of a stabilising agent. The slip was foamed by the use of either high-speed rotating whisk or blades or by bubbling air through the slip via a Buchner funnel. These foamed slips were then sintered to produce porous hydroxyapatite ceramics with varying degrees of success.

The most successful technique involved the use of an agar-stabilised slip that was foamed using high-speed rotating blades. The resultant foamed slip was then cast into a filter paper mould and refrigerated to 6°C to set the agar stabilising agent before the slip was allowed to dry. The set green body was dried at room temperature for one or two days. This green body was then sintered at between 1000°C and 1300°C. The sintering process burns off the organic stabilising agent leaving a porous ceramic structure.

In a related study Binner[56] demonstrated the production of porous ceramic materials by the *in situ* polymerisation of an organic monomer in a foamed ceramic slip to produce a robust porous green body that could subsequently be sintered. Both the above foamed slip processes produce a bulk porous ceramic material. Fabbri *et al*[57] demonstrate the production of near spherical granules of porous hydroxyapatite by dripping a hydroxyapatite slip stabilised with an amino acid binder into liquid nitrogen. This produced a freeze-dried green body that was subsequently sintered to form porous crystalline hydroxyapatite granules.

The materials produced via the stabilised foamed slip method formed a network of interconnecting pores. The cells become interconnecting as gravity drains the slip from the cell walls, leading to cell wall rupture. The size of these channels was determined by the viscosity of the slip and the foaming techniques. Structures with a macropore size in the range of 100-250 micron were successfully produced. Due to the non-dispersed nature of the slip the walls of the structure showed a high degree of microporosity.

A similar method of producing porous HA ceramic materials has been developed by Sepulveda *et al* where in a ceramic slip, with surfactant and acrylic monomer additions, was foamed by agitation and then set by polymerisation of the acrylic monomer. This gelled body was subsequently sintered at 1350°C to produce a macroporous HA ceramic material[58].

Reticulated Foam Method

Another method of producing architectures similar to those of natural bone is to impregnate or coat a foam structure with a ceramic slip. During sintering the foam support structure is burned off leaving the porous ceramic to sinter.

Work by Fabbri *et al*[59] used cellulose spongy substrates that were impregnated with ceramic particles to produce, on sintering, HA products of diverse porosity. A commercial grade HA powder of the order of 0.3 micron in size was mixed with an acrylic binder in an aqueous solution. The resultant slip was subjected to ultrasonic vibration treatment to homogenise and de-gas the slurry. The foam substrate was ultrasonically cleaned in distilled water so as to promote the absorption of the ceramic slip.

The foam substrate was then impregnated with the ceramic slip, taking care to obtain a uniform coverage while preserving the open pored structure. Once impregnation was complete the system was allowed to dry in air for three to four days. The dried structure was then fired at 1280°C. During the firing process the foam support structure was burned out leaving the ceramic powder to sinter and form a highly crystalline HA structure with interlinked open porosity.

One of the advantages of this method is that the structure of the sintered ceramic article can be controlled by controlling the structure of the foam support media, which can be chosen to produce materials across a large range of porosities. The flexibility of this technique also allows the manufacture of porous ceramic structures with a porosity gradient across the material or with discrete changes in porosity across the material[60].

Optical microscopy carried out on the ceramic foams produced via the reticulated foam method showed a texture similar to that of cancellous bone with an interlinked open pore structure. The structure of the foam substrate was replicated in the finished ceramic foam.

The choice of cellulose foam as a substrate by Fabbri was a good one as this material is not only conducive to binding the slip to the surface of the foam struts, but the permeable nature of the material allowed slip penetration into the microporosity of the strut itself. This property of cellulose avoids the formation of hollow ceramic struts which can form when a non-permeable material such as polyurethane is used as the support foam. The downside of using cellulose is that the structures and pore distributions available in this material are limited and its porous nature may well have contributed to the long drying times necessary in the process.

A significant improvement of this method was developed by Tain and Tain in which a pH activated flocculent was used to encourage the deposition of the ceramic slip onto a pre-acidified polyurethane foam support[61]. The subsequent gelation of the slip adjacent to the foam struts allowed the stable formation of thick coatings of slip around the support strut. On drying and sintering these thick coatings formed strong, uniformly distributed ceramic struts, resulting in a robust material with a high degree of interconnected porosity.

Lost Wax Method

In work by Tancred, Carr and McCormack[62] the cancellous structure of bovine bone was directly replicated by means of a variation on the lost wax process. In this work cancellous bone was extracted from bovine long bones, then cleaned and denatured. This structure was then filled with molten wax and allowed to set. The infiltrated block was then immersed in 10% hydrochloric acid which acted to dissolve out the calcified material leaving a wax negative. This negative was then impregnated under vacuum by a high loading slip of HA or TCP and dried to produce a green body. These blocks were then fired to burn off the wax and sinter the material to produce the replica cancellous bone.

All three of the above techniques have one common and inherent limitation, that of low strengths in the resultant ceramics. This low strength is inherent in the materials due to the fact that the strength of high temperature HA is only a fraction of that of biologically deposited HA in bony tissue. This difference in strength was quantified in work by O'Kelly *et al*[52] where glass reinforced HA was compared with cleaned bovine cancellous bone. The results of this work demonstrated that the synthetic HA material would be required to have an apparent density 70% greater than that of the bovine bone to match the UCS produced.

1.10 Mechanical Properties of HA and TCP

This low strength in sintered HA with a simulated cancellous structure is illustrated in the compressive strength results obtained from material produced via by the lost wax processing route. In that study[52] the 60% macroporous material achieved a UCS of slightly more than 3MPa whereas the denatured bovine bone in their study demonstrated a UCS of 8MPa at 76% macroporosity.

The mechanical properties of sintered HA and TCP have been evaluated in a number of studies. In work by De With *et al*[63] a number of HA samples were produced under different sintering conditions, with sintering temperatures ranging from 1100°C to 1250°C, producing sintered materials with densities from 75% to 98% of the theoretical density of 3.156 g cm^{-3}. These samples were tested under compression and values for Young's modulus, fracture toughness and ultimate compressive strength were found. These results showed the sintered HA materials with 98% theoretical density to have a modulus of 113 GPa, a K_{Ic} of 1 MPa $m^{1/2}$ and a UCS of 798 MPa when tested under dry conditions. Work by Jarcho *et al*[64] obtained an UCS of 917MPa for near fully dense HA. These properties were found to fall off rapidly with decreasing density, so that at 75% of theoretical density the material had a strength of only 50 MPa. From this work a clear relationship between sintering temperature, material density and mechanical properties can be seen.

The normal limit on the upper sintering temperature that can be used in sintering HA is 1300°C, as above this temperature the HA will tend to dissociate into α-TCP and tetracalcium phosphate, liberating water in the process. It has been demonstrated[65] that control of the moisture content of the atmosphere in which the material is sintered can extend the stability of the HA. Therefore it is possible to sinter HA at temperatures above 1300°C without significant degradation of the HA and thus produce highly dense material. It has in fact been shown that it is possible to produce highly dense , high strength HA by sintering at 1400°C with little effort being made to control the sintering atmosphere[66], indicating that the moisture content necessary to suppress the transformation of HA to α-TCP to be low.

Other efforts to improve the mechanical properties of sintered HA have focused on the additions of SiO_2 and P_2O_5 glass reinforcements[67][68]. These additions act not only as a reinforcement but also provide a liquid phase in the sintering process and act as a sintering aid in the normal HA sintering process. In a similar vein work by Royer *et al* demonstrated the possible increase in strength obtained by the use of biphasic HA/TCP materials as opposed to single phase HA[69].

Mechanical Properties *in vivo*

All of the above discussion on mechanical properties relates to dry HA materials in terms of an engineering ceramic. The physical properties of HA change significantly after the material has been implanted for any period of time. The change in the mechanical properties of implanted HA based bone substitute materials with time *in vivo* was studied by Hing *et al*[25][23]. This study involved the implantation of cylindrical Endobon™ plugs into the femurs of New Zealand rabbits. The animals were sacrificed at set time periods up to 180 days and the femur removed. The implants were tested by two distinct methods. In half the cases the implants were carefully cut from the implant site and compression tested. The remaining samples were subjected to push out tests where the force required to push the implant plug out of its bone section was measured. It was found that the UCS of the implant increased dramatically from an initial value of 3MPa to a value of 19MPa at 100 days *in vivo*. This increase in compressive strength was accompanied by a corresponding increase in the interfacial shear stress measured in the push-out testing. It was found that these strength increases correlated well with histological measurements of bone ingrowth into the implant. It was noted that at three and six months *in vivo* the failure mode in the push out testing changed from extrusion to internal fracture of the implant indicating that the strength of the interface between bone and implant was greater than that of the implant itself.

In a similar trial by Hong and de Groot[70] the tensile strength of the interface between bone and a microporous HA implant was measured at set periods of time *in vivo*. The most interesting result from this work was that in samples tested after 16 weeks *in vivo* failure occurred in the HA implant rather than at the interface indicating the interface was stronger in tension than the HA itself. This result is all the more interesting as the scale of the porosity in the implants used was too small to allow bone ingrowth, demonstrating that a good mechanical interlock between bone and a HA implant can be achieved without penetration of bone into the implant.

1.11 X-Ray Diffraction Analysis

As has been discussed earlier the phase composition of the calcium phosphate ceramic will radically effect its dissolution rate and osteoconductive behaviour *in vivo*. It is important therefore to be able to determine the phase composition of any candidate bone substitute material in its fully sintered form. To do this an understanding of thermal transformations that occur during sintering must be gained. Secondly a method of identifying and quantifying the phases in sintered material must be established.

Qualitative XRD

Identification of the phases present is normally achieved using X-ray diffraction analysis (XRD) of a fine powder sample loaded onto a flat plate in the diffractometer. For any given X-ray source (Cu Kα being the most common) every crystalline material produces a distinct diffraction pattern of reflection intensity, in counts, against X-ray incident angle. Where only a single phase is present a diffraction pattern of reflection intensity against incident angle can be matched with the JCPDS standard diffraction patterns using the Hanawalt method[71] to match the three strongest reflections from the standards file against those present in the samples' diffraction pattern.

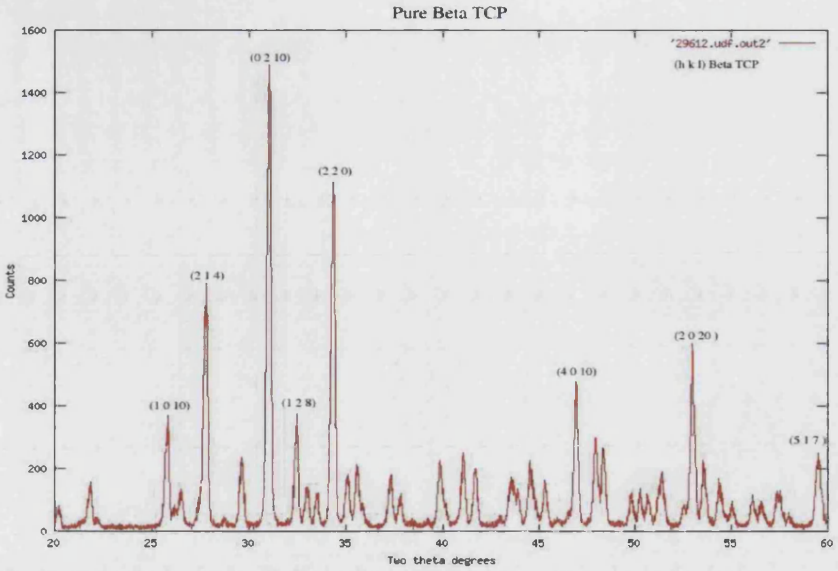

Figure 5 XRD trace for high purity β-TCP with all major reflections marked with their respective Miller indices

The identification of mixed phase materials is a good deal more complicated as the strong reflections from different phases can overlap and this superposition creates strong reflections and to some degree disguises the distinctive diffraction patterns of the phases present. This makes identification of the phases present in a completely unknown mixture, by trying to match a standard diffraction pattern to a subset of the reflections produced by the unknown, very difficult and unreliable. This difficulty can be reduced if the elemental make up of the sample can be determined by some other means, such as EDAX analysis.

In the case of the current work, XRD was used to identify unknown materials where the majority of the material was known to be one of a number of calcium phosphate phases . In this case the list of candidate materials for which the standard must be compared against the diffraction pattern of the unknown is reduced to some five or six materials, allowing an easier and more reliable identification than would otherwise be possible. Figure 5 shows a typical XRD trace for β-TCP where the main marked peaks are identified by their corresponding Miller indices.

Quantitative XRD

Another key feature of XRD analysis is that the intensity of the reflections produced by a given phase in a sample are proportional to the concentration of that crystalline phase present in the sample. It is therefore possible, by use of XRD, to identify the phases in an unknown mixture and to determine the proportions in which those phases are present in the sample.

However in a sample where two or more phases are present the relationship between the intensity of a phases' diffraction pattern and its concentration in the mixture is not generally linear. The diffracted intensity of the phase depends strongly on the relationship between the adsorption coefficient of the phase and the adsorption coefficient of the mixture. This relationship varies with concentration, usually in a non-linear manner[71]. For an unknown mixture, the intensity of the diffraction pattern of a given phase (phase a) in that mixture can be related to its concentration in the mixture by the following:

$$I_a = \frac{K_1 c_a}{\mu_m}$$

Where I_a is the intensity of the diffraction for the phase a, and c_a is the concentration of this phase. K_1 is an unknown constant and μ_m is the linear adsorption of the mixture. However this linear adsorption co-efficient is itself dependent on c_a , thus introducing complexity into the relationship.

Several methods of analysis have been derived, chiefly by Alexander and Klug[72], to overcome this complexity and allow the determination of the concentration of the phase a. One such method involves the introduction of a known quantity of an internal standard into the mixture to be analysed. It has been shown[72] that the relationship between the diffracted intensity of the phase a and the diffracted intensity of the internal standard can be related to their relative concentrations by :

$$\frac{I_a}{I_s} = \frac{K_3 c_a}{K_4 c_s}$$

Where I_s and c_s are the diffracted intensity and concentration of the internal standard respectively.

In real terms this result means that the variations in adsorption caused by the other constituents of the mixture need not be considered as their contributions effect I_a and I_s to the same degree. Therefore a calibration curve of I_a/I_s can be created by measuring the diffraction strengths for the standard and phase a from a set of standard dilutions using a fixed quantity of internal standard and in which the ratio of standard to phase a is known. Once this calibration curve has been established the concentration of phase a in an unknown mixture can be determined by the addition of a known quantity of the internal standard material and measuring the ratio of I_a:I_s by XRD.

An example of the use of this technique can be seen in work by Klein *et al*[38]where just such a set of techniques were used to determine the effect of sintering on two calcium

phosphate powders by XRD pre-sintering and post-sintering. The two powders used were $Ca_{10}(PO_4)_6(OH)_2$ from Merck and $Ca_3(PO_4)_2$ from BDH. The former showed an HA structure while the latter was shown to be 90% β-TCP and 10% α-TCP. On sintering, the apatite material retained its structure while the TCP material was transformed to 100% β-TCP. It is interesting to note that Klein also found that the sintered apatite material sourced from Merck developed a blue colour where as the TCP material remained white after sintering. This result is interesting as a similar phenomenon was noted to occur in the current work and in fact served as a useful marker for the presence of HA in the material.

1.12 Project Background

The current work and subsequent materials development has its origins in a project to characterise a bone graft extender material at that time under late stage development by Stryker Howmedica Osteonics. This material was a precursor to the now commercially available Bone Save material.

Early Production Methods

The material initially investigated was a biphasic porous calcium phosphate material produced by a modified BurPS method.

In the production of this material two grades of calcium phosphate powders were blended with a quantity of organic filler. One of the calcium phosphate powders used was a low stability powder reported to thermally transform to β-TCP at temperatures above 1000°C (listed as TCP118), the other powder was a high crystallinity HA material (listed as TCP130). Both powders were supplied by Rhodia Specialty Phosphates (see Appendix 3).

This blend of ceramic powders and organic filler was wet mixed thoroughly in a blending drum and then pressed in a tablet press to produce a green body of the material. These green body tablets were crushed and sieved to the required granule size prior to sintering at 1100°C for the time required to allow the material to undergo consolidation and thermal transformation. The sintering process also resulted in the burning out of the organic inclusions to produce a sintered material with a distinct macroporosity.

Application and Characterisation

This material was developed to act as an extender to allograft for use in impaction grafting, particularly in impaction grafting for revision hip arthoplasty. In this application the synthetic material is mixed up with the allograft material immediately prior to implantation[40]. This bulking out of the allograft serves in the first instance to alleviate pressure on allograft supply[2]. It has additionally been postulated by Grimm *et al*[73][74] that

the use of this material may serve to improve both short and long term stability of the graft mantle and prosthesis fixation and reduce the impact of variability of allograft quality on graft mantle stability[75].

Characterisation work carried out on this material (see Appendix 1) confirmed the presence of large scale macroporosity in the size range generally accepted to promote osteoconduction. Qualitative XRD analysis determined that the material was composed of a mix of HA and β-TCP.

Materials Limitations

From characterisation work, however, some the limitations of the material were highlighted. As mentioned previously, the formation of isolated porosity is one of the inherent drawbacks of the BurPS process. It was found that the porosity in the material was largely isolated and not uniformly distributed thought the material, but was found to be clumped together, usually near the surface of the granules. It was also found that the overall degree of macroporosity present in the material was lower than anticipated given the amount of organic porosifer in the powder mix.

The form factor of this material was also limited to being granular due to the fact that cracking in the tablet green body was very common. This combined with the friablity of some of the material precluded the option of producing specifically shaped components from this material.

It was as an effort to address the limitations of this, and indeed many of the other materials already mentioned, that the current program of work was conceived.

1.13 Aim of Current Project

The aim of the current work was to develop a methodology to produce a porous ceramic material in which the pore size and distribution could be carefully controlled. The pore structure of this material would be designed such that interconnections between macropores could be guaranteed. This interconnected pore structure would be designed to have a pore size range optimised to promote osteoconduction .

Previous work on the development of the BoneSave material demonstrated that the use a blend of a stable HA and a thermally transforming calcium phosphate powder could be used to generate a HA ceramic with a specific amounts of α-TCP or β-TCP thus combining the surface bioactive ability of the HA with the resorption and replacement mechanism of bone ingrowth observed with the TCP materials.

The final requirement of this new process was that it should be capable of producing large components that were sufficiently mechanically robust to allow them to be machined to shape, thus removing the limitations imposed by a fixed form factor on the Bone Save material.

1.14 Outline of Work

As stated above, the starting point for the development of new bone graft was based on the experience gained by the characterisation of the early BoneSave material. Therefore the same calcium phosphate powders used in the fabrication of the BoneSave material were also used in the current work. This allowed the expertise developed in the sintering and thermal transformation of these powders to be built upon in the current work. In addition to the transfer of technology, the use of common powder precursors meant that the *in vitro* and *in vivo* work ongoing with the BoneSave material would have greater relevance to the materials produced as part of the current work.

To establish a practical baseline for the development of a new bone substitute material a number of established techniques were used to produce materials to which any newly developed material could be compared. These materials varied from low porosity materials produced by isostatic pressing and slip casting methods through to highly porous structures produced by the BurPS technique.

Initial development work focused on attempts to utilise and improve the coated foam method of producing porous ceramics. Though success in this area was limited substantial expertise was developed in the handling of foams and slips and in the burnout and sintering processes.

Through major modifications of the coated foam technique a novel technique for the production of a bone substitute material was developed. This technique involves the total impregnation of a reticulated organic foam with a highly loaded calcium phosphate slip. The impregnated foam is then dried to a green body and sintered leading to the burnout of the organic foam generating a network of interconnected macroporosity, the scale and density of which is strongly determined by the structure of the organic foam.

The following report outlines the development of this methodology and the characterisation of the resultant materials. Comparisons between these new materials and those currently available are made and the possibility of their use in a range of orthopaedic and maxillofacial applications is explored.

The limitations of the new production process and the new materials are also critically examined and a program of further work proposed to overcome these limitations and to develop materials and structures tailored for specific biomedical applications.

2 Materials and Methods

2.1 Section Overview

The main method presented here is for the production of a porous bone substitute material by a vacuum pressure impregnation process. This method has gone through several levels of refinement and consists of a number of sub-processes that are also outlined here. The final vacuum pressure impregnation method is a culmination of these sub processes which is a core part of the program of work, and as such is treated in some detail.

This chapter outlines the materials used in the construction of the bone substitute, the method of fabrication and the techniques employed to characterise the materials at each stage of the process. The structure of the chapter attempts to be constructive, working from the base input products through the various processing techniques to the final fabrication method. In addition to the processes central to the production of the bone substitute, the method of fabrication of some materials produced solely for the purposes of comparison are also outlined. These materials were produced to set a reference point against which the developed bone substitute could be compared.

A number of techniques were used extensively in the characterisation of the materials produced. These were optical microscopy, scanning electron microscopy (SEM), X-ray analysis, and mechanical testing. In addition to these techniques, image analysis was used to extract data as to the material's physical structure from the images produced using SEM.

2.2 Starting materials

The starting materials fall into two broad categories, ceramic powders and organic poroisifers such as polymethylacrylate (PMMA) spheres or polyurethane (PU) foams. The following sections describe these materials and the techniques employed in their characterisation and that of the starting materials used.

2.2.1 Powders

With the exception of the titanium dioxide, used as a standard in the X-ray work, all the powders used were composed of calcium phosphate with various phase compositions. These powders were used either directly in the manufacture of materials, or as reference materials against which the new materials could be compared.

Description

All the sample materials produced in this work were based on two powders produced by Rhodia specialty phosphates group. These powders are sold as tricalcium phosphate grade

118 and tricalcium phosphate grade 130, though is will be shown later that this designation was a misnomer. Both are fine white powders and are sold in bulk for use in the food industry. Copies of the product data sheets are shown in Appendix 3. The use of these materials was inherited from prior work done between Stryker Howmedica Osteonics and TCM in conjunction with the University of Bath. The description of these powders as given below reflects the received wisdom as to the nature of these powders at the start of the project

In addition to these powders used for the bulk of the manufacture, two high purity powders were used for comparison and for the calibration of the adsorption curve in the internal standard method for quantitative X-ray analysis.

Powder	*Description*
Grade 118	Calcium phosphate powder with low crystallinity HA which can undergo thermal transformation to produce β–TCP.
Grade 130	Calcium phosphate powder with high crystallinity HA. Does not undergo thermal transformation at normal sintering temperatures
HA ex Howmedica	High purity, high crystallinity HA powder as produced by Stryker Howmedica as a part of their periapatite production process. This was a white powder with large flaky agglomerate particles.
P223S **High purity TCP**	High purity, high crystallinity β–TCP supplied by Plasma Biotal Ltd. designation P223S (see appendix 3 for product data sheet). This was a very fine white powder.

Table 1 Ceramic Powders

Characterisation

Qualitative XRD

To determine the phase composition of the powders as-received, and prior to thermal treatment, XRD analysis was carried out. Thermal treatment of the powders was designed to replicate the sintering process used to produce the bone substitute material.

Sample preparation

The thermal treatment consisted of heating the powder at a rate of 120°C per hour until the desired dwell temperature had been reached. This dwell temperature was then held for 4 hours before cooling at 250°C per hour to 100°C.

The dwell temperatures of 1150°C and 1280°C were chosen based on preliminary studies of the sintering behaviour of the BoneSave material carried out for Stryker Howmedica

Osteonics. These temperatures represented the upper and lower ends of the temperature range in which useful materials were produced in these studies.

Each of the four powders were analysed in their as-received condition, and after thermal treatment at 1150°C and 1280°C. Thermal treatment of the powders at these temperatures produced a loosely sintered solid which required grinding before powder XRD could be carried out. Additionally the HA powder as-received from Howmedica required grinding to break up the flaky agglomerates. Grinding was done with a pestle and mortar using alcohol as a grinding aid.

X-ray analysis

Sample powders were loaded into a Philips X-ray diffractometer and analysed using Cu radiation with a wavelength of 1.54Å. The data range was set $20° < 2\theta > 59.99°$ with a scan step size of 0.01°. This produced a file containing the counts recorded at each step. A Perl script was written which extracted the relevant header data and plotted the counts against the 2θ angle. An HTML index of these plots was also generated to allow easy cataloging of the XRD traces (see Appendix 2). The strong reflections in the traces were then matched against the JCPDS standard diffraction patterns for all calcium phosphate materials using the Hanawalt[71] method as outlined in the introduction.

Quantitative XRD

Determination of the phase composition of the powder samples was carried out by use of the internal standard method, as discussed in the introduction. The method requires that the relationship between the integrated peak intensity for the phase to be measured, and the intensity for a fixed quantity of standard be calibrated. In this case the concentration of HA was calibrated against TiO_2 as an internal standard using the β-TCP as a dilutant. This allowed the HA and TCP response to be measured in terms of the response of the internal standard.

Calibration curve

The calibration curve for the HA was produced by measuring the peak intensities for the HA against the TiO_2 internal standard in 11 synthetic samples containing known concentrations of HA. The synthetic samples were as listed in Table 2. The strong lines for the HA the TCP and TiO_2 were noted and the average integrated peak intensities determined. These were then plotted to produce a calibration curve.

Sample No.	*HA content*	*TCP content*	*TiO_2 content*
1	1g	0g	0.5g
2	0.9g	0.1g	0.5g
3	0.8g	0.2g	0.5g
4	0.7g	0.3g	0.5g
5	0.6g	0.4g	0.5g
6	0.5g	0.5g	0.5g
7	0.4g	0.6g	0.5g
8	0.3g	0.7g	0.5g
9	0.2g	0.8g	0.5g
10	0.1g	0.9g	0.5g
11	0g	1g	0.5g

Table 2 XRD calibration curve samples.

These synthetic samples were analysed again using Cu α radiation with a wavelength of 1.54Å. Two analysis runs were carried out on each sample, one with the data range of 20°< 2θ>59.99° with a scan step size of 0.01° and the second with two data ranges 24°< 2θ>27° and 30°< 2θ>33° which focused more closely on the areas of key interest. The strong lines for the HA the TCP and TiO_2 were noted and the average integrated peak intensities determined. These were then plotted to produce a calibration curve.

Determination of unknowns

Samples of the powders grade 130 and grade 118 in the as-received condition and thermally treated at 1150°C and 1280°C were prepared as above. To one gram of each of these samples 0.5g of the TiO_2 internal standard was added. Samples were blended and analysed using Cu α radiation with a wavelength of 1.54Å. The data range was set 20°< 2θ>59.99° with a scan step size of 0.01°. The strong lines for the HA the TCP and TiO_2 were noted and the average integrated peak intensities determined. These were then cross-referenced with the calibration curve to determine the HA and TCP concentrations in the materials.

Thermal Analysis

Thermo gravimetric analysis

The TGA technique measures the mass change of a sample as it is subjected to a fixed heating rate. This measurement provides information useful for the determination of organic content, moisture content and water associated with the samples.

Differential Scanning Calorimeterey

DSC provides a measure of the change in the energy taken up or given out by a system as it is heated through a specific thermal ramp. The material to be analysed is loaded against a known reference material and the power input and sample temperature measured. Both

sample and reference material are then heated. The DSC can be run in power control mode, where the power input is set and the sample temperature measured, or temperature control mode, where the heating rate on the sample is set and the power input varied and recorded. Data from DSC can be used to find endothermic or exothermic phase changes in the material. This technique is commonly used in conjunction with TGA to determine the nature of the reactions occurring in the sample.

TGA and DSC was carried out on the two main powders, grade 118 and grade 130, by Stryker Howmedica Osteonoics on our behalf using the facilities at the University of Limerick.

2.2.2 Foams

Organic foams were used in the production of ceramic materials with a structured porosity. These foams were used in two distinct manners. Initially the foam was used as a support framework onto which a coating of ceramic slip was applied. Later in the project the foam was utilised as a structured porosifier that was impregnated with the ceramic slip. In both cases the foam, incorporated in the green body, was fugitive on firing. Though a wide selection of foams were considered at the outset reticulated PU foam was selected as the most suitable, and it was on these foams that the work was focused.

Description of organic foams

The foams used were reticulated polyurethane foam supplied by Sydney Heath & Sons. These were open structured foams with no apparent closed pore volumes. Foams were supplied rated by pores per inch (ppi). Foams of 90 ppi, 65 ppi, 45 ppi, 30 ppi, 20 ppi and 10 ppi were used. As fire retardants are commonly added to these types of foams care was taken to select the non fire retardant variant of each type to ensure burnout of the foam was not unduly hindered and also to reduce the likelihood of the sintered ceramic being contaminated with by-products of the foam burn out.

Characterisation of foams

Characterisation of the foams was carried out to assess how the foam would burn out during a firing process and to assess the likelihood that the burnout process could contaminate the sintered ceramic. As the foams were used as porosifiers, the structure of the foam and the shape and size of the foams strut cross sections were also examined.

SEM

SEM was used to characterise the pore structure of the foams and to measure the size and shape of the foam strut cross-sections. To best accomplish these goals, samples of foam were examined both in their normal state and as resin mounted polished sections.

Non-mounted foams

Small sections of each of the foams were stuck on metal specimen platens with conductive carbon slip. These samples were then gold sputter coated for SEM examination. Images were taken at low magnification to show the foam's overall structure and at higher magnification to show the surface texture of each foam. In addition to the SEM examination EDAX analysis was employed to analyse the elemental composition of foam surface.

Mounted foams

Samples of each of the foams were mounted in epoxy resin. Specifix low viscosity epoxy resin was impregnated into the foam samples under vacuum and then placed in a pressurised vessel to cure. This process ensured a high level of resin impregnation into the foam samples.The mounted samples were then ground and polished. Prior to gold sputter coating the mounted samples were photographed using light microscopy and macro images obtained by scanning on a flatbed scanner. Gold sputter coating was carried out and the samples were then examined and photographed using the 6310 scanning electron microscope.

Optical

Samples mounted and prepared above for SEM examination were examined and photographed using a Zeiss light microscope. Images taken with the light microscope were cross-referenced with scaling shots taken at the four available magnifications to allow easy measurement of feature size during image analysis.

Other porosifiers

In addition to the polyurethane foams other organic fillers were used as porosifiers to produce porous materials as part of the exercise to produce baseline materials.

Description of organic fillers

Filler	*Description*
Sugar	Standard granulated white sugar.
PEO	Polyethlyeneoxide, fine free flowing powder of hard particles
PEG	Polyethlyeneglycol, powder consisting of soft particles which have a tendency to bind together
PMMA	Polymethylacrylate, hard polymer spheres forming a free flowing powder

Table 3 Description of organic fillers

Characterisation of organic fillers

The role of these organic fillers was to act as porosifers and as such the size and shape of the filler particles would have a strong effect on the porosity produced. The size and shape of the fillers was assessed by SEM imaging. Samples of filler material were mounted on metal sample platter using adhesive carbon pad. These samples were then gold sputter coated and photographed using the 6310 scanning electron microscope. Images obtained were analysed using image analysis to measure particle size and shape.

2.3 Fabrication processes

The following sections describe the processes involved in the production of solid CaP ceramic artefacts and porous CaP ceramic artefacts from the base input materials described in the previous sections. The production control processes are described in addition to the characterisation techniques used in the analysis of the resultant materials.

The processes discussed include the production of reference materials for comparison to the bone substitute material produced. These reference materials were high density ceramic materials produced using uniaxial and isostatic powder pressing, and macro porous ceramic materials produced by the BURPS method, described below.

The processes of slip production and the production of macro porous CaP ceramic materials by the coated foam and impregnated foam routes are also discussed. The key process, that of vacuum pressure foam impregnation, is described in detail.

2.3.1 Baseline materials

Produced as reference or control materials, against which the synthetic bone graft replacement material was to be compared, the baseline materials were produced by pressing the powder components into a green body and then sintering to produce the ceramic artefact.

Two distinct types of material were produced in this section of work. Firstly high-density ceramic material produced from the two base input powders, both in their pure form and blended together, were produced. Secondly macro porous materials were produced via the BURPS method, utilising a number of organic fillers to act as the porosifer.

Production of baseline materials

High density materials

High density ceramic materials were produced from the two base powders, grade 118 and grade 130 via uniaxial pressing and isostatic pressing routes.

Two three gram green bodies were pressed from each powder grade, one via uniaxial pressing and one via isostatic pressing (see below). These samples were then sintered to 1280°C using the thermal ramp shown in Figure 6.

The initial heating rate shown was 60°C/hour up to 600°C, the material was then held at 600°C for one hour before heating at a rate of 120°C/hour to the final sintering temperature. The material was then allowed to dwell at this sintering temperature for four hours. Cooling at a rate of 250°C/hour was then carried out. This sintering regime was designed based on work done at the University of Bath on characterisation of the sintering profile of HA materials[76].

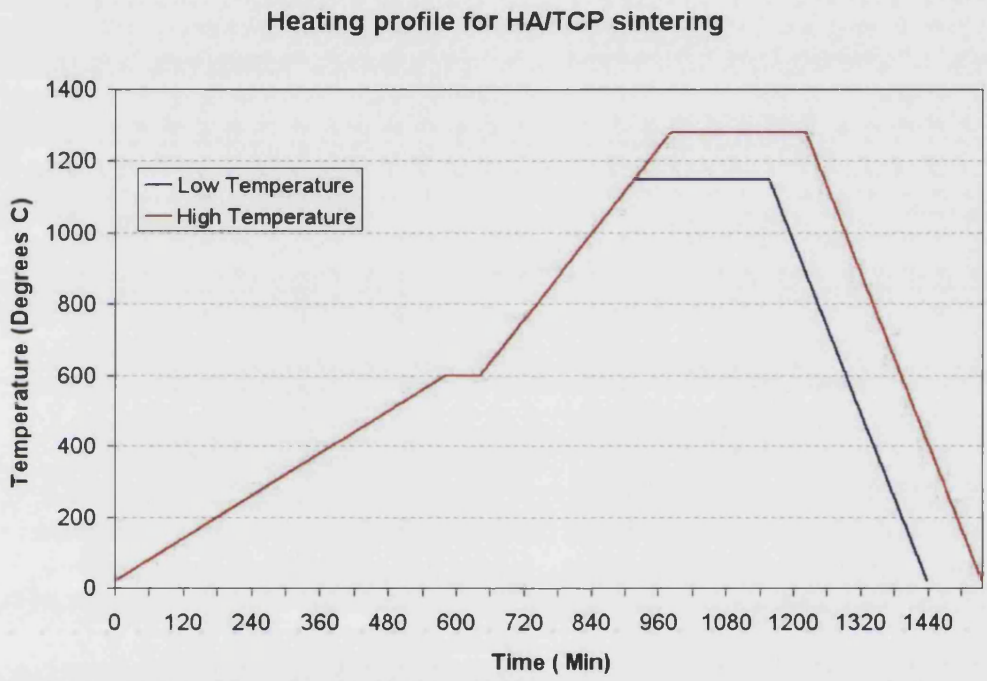

Figure 6 Sintering regime for HA/TCP ceramics

Uniaxial pressing

Three grams of powder was loaded into a 12mm diameter die and pressed at a pressure of 110-130MPa using a hydraulic hand press. The pressure was maintained for three minutes before the sample was unloaded and carefully removed from the die.

Isostatic pressing

3g of powder was loaded into a 12mm diameter die and pressed at a pressure of 80MPa using a hydraulic hand press. The pressure was maintained for 1min before the sample was unloaded and carefully removed from the die.

The resultant green body was placed within a rubber sheath, one end of which had been sealed. The sheath was then evacuated using a vacuum pump. Care was taken to ensure there were no air inclusions in the sheath and that it made good contact with the green body at all points. The sheath was then loaded into the oil bath of the isostatic press.

The oil bath was pressurised to 100MPa and held at pressure for 1min. The pressure was then released and the rubber sheath removed from the oil bath. The oil was cleaned thoroughly from the surface before the sheath was cut and the green body removed.

BurPS

Macroporous ceramic materials were produced using a range of organic fillers, detailed above, via the BurPS route. In all cases, other than with the sugar filler, the organic component was dry blended with the ceramic powder prior to pressing and sintering. In the case of the sugar filler the ceramic and filler were mixed with 4.5ml of distilled water per 100g of powder blend. Mixing was accomplished by ball milling the powder blend overnight with a small quantity of 10mm diameter zirconia milling media, typically 6 per 50g of powder.

The mixed powders were then pressed uniaxially or isostatically, as above, prior to sintering to 1150°C or 1280°C as desired. The thermal ramp used for sintering was as shown in Figure 6.

Table 4 below shows the blends of powder and organic fillers for which pressing was attempted in the production of BurPS materials. In all cases the ceramic powder used consisted of 20% grade 118 and 80% grade 130.

Filling Agent	*Filling Agent (Vol%)*
Sugar	16.7%
	37.5%
PEG	16.7%
	37.5%
	44.4%
PVA	16.7%
	28.6%
	37.5%
	44.4%
PMMA	13%
	20%
	28.6%
	37.5%
Polyethylene Oxide	16.7%
	28.6%
	33.00%
	37.5%
	44.4%
	57%

Table 4 Organic fillers and ceramic powder pressed for BurPS materials

2.3.2 Characterisation of baseline materials

The characterisation of these materials focused on the measurement of the pore size and pore morphology at both the macropore and micropore level. This was accomplished by SEM coupled with some basic image analysis.

SEM

Electron microscopy was carried out on all of the baseline materials. Samples were examined both as polished sections and in an unpolished state with exposed fracture surfaces. Polished samples were prepared as shown in Table 5 below.

Preparation stage	*Method employed*
Mounting	Specifix low viscosity epoxy resin impregnated into the samples under vacuum and cured under pressure
Grinding	Rough planar ground using progressively finer silicon carbide paper from 240 grit to 600 grit
	2 mins on 600 grit silicon carbide paper at 150 rpm, complementary rotation at 5 lb. load per sample
	2 mins on 1200 grit silicon carbide paper at 150 rpm, complementary rotation at 5 lb. load per sample
Polishing	2 mins on a 0.05μm Texmet cloth at 150 rpm using Masterprep colloidal silica water based suspension, complementary rotation at 5 lb. load per sample
Coating	Gold sputter coating was carried out and the samples examined and photographed using the 6310 scanning electron microscope.

Table 5 Preparation of HA/TCP ceramics for SEM

Fracture surface samples were prepared by cracking the material, typically with a pestle and mortar, and mounting the resultant chips on a metal sample platen using conductive carbon slip. Samples were gold sputter coated to allow SEM examination.

Pore size, shape, and distribution were determined by image analysis of the polished sections of the macro porous materials. The techniques involved in the determination of pore size are outlined in the section on image (section 2.6.2.3).

2.4 Slips

All methods involving the use of organic foams, as either a carrier or as a porosifier, to produce porous bone graft substitute relied on aqueous ceramic slip to deposit the ceramic particles in place to form a green body. Therefore the ceramic slips were the main precursor in the production process and as such play a pivotal role in the project.

All slips used were aqueous suspensions of the powder grades 130 and or grade 118 with low organic additions. Organic additions were in the form of either binders or dispersants. In the main, slips were ball milled, though some work on high speed dispersion mixing was also carried out. It is also worthwhile to point out that although viscosity measurements were used in the characterisation of the slip, viscometery was also extensively used as a production control tool.

2.4.1 Slip production methods

Various slips were produced during the course of the work varying in powder content, viscosity, dispersion method and organic additions. The slips are presented here in the order they were produced and are indicative of the level of refinement of the impregnation/coating method in which they were employed.

High loading slip

These slips were produced to have a high viscosity and high ceramic powder content. The target fabrication process for these slips was the coated foam process, discussed later. To improve green body strength and reduce cracking these slips included an organic binder component.

Slip production was carried out as follows:

- A solution of 2%PVA was made up by dissolving the PVA in warm water.
- To 100ml of the PVA solution 20g of base powder was added plus 30g of zirconia milling media.
- This mix was then ball milled for two hours before an addition 20g of powder was added.
- The incremental addition of powder was repeated until the desired powder loading was attained.
- The slip was then milled overnight.

Slips were produced with powder contents in the range of 60g –100g of powder per 100g of PVA solution. The resultant slips were found to be highly viscous.

Ball milled

These slips were a refinement of the high loading slips designed to have, in general, a lower viscosity and to be produced on a larger scale. These slips had no organic additions made to them. The target application for these slips was the impact impregnation process.

Slip production was carried out as follows:

- The desired amount of powder was weighed out in the desired ratio of grade 130 to grade 118. Typically 400g – 800g were used.
- The powder was added to 1 litre of distilled water under constant stirring. To this mix 200g of zirconia milling media was added.

- The mix was placed on a ball mill and milled for 18hrs-24hs.
- The viscosity of the slip was measured using a Brookfield viscometer (see below).
- In the event that the slip was allowed to stand for any significant period of time it was returned to the ball mill for an hour to re-mobilise prior to use.

High shear dispersion mixing

In an attempt to speed up the process of slip production the use of a high shear dispersion mixer was trialled. Slips produced by this method were targeted to directly replace those produced by ball milling.

Slip production was carried out as follows:

- The desired amount of powder was weighed out in the desired ratio of grade 130 to grade 118. Typically 400g – 800g were used.
- The powder was added to 1 litre of distilled water under constant stirring.
- The mix was dispersed using a high shear dispersion mixer at a speed of 2400rpm for three minutes.
- The viscosity of the slip was measured using a Brookfield viscometer.

Ball milled and dispersed

These slips were produced as a refinement of the ball milled slips so that a high loading slip could be produced with a lower viscosity than its non-dispersed equivalent. This lower viscosity per powder content was required by the vacuum pressure impregnation method discussed later. The dispersant used was Dispex A40, an ammonia salt based dispersant produced by Ciba (see data sheet Appendix 3) . This dispersant was chosen as it contained no metal salts and was completely fugitive on firing.

Slip production was carried out as follows:

- The desired amount of powder was weighed out in the desired ratio of grade 130 to grade 118. Typically 400g – 800g were used.
- The powder was added to 1 litre of distilled water under constant stirring. To this mix 200g of zirconia milling media was added.
- The mix was placed on a ball mill and milled for 18hrs-24hs.

- The viscosity of the slip was measured using a Brookfield viscometer as detailed below.
- An addition of 0.5ml of Dispex was added and the mix stirred thoroughly.
- Viscosity readings were again taken.
- Additions of dispersant were continued in this manner until the desired viscosity was attained.
- In the event that the slip was allowed to stand for any significant period of time it was returned to the ball mill for an hour to re-mobilise prior to use.

2.4.2 Characterisation of slips

Characterisation of the slips was focused on two areas, assessing the suitability of the slip for the target coating or impregnation process, and secondly to determine the effect of processing changes in slip production on the properties of the sintered ceramic. To these ends viscosity measurements were made on the slip, and sintered artifacts were produced from the slips either as high-density materials or as small-scale coated foam samples.

Viscosity

It was obvious that the success of an impregnation or coating processes was strongly determined by the flow of slip into and out of the foam. Therefore the viscosity of the slips used in these processes was vital to their success or failure in the production of an artefact with evenly distributed porosity. During the early work using the high loading slips, the viscosity was determined purely by the weight fraction of powder in the slips and viscosity measurements were not taken. Later use of a dispersant allowed greater control of the slip viscosity and so the use of viscosity measurements as a characterisation method and process control tool became more useful.

As the dispersant was being used chiefly to control slip viscosity the effect of dispersant additions on viscosity was measured as follows:

- Slips were produced with powder loading of 500g and 600g per by ball milling as detailed above. Powders consisted of 50% grade 118 and 50% grade 130 in both cases.
- A 0.5g/l addition of Dispex was made to the slips, which were then stirred thoroughly.

- The viscosity of the slips were measured using a Brookfield viscometer (circa 1954) using a spindle speed of 10rpm and a No. 5 spindle.
- To take a measurement the spindle was inserted in the slip up to the prescribed level, the rotor switched on and the reading taken from the rotating dial. The first reading was taken 60 seconds after the rotation had been started and two further readings were taken at 30 second intervals.
- Three separate measurements taken for each dispersant addition. The spindle was cleaned and the slip stirred between each of these three measurements.
- This measurement process was repeated with further additions of Dispex in 0.5g/l steps up to a total Dispex content of 3g/l.

Slip Casting

To determine the effects of production via a slip casting route, and the addition of dispersant, on the microstructure of a sintered component a high-density ceramic was produced from the dispersed and non dispersed slips by slip casting.

- A slip was prepared with 600g/l powder loading consisting of 50% grade 130 and 50% grade 118, by ball milling.
- To one half of this slip an addition of 2g/l of Dispex dispersant was made.
- Both slips were cast in filter paper lined funnels, dried and subsequently sintered at 1280°C using the thermal ramp described previously.
- Sintered materials were sectioned and mounted in epoxy resin prior to polishing as described in Table 5.
- These polished sections were gold sputter coated and photographed using high magnification scanning electron microscopy sectioned. Resultant images were analysed using image analysis techniques.

Trial usage

To evaluate the suitability of the slips as produced, small-scale trial samples were made by coating or impregnating the foams with the slips as appropriate for the slip type. This process was carried out to eliminate some of the many production variables so as to narrow the field of interest for the more extensive sample production.

Small sections measuring 1.5cm x 1.5cm x 2.5cm were cut from each of the available foams in the pore size range of 10ppi-90ppi. In the case of the high loading slips with binders, these foam samples were coated with the slip in accordance with the method outlined for coated foams, below. In the case of all other slips the foams were impregnated with the slip using the impact impregnation method (see section 2.6.1).

Samples were dried and sintered to 1280°C using the heating ramp shown in Figure 6. Sintered materials were sectioned and visually inspected, the appearance of these sections was recorded by scanning on a flatbed scanner.

2.5 Coated Foams

This method is the classic method of production of porous ceramic materials using a reticulated foam support. The technique relies on slip adhering to the foam support and drying in place thus producing a green body with a pore structure similar to that of the base foam. Sintering caused the foam support to burn off resulting in a porous ceramic material. In the case of this work, coated foam samples were produced from the high loading slips with PVA binder. Variations in the process centred on the method of removal of the excess slip, and the number of slip coats applied to the foam.

2.5.1 Coated foam method

Coated foam samples were produced by the following method:

- Three high loading slips produced as detailed above with powder contents of 600g/l 800g/l and 100g/l respectively.
- Sections of foams were cut to 2.5cm x 2.5cm x 2.5cm from foams with pore sizes of 10ppi, 20ppi, 30ppi, 45ppi, 60ppi and 90ppi.
- The foam supports were submerged under the selected slip and mechanically worked to ensure good penetration of the slip into the foam structure.
- The foam was removed from the slip and pulled between two rollers set 1cm apart so as to remove the excess slip and evenly distribute the slip across the foam support.
- Coated foams were dried on tissue overnight prior to drying in an oven at 40°C for 12 hours.
- The resultant green body was sintered at 1150°C or 1280°C using heating ramp shown previously.

Variations

Variations were carried made on the above method. In the first instance the use of the rollers to remove excess slip was replaced by the use of compressed air to blow out excess slip from the foam and to rupture any cells formed.

The second variation employed was the second dipping of the coated foam. The foam was coated using the compressed air method as above and subsequently tissue dried overnight on tissue. The coated foam was returned to the slip and the system agitated to promote slip ingress into the green body. The brittle nature of the coated foam precluded mechanical working as a method of promoting slip ingress.

The coated foam was then removed from the slip and the excess removed using compressed air. The resultant green body was then dried and fired as before.

2.5.2 Characterisation of materials by coated foam route

Characterisation of these materials comprised of macroscopic examination and SEM imaging and photography.

Optical

Samples were photographed using an Olympus 2.2 megapixel digital camera in macro mode. Images were taken of intact and fractured samples.

A selection of samples were sectioned and ground flat, these samples were scanned on the flatbed scanner, at high resolution, to show internal structure. Sectioning and grinding was limited to the more mechanically robust materials produced by this method.

SEM

A selection of samples, showing fracture surfaces, were prepared for SEM examination. These samples were mounted on metal sample platens using carbon slip and then gold sputter coated. These samples were then imaged and photographed using the 6310 scanning electron microscope.

2.6 Impregnated Foams

The impregnated foam method was the core fabrication technique of this project, with the focus of the work being the vacuum pressure impregnation technique. This technique varies radically from the coated foam technique as it produces a negative image of the foam in the final ceramic artifact. The organic foam in this method acts as interconnected porosifier, which is fugitive on sintering leaving behind an interconnected network of pores.

The two main techniques discussed, impact impregnation and vacuum/pressure impregnation, differ in the means by which the slip is introduced into the organic foam. The aim of the impregnation was complete filling of the foam pore structure with slip.

2.6.1 Foam impregnation methods

The technique has undergone a series of refinements from the crude impact impregnation method using non-dispersed slips up to the double impregnation method using the vacuum/pressure technique with dispersed slips. The various techniques are presented here in order of refinement.

Impact impregnation method

Initial impact impregnation method used non-dispersed ball milled slips with powder loadings in the range of 400g/l to 800g/l. Subsequent refinement of this technique used dispersed slips with powder loadings in the range 450g/l to 600g/l

Impact impregnation with non-dispersed slips was carried out as follows:

- Non-dispersed ball milled slips were made up with powder loadings in the range of 400g/l to 800g/l as required.
- Sections were cut from the 20ppi, 30ppi, 45ppi, 60 ppi and 90ppi foams. Sections were 2.5cm x 2.5cm x 2.5cm in size.
- Foam sections were submerged under the slip and mechanically worked to expel the majority of entrapped air.
- The vessel containing the slip and submerged foam was then impacted repeatedly on a solid surface. Care was taken to ensure the foam remained submerged throughout the process. Impaction promoted the ingress of slip into the foam and the release on any remaining entrapped air.
- The impregnated foam was then removed from the slip and allowed to dry on a mesh or on tissue prior to drying overnight at 40°C. Details of the drying techniques used are covered in a dedicated section below.
- The resultant green body was then sintered to 1150°C or 1280°C as required using the heating rate shown in Figure 6.

A modification of the above method using dispersed slips was developed to allow higher loading slips to more effectively penetrate into the organic foam structure.

- Dispersed ball milled slips made up with powder loadings in the range 450g/l to 600g/l.
- Target viscosity of the slip was set for each foam type used based on the experience gained from the slips trial usage.
- Foam sections were cut and impregnation carried out as above.
- Samples were dried on mesh or tissue prior to sintering at 1150°C or 1280°C.

Vacuum/pressure impregnation method

The vacuum pressure impregnation method works by evacuating the foam in a vacuum chamber prior to pumping in the ceramic slip. The re-introduction of atmospheric pressure into the vacuum chamber forces the slip into the foam, thus achieving impregnation. In the original trials of this technique using a hyper jet vacuum/pressure impregnation machine were unsuccessful. One of the limitations of this machine was its stainless steel vacuum chamber, which did not allow the observation of the impregnation in process. This fact coupled with a requirement to utilise lower volumes of slip prompted the adaptation of a resin impregnation device to serve the needs of the slip impregnation technique.

Rig Design

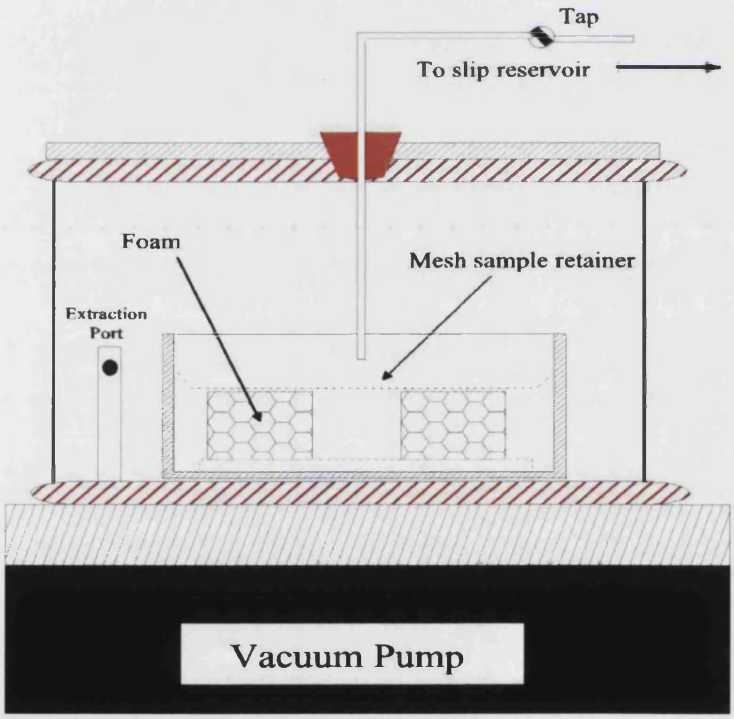

Figure 7 Schematic of vacuum impregnation rig

The vacuum/pressure impregnation rig, as shown in Figure 7, comprised of a glass chamber sealed at the top and bottom with rubber seals to two metal plates.

Placed inside the chamber was a round glass vessel. On the floor of this vessel a mesh support platform was placed, which would serve to raise the foam materials off the floor of the vessel, thus allowing better slip ingress. Foam materials were held in place by a mesh retainer, which clamped securely against the sides of the vessel. Through the centre of the top plate a pipe passed out of the chamber to the slip reservoir. Flow through this pipe was controlled by a simple tap. Air was evacuated from the chamber through the extraction port that was set on a riser inside the chamber and connected to the vacuum pump through the bottom plate.

Impregnation process

- Slips of the required powder loadings were made up by ball milling and the viscosity set by the addition of dispersant as detailed earlier .
- The slip was then placed in a large vacuum and pumped down to 1000 mbar. The low pressure led the formation of gas bubbles in the slip, causing the slip to foam and rise. The rise of the slip was curtailed by the controlled release of air into the chamber. The process of pumping down and partial re-pressurisation was repeated until large gas bubbles grew and burst causing a large release of gas and collapse of the foamed slip.
- Sections were cut from the 20ppi, 30ppi, 45ppi, 60 ppi and 90ppi foams. Sections were 2.5cm x 2.5cm x 2.5cm in size. Theses foam sections were soaked in distilled water and rinsed to ensure cleanliness and to remove any surface treatment.
- Up to three foam sections were placed in the impregnation rig. Sections were placed on the mesh support platform within the glass vessel. These sections were then secured in place by the mesh retainer as shown above (see Figure 7).
- The chamber was then evacuated with the slip flow tap set to closed. This removed the air from the pores in the foam sections. The chamber was pumped down to 1000mbar negative pressure and held at this pressure for five minutes.
- The slip flow tap was then set to open and a quantity of slip drawn across into the vessel. Sufficient quantity was drawn across to completely cover the foam section with one centimetre or more of slip. The tap was then closed and the vacuum pressure allowed to return to 1000mbar.
- The air inlet valve on the vacuum pump (not shown) was then opened allowing partial re-pressurisation of the chamber. This pressure forced the slip into the

evacuated foam sections. The air inlet valve was set to closed and the vacuum pressure allowed to return to 1000mbar.

- The process of evacuation and re-pressurisation was repeated until no bubbles or off gassing were observed from the slip during the evacuation stage. This usually occurred after three cycles.
- When impregnation was completed the vessel was removed from the chamber and the excess slip returned to the slip reservoir. The impregnated foam sections were then removed and placed on drying surface.
- Drying was usually carried out on tissue paper, though other drying methods were tried. Details of the drying procedures employed are given below.
- The dried green bodies were then sintered at 1150°C or 1280°C using the heating ramp shown in Figure 6. The slow heating rate and dwell at 600°C were designed to allow burn out of the organic foam prior to sintering.

Drying

Variations in the drying techniques were made as mentioned above. These variations were made to determine the effect of drying conditions on slip distribution within the foam structure and the overall quality of the sintered article.

Impregnated foams were placed on layers of tissue, fine wire mesh or non-permeable polyethylene sheet. These samples were turned every hour for the first four hours of drying and then allowed to dry for a further eight hours. Samples were then placed in an oven at 40°C and allowed to dry for 12 hours.

In addition to these trials freeze-drying was also explored as an option. In this case the impregnated foams were placed in liquid nitrogen for 30 seconds before being dried on tissue as above.

Modification: Double impregnation methods

Two significant modifications to the vacuum/pressure impregnation technique were trialed. In the first instance the dry foam and slip composite green body was returned to the impregnation chamber and the impregnation process repeated.

In the second instance the impregnated foam was removed from the slip after the primary impregnation and placed on tissue to dry. A layer of tissue was also placed over the sample to aid uniform drying. Drying in this manner was carried out for 15 minutes so that the excess water had been removed from the system.

The partially dried sample was then returned to the vacuum chamber and a second impregnation carried out. This modification also allows additional flexibility in the process as the slip for the first and second impregnation process need not be the same in terms loading, viscosity or chemical composition.

2.6.2 Characterisation of materials by foam impregnation method

The characterisation of the materials produced centred around the measurement of the pore size, shape and distribution within the materials. The tools used in this characterisation were microscopy coupled with image analysis. Macroscopic examination and photography was used extensively to examine and record the less successful combinations of fabrication variables.

The compressive strength of some of these materials was also measured so as to evaluate the effect of the process variables on the mechanical properties of the material and to examine any correlation between pore size/distribution on mechanical strength.

Macroscopic examination

Macroscopic examination was used to evaluate the overall pore distribution throughout the sample material. In the case of mechanically robust materials, sections were cut and ground so that the distribution of pores within the bulk of the samples could be observed. Any colour variation within the material or any large-scale flaws were also noted at this stage.

A record of the appearance of the material was kept either by scanning sections on a flatbed scanner or by photographing the materials with an Olympus 2040-Z digital camera in macro mode.

Microscopic examination

Microscopic examination took two main forms. Firstly darkfield optical microscopy was employed to qualitatively access the nature of the porosity in the materials and to verify the pore formation mechanisms occurring in the process.

Secondly SEM was employed to take high contrast images of the materials so that macroporosity and microporosity could be quantitatively accessed by means of image analysis.

In both cases polished sections of epoxy mounted materials were used. Samples were mounted and polished by the method shown in Table 5, with great care being taken at the mounting stage to ensure good resin impregnation into the ceramics pore structure.

Prior to gold sputter coating the sections were examined and photographed on the Zeiss optical microscope using darkfield illumination. The gold sputter coated sections were examined and photographed on the JEOL 6310 scanning electron microscope.

In addition to the polished section samples, fracture surface samples were mounted and gold sputter coated. These fracture surface specimens were also photographed using the 6310 scanning electron microscope.

Image analysis

Image analysis of the SEM images was used to make quantitative measurements of the porosity in the sample materials. This technique allowed the pore size and pore size distribution to be assessed.

The negatives from the SEM microscopy were scanned using a flatbed scanner and a light box for back lighting. The image contrast and levels were adjusted using GIMP (GNU image manipulation program 1.2.3) to enhance the images and optimise the contrast between the pores and the ceramic material.

Optimised images were loaded into NIH image, an image analysis program, as 8 bit greyscale images to simplify the process of thresholding. Baseline JPEG file format with a low compression ratio was used to minimise file size and allow good portability between systems.

Each image was spatially calibrated to allow conversion from pixels count to micrometers. The scale bar on the SEM images was used for this calibration. Scaling shots of a known rule were taken to calibrate the optical images that were analysed.

The image threshold was set so that the pore volume was identified as one phase and the ceramic material identified another phase. In terms of the analysis software this effectively creates a binary image where pixels are either black or white. Using the threshold the software was then set to find the areas of the pore phase in the material. The algorithm finds groups of dark pixels and finds where they border with the bright phase. If the number of pixels contained within this border was above a minimum, as set by the operator, the area was marked and counted.

Data for each of these found areas was extracted and exported as a comma separated value (csv) file. The data fields extracted were; area, area equivalent diameter, long axis, short axis, circularity and mean grey value. Features of particular interest that could not usefully be measured using the area method were measured with line objects calibrated against a scale bar.

The extracted csv file can then be treated with a number of programs to extract statistical data about pore size and distribution from the results. In this instance the statistical analysis package provided by the Gnumeric spreadsheet program was used extensively.

Compression Testing

Compression testing was carried out to establish the load bearing capability and to demonstrate the robust nature of the developed material. A fixed platen compression test was chosen, as this was the simplest to perform and to produce samples for.

Sample production

Samples were produced by both the impact impregnation and vacuum pressure impregnation routes. All samples were produced using dispersed ball milled slips with a grade 118:grade 130 of 1:1. Foams with pore sizes on 20ppi, 30ppi and 45ppi were used. The foam sections for all samples were 2.5cm x2.5cm x 2.5cm.

The following samples were produced for compression testing:

Impregnation Method	*Foam*	*Slip*	*Drying Conditions*	*Sintering Conditions*
Impact Impregnated	30ppi, 45ppi	Ball milled and dispersed 500g/l	Tissue dry, Mesh dry	1150°C, 1280°C
Double shot vacuum pressure impregnated	20ppi, 30ppi	Ball milled and dispersed 500g/l	Tissue dry	1280°C

Table 6 Samples produced for compression testing

Sample testing

The sintered samples were cut and ground into cubes, measuring 1.5cm on each side. Care was taken to ensure all opposing faces were parallel.

These ground samples were dried to ensure any water from the wet grinding stage had been removed. The dry samples were then weighed and their density calculated from their weight and geometric volume.

The cube shaped samples were then compression tested on an Instron 4303 test machine using fixed platens. Testing was carried out at a crosshead speed of 2mm/min. Load data was output and plotted against time on a chart record. All samples were tested to destruction.

XRD analysis of sintered materials

Selected materials produced via the impact impregnated and vacuum pressure impregnation methods were ground to powder and analysed by qualitative and quantitative XRD. Grinding was carried out with a pestle and mortar using ethanol as a grinding aid.

These samples were selected to ensure all variables of; slip composition, impregnation method and sintering temperature were represented. Anatase TiO_2 was added to the powders to act as an internal standard to facilitate quantitative analysis.

3 Results

3.1 Overview

This chapter presents the results of the experiments to characterise synthetic bone material produced by a number of methods including vacuum pressure impregnation and briefly outlines some of the key findings of these results. The aim therefore is to present the important experimental results and to highlight the key findings in the context of the desired application.

The chapter breaks down into four broad sections covering the characterisation of the ceramic powders used, the characterisation of the organic porosifers, the characterisation of reference materials and the characterisation of materials produced utilising an organic foam support. The last of these sections is the most substantial and the results presented are representative of the state of the art in terms of the materials produced in the project.

3.2 Powder Results

3.2.1 Base Powder

XRD and thermal analysis of the four ceramic powders were used throughout the project, with particular emphasis on the Grade 118 and Grade 130 powders that were the mainstay of the sample manufacture process.

The results showed the powder composition in the as received state and track the changes in composition as the powders were sintered to 1150°C and 1280°C.

Qualitative Analysis

This section details the results of the qualitative XRD analysis of the ceramic powders in the as received condition and after sintering at 1150°C and 1280°C. This analysis focuses on matching the XRD trace produced in each case to the JCPDSS standard data for all of the compounds likely to be found in the powder. Matches were made with regard to peak position and relative peak heights.

Grade 118 as-received

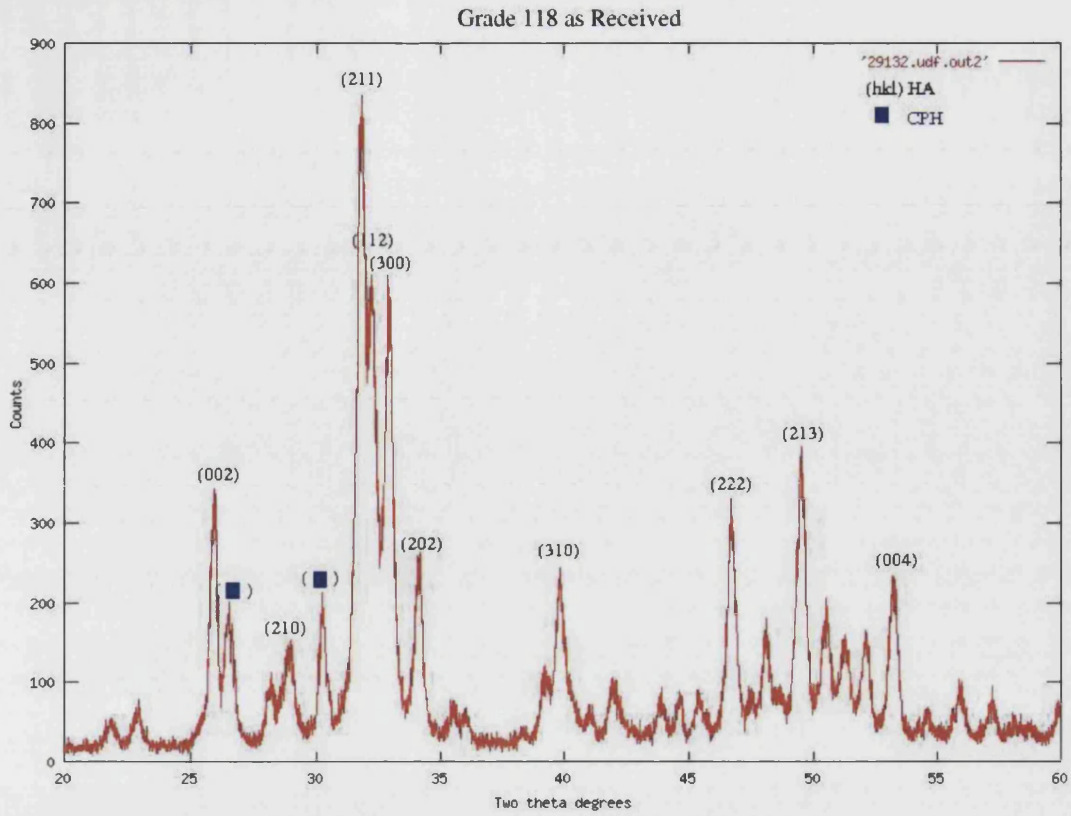

Figure 8 XRD trace for Grade 118 powder in the as-received condition.

Figure 8 shows the XRD trace for the Grade 118 material prior to any heat treatment. The trace shows a strong match for the JCPDS standard for HA (JCPDS 9-432), the main matched peaks shown with their corresponding index. In addition to the HA peaks, two further strong peaks can be seen (marked with blue) at 26.4° and 30.4°. These were identified as calcium phosphate hydrate (JCPDS 44-726), this compound was know to be unstable. Index numbers for these peaks are not given, as the standard is un-indexed. Calcium phosphate hydrate is known to be unstable and its presence in the powder was an indication that it had not undergone heat treatment.

Grade 130 as-received

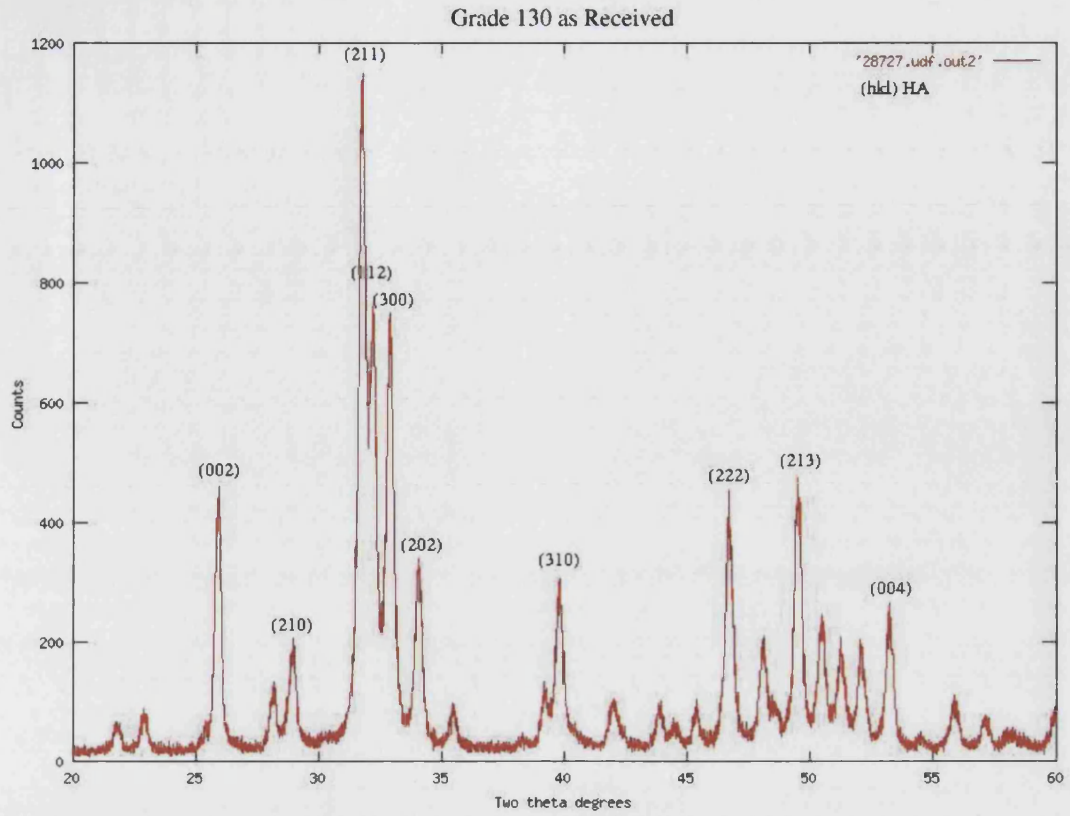

Figure 9 XRD trace for Grade 130 powder in the as-received condition.

Figure 9 shows the XRD trace for the Grade 130 powder in its as received condition. This trace shows a perfect match to the JCPDS standard for HA. Of note in this trace was the low level of background counts observed, indicative of a high degree of crystallinity.

HA reference powder supplied by Howmedica

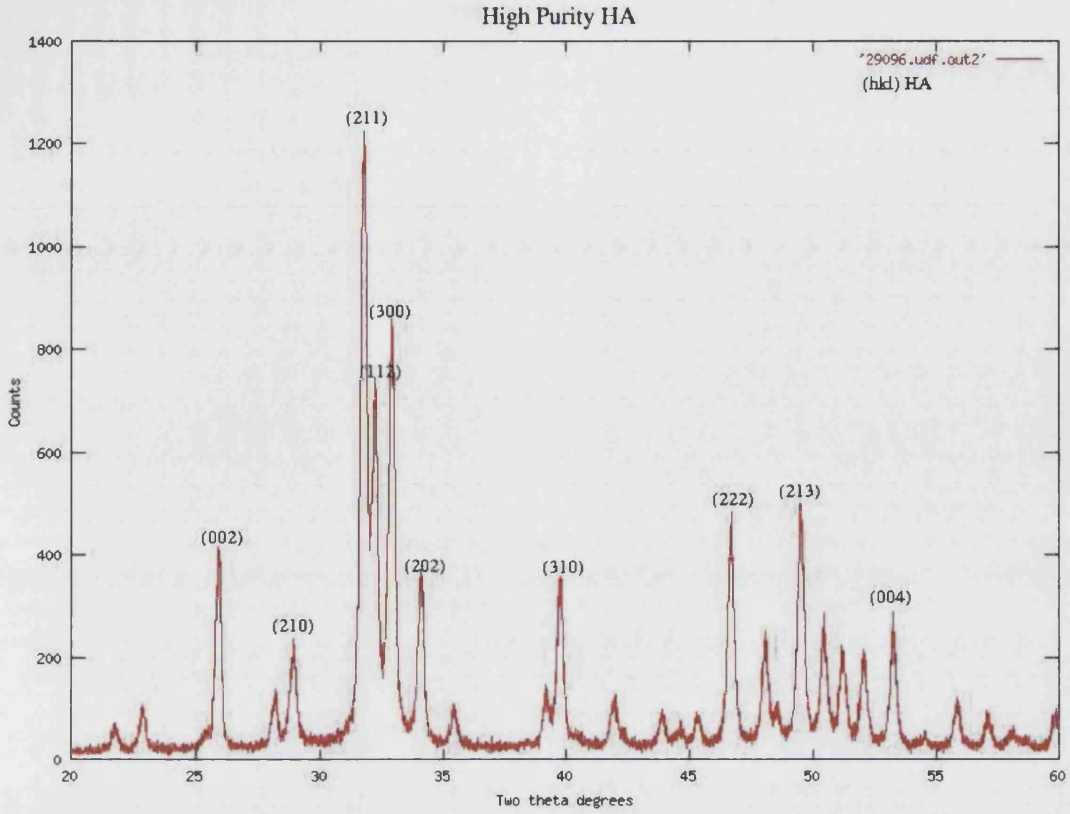

Figure 10 XRD trace for HA reference powder as-received from Howmedica.

Figure 10 shows the XRD trace for the HA powder supplied as a reference by Howmedica. This trace also matches the HA standard and can be seen to be almost identical to that of the Grade130 powder shown above.

High purity β–TCP standard

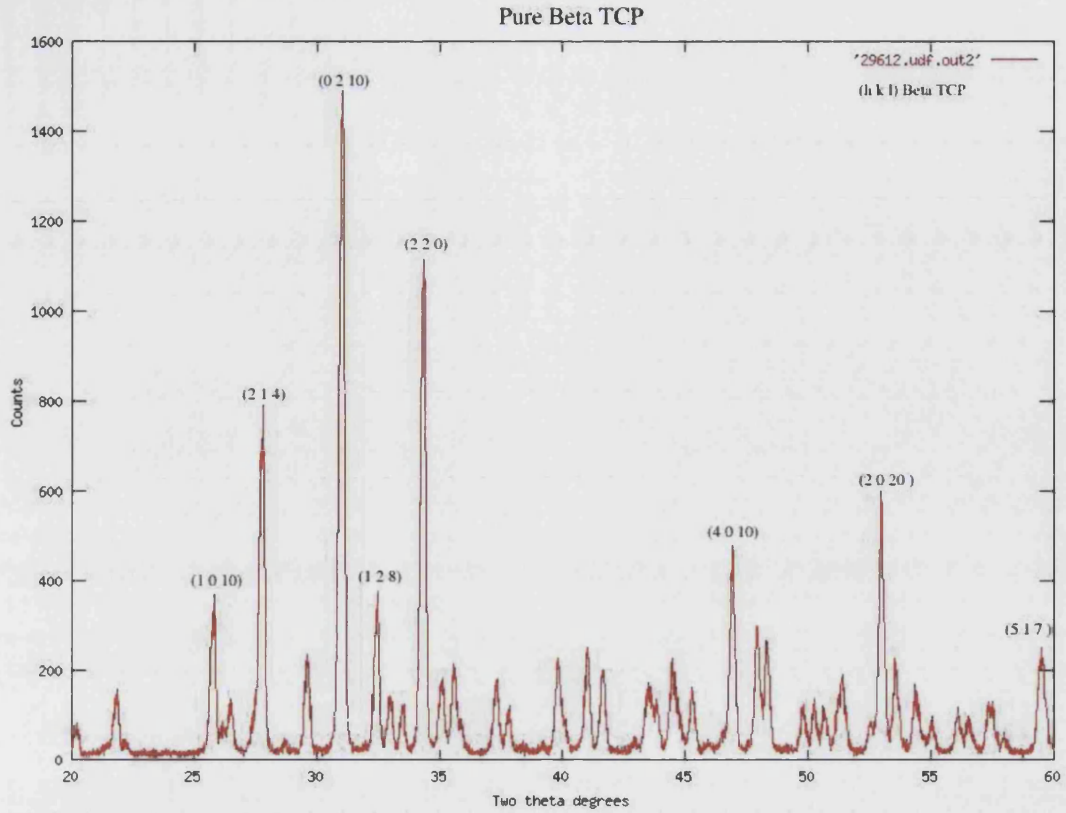

Figure 11 XRD trace of high purity β–TCP standard.

The trace for the high purity β–TCP supplied by Plasma Biotal (see Figure 11) shows a perfect match with the JCPDS standard (9-169) for β–TCP, or Whitlockite, with a low level of background noise indicating a high degree of crystallinity.

Grade 118 after heat treatment for 4 hours at 1150°C

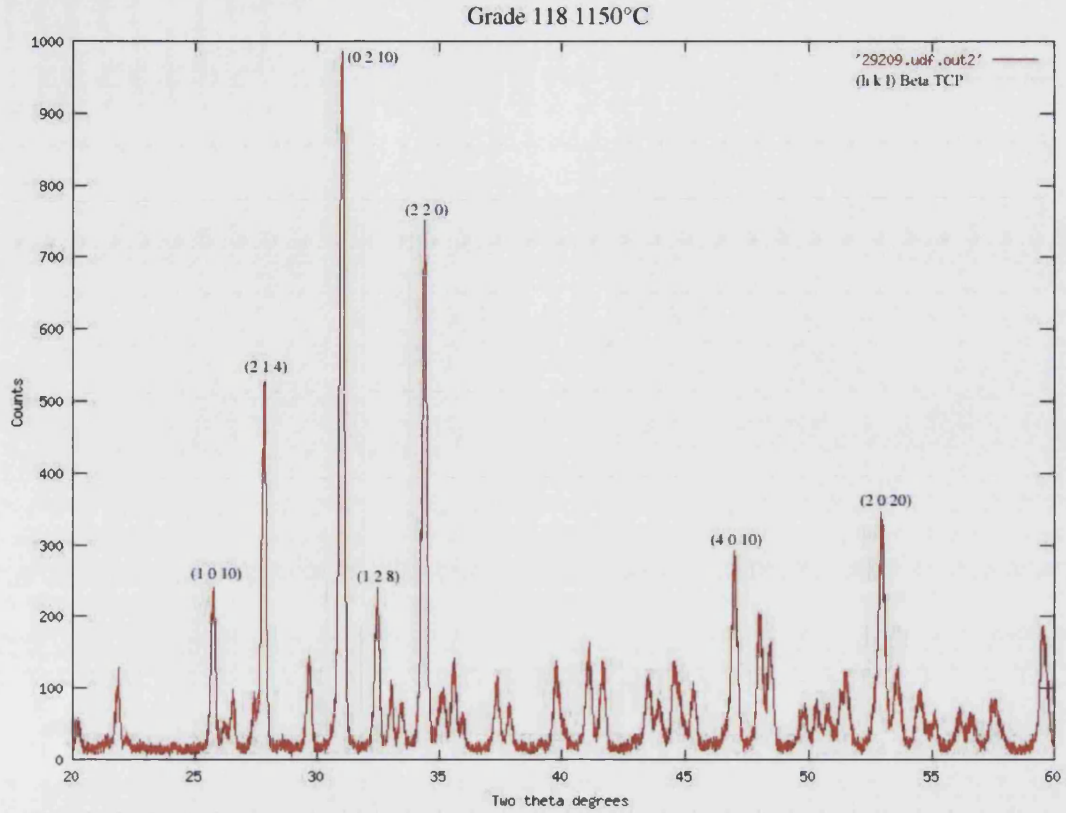

Figure 12 XRD trace of Grade 118 after 4 hours at 1150°C.

The composition of the Grade 118 material after heat treatment at 1150°C was shown to be radically different to that of the non heat-treated Grade 118. Figure 12 above shows the XRD trace obtained from the material heat-treated at 1150°C. This trace shows that all of the HA and CPH has been transformed to β–TCP by the heat treatment.

Grade 130 after heat treatment for 4 hours at 1150°C

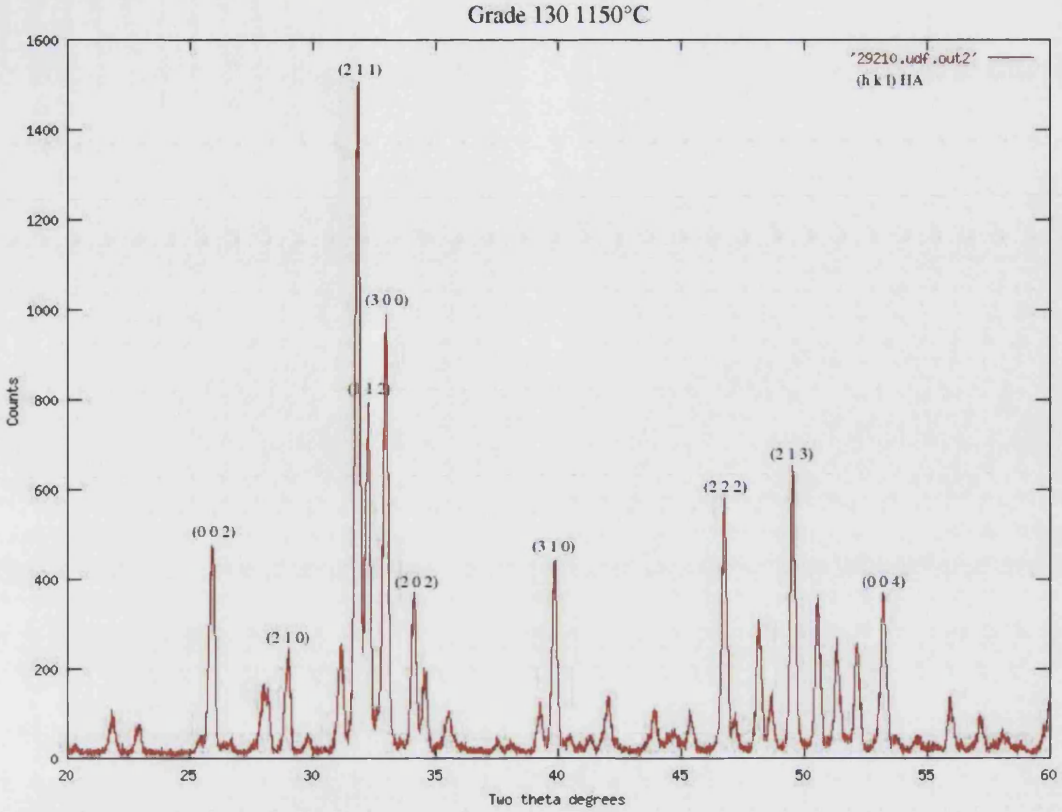

Figure 13 XRD trace of Grade 130 after 4 hours at 1150°C.

Figure 13 shows the XRD trace for the Grade 130 material after heat treatment for 4 hours at 1150°C. The trace shows an increased signal : background ratio to that of the non heat-treated Grade 130, indicating that the crystallinity of the HA has increased. It should be noted that no TCP has been formed in this powder after heat treatment at 1150°C, this is in contrast to the findings with the HA powder ex-Howmedica shown below.

HA supplied by Howmedica after heat treatment for 4 hours at 1150°C

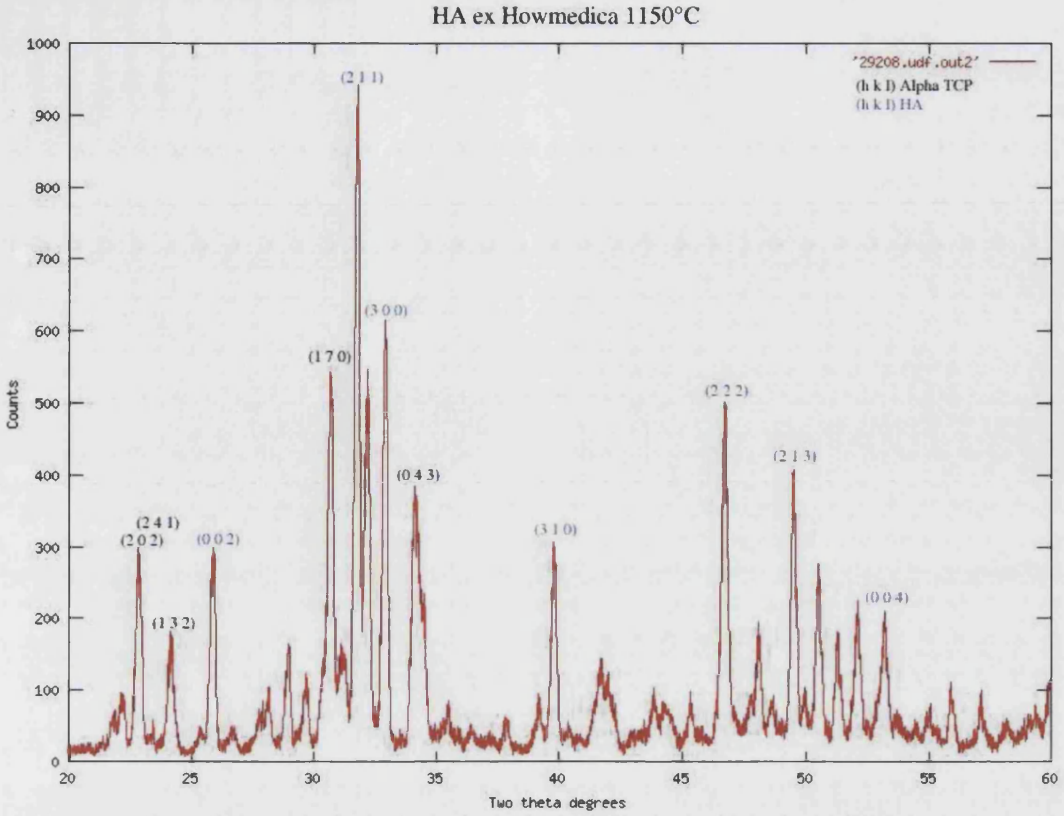

Figure 14 XRD trace of HA ex- Howmedica after 4 hours at 1150°C.

Figure 14 shows the XRD trace from the HA powder provided by Howmedica. In contrast to the Grade 130 material, heat treatment at 1150°C has caused a significant portion of HA to transform into α–TCP (indexed in black). This demonstrates a marked difference in the stability of the two powders.

Grade 118 after heat treatment for 4 hours at 1280°C

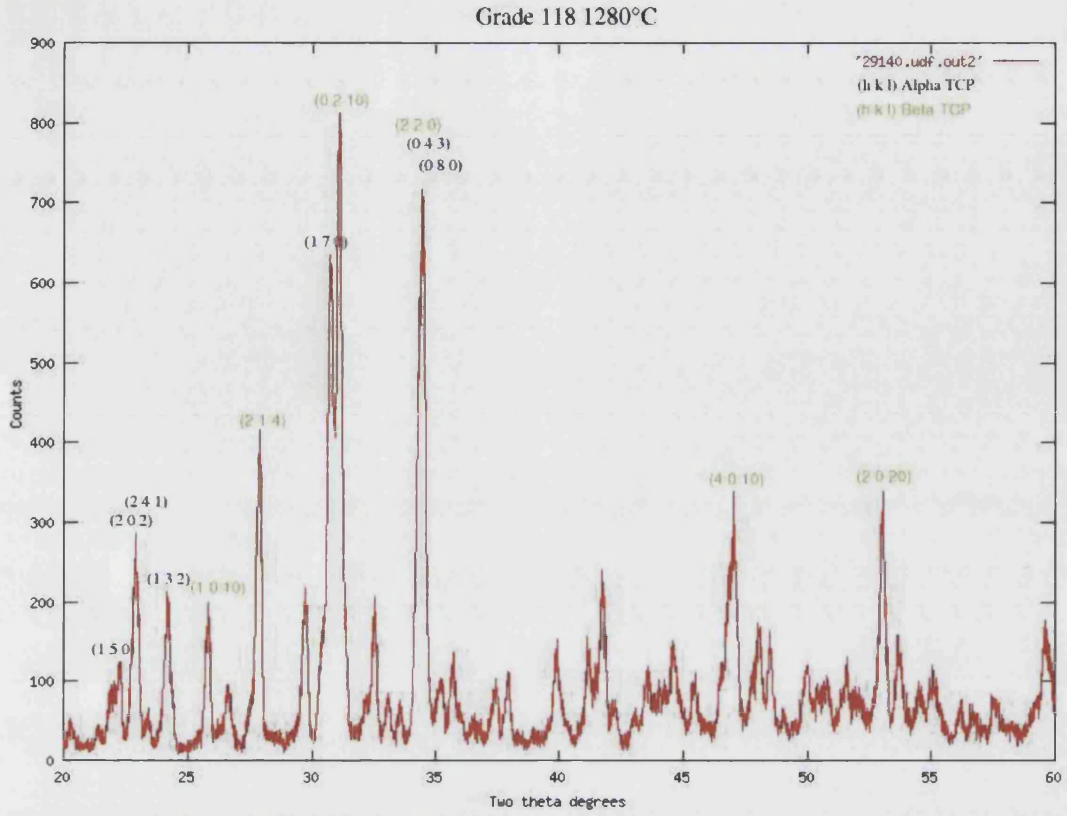

Figure 15 XRD trace of Grade 118 after 4 hours at 1280°C.

Figure 15 shows the XRD trace for the Grade 118 material after heat treatment at 1280°C for 4 hours. The β–TCP peaks found in the Grade 118 treated at 1150°C are still evident here (indexed in green). In addition to the β–TCP peaks for α–TCP were also found. In this trace the height of the α–TCP (1 3 2) peak provides a useful indication of the quantity of α–TCP present, as there was no overlap with any of the strong peaks from the β–TCP. The strength of this peak, which is a 40% intensity peak, indicates a significant quantity of β–TCP has transformed into the high temperature α form between 1150°C and 1280°C.

Results from the XRD analysis of the high purity β–TCP supplied by Plasma Biotal demonstrates that this powder also undergoes transformation from β–TCP to α–TCP between 1150°C and 1280°C.

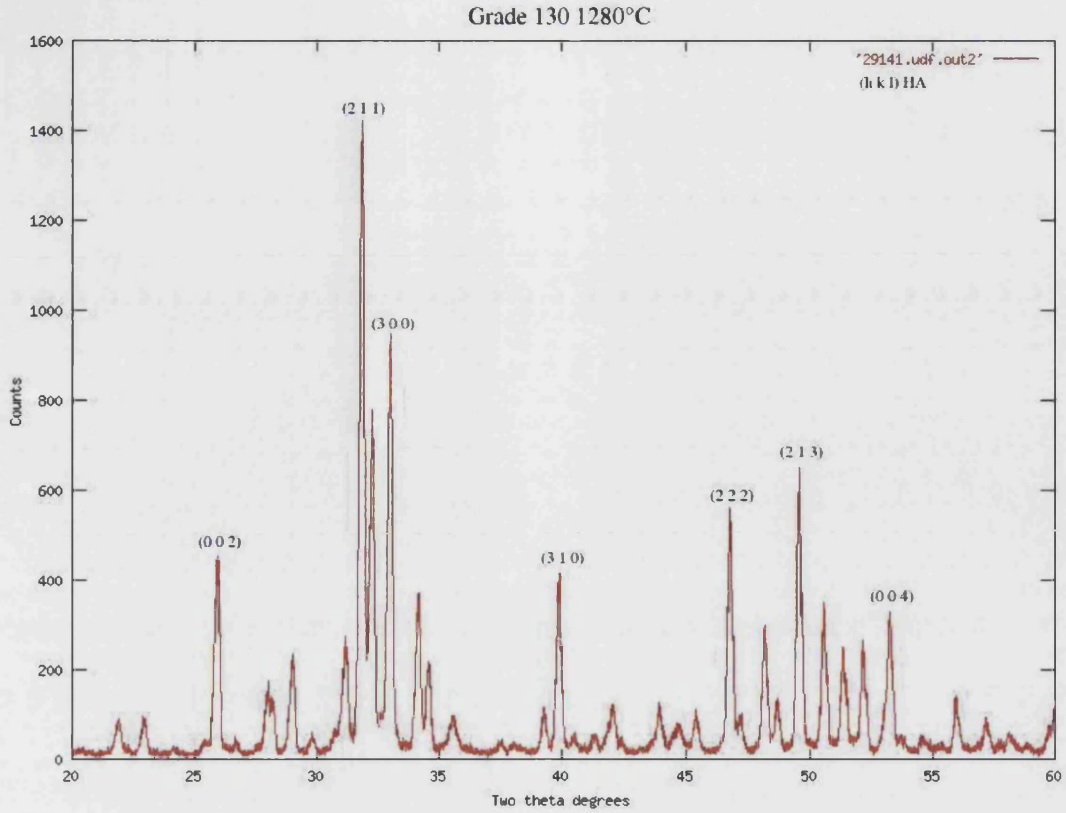

Figure 16 XRD trace of Grade 130 after 4 hours at 1280°C.

Figure 16 shows the XRD trace from the Grade 130 after heat treatment for 4 hours at 1280°C. The traces markedly similar to that of the 1150°C treated material indicating that this no compositional changes occur between these two temperatures in this material. The trace again shows a match for the JCPDS standard for HA. There are no indications of the presence on either α–TCP or β–TCP.

Quantitative Analysis

The quantification of the mass fraction of HA and β–TCP present in the sintered materials was achieved by measure of the integrated peak intensities of the relevant marker peaks for each compound. To adjust for mass adsorption effects these integrated peak intensities were normalised against a TiO_2 internal standard and calibrated using standard dilutions of β–TCP with HA.

The resultant calibration curve was then used to determine the mass fraction on these compounds in the sintered bone materials produced in the later stages of the project.

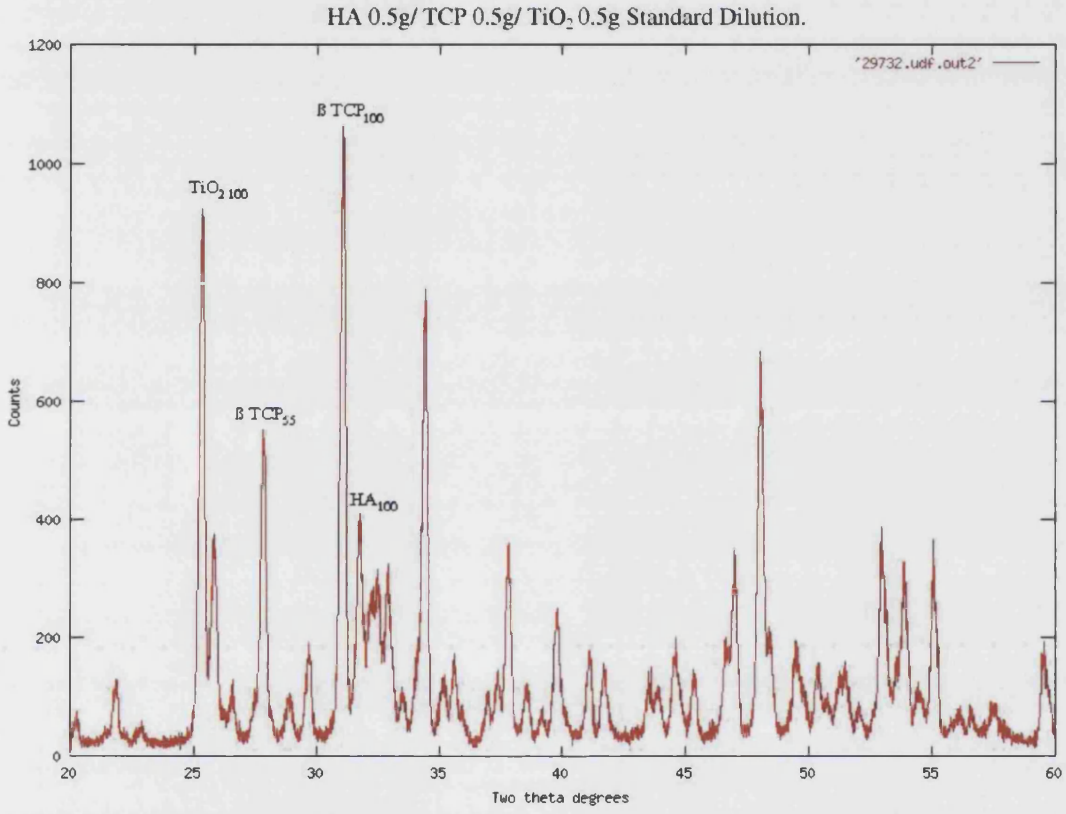

Figure 17 XRD trace of sample No.6 with marker peaks for each compound shown.

Figure 17 shows the XRD trace for sample No.6 (see below) of the calibration run with the marker peaks for HA, β–TCP and TiO_2 shown. The integrated peak intensity of these peaks was used as the measure of the compounds presence in the mixture. Peaks were chosen as markers due to their strength and clarity. In the case of the β–TCP two marker peaks, the 100% and the 55% peaks were used. These two peaks were normalised to allow a more reliable determination of peak intensity. Sample No. 6 is shown above as it was the midpoint in the standard dilutions and illustrates all points of interest.

Sample HA/TCP/ TiO_2	TiO_2 Normalised Peak Intensity	HA Normalised Peak Intensity	β–TCP Normalised Peak Intensity
No. 1 1/0/0.5	43407	40917	6355
No. 2 0.9/0.1/0.5	43737	37595	11853
No. 3 0.8/0.2/0.5	39977	30918	16618
No.4 0.7/0.3/0.5	39196	26848	20377
No. 5 0.6/0.4/0.5	27918	22068	27834
No. 6 0.5/0.5/0.5	27725	19711	32225
No. 7 0.4/0.6/0.5	25011	14813	34106
No. 8 0.3/0.7/0.5	22746	12042	39792
No. 9 0.2/0.8/0.5	19553	6295	31861
No. 10 0.1/0.9/0.5	18273	4863	35590
No.11 0/1/0.5	17581	2619	36375

Table 7 Peak intensity values for marker peaks

Table 7 shows the normalised integrated peak intensities, in terms of total counts, for HA and β–TCP in each of the standard dilutions. The internal standard response for each dilution is also shown.

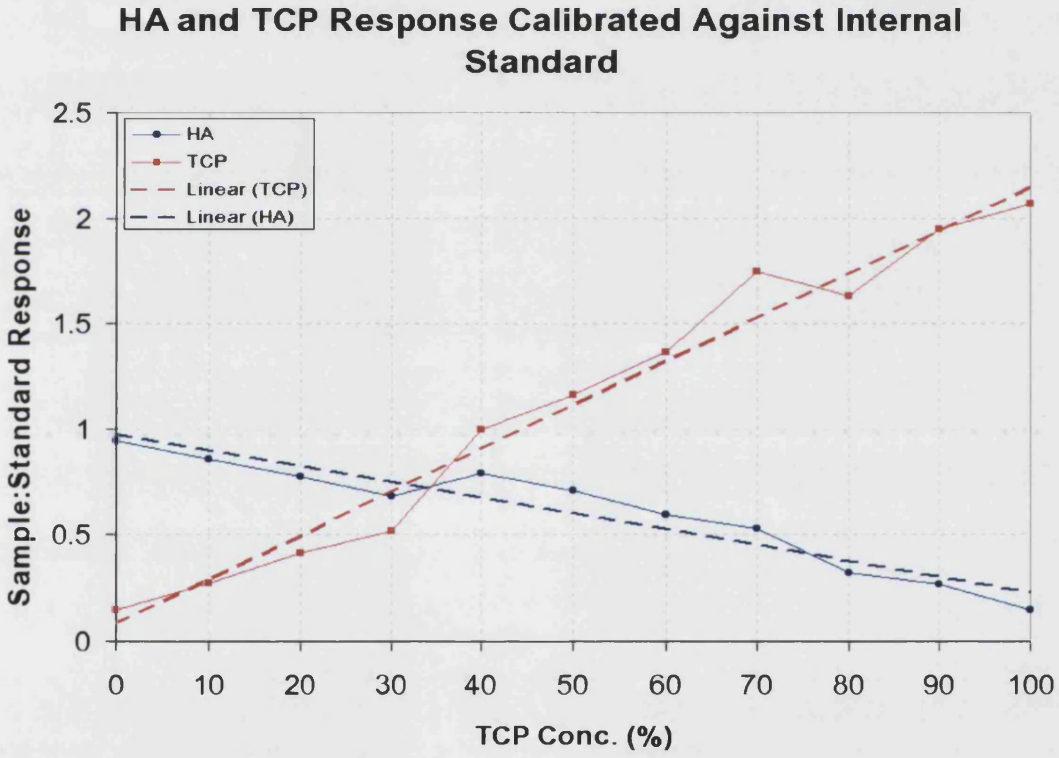

Figure 18 HA and β–TCP response in standard dilutions normalised against internal standard.

Figure 18 shows the HA and β–TCP response for each of the standard dilutions against the mass fraction of β–TCP. The response plotted here is the normalised integrated peak intensity for each compound divided by the internal standard response for that dilution. The dashed line shows the least squared liner fit to each series. From this calibration curve

the mass fraction of β–TCP and HA in an unknown mix of the components can be determined by use of the internal standard method.

Determination of HA and β–TCP concentrations in sintered products

Using the results from the calibration run (above) the phase composition of the sintered CaP ceramics produced in the later stages of the project was quantified. The composition of the slips for the bulk of the materials produced in the later stages of the work had been fixed at 50% Grade 118 and 50% Grade 130. The results of the quantitative analysis of these materials are presented below.

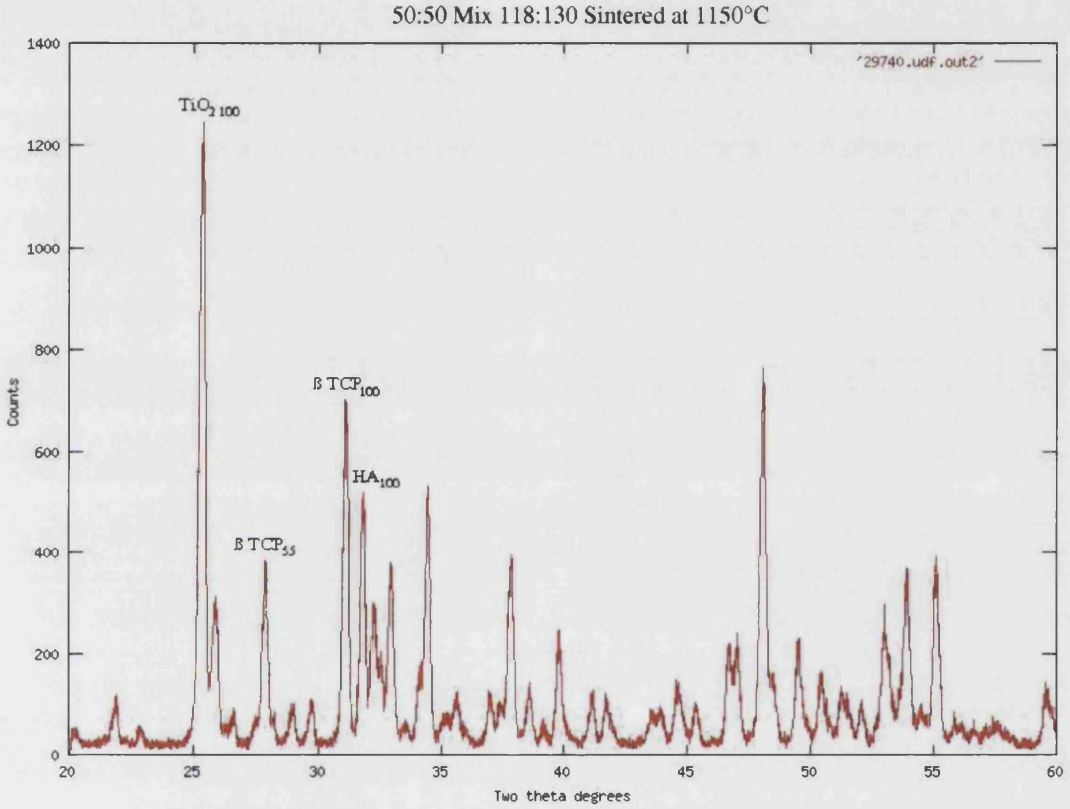

Figure 19 XRD trace from 1150°C sintered material with fixed addition of internal standard.

Figure 19 shows the XRD trace for one such sample sintered at 1150°C. A fixed addition of 0.5g of TiO_2 per 1g of sample was made to facilitate analysis by the internal standard method. The peaks of interest for HA β–TCP and TiO_2 are marked. It was noted that the response from both the HA and TCP was lower than anticipated as the qualitative analysis had suggested that the profile should have resembled that shown in Figure 17.

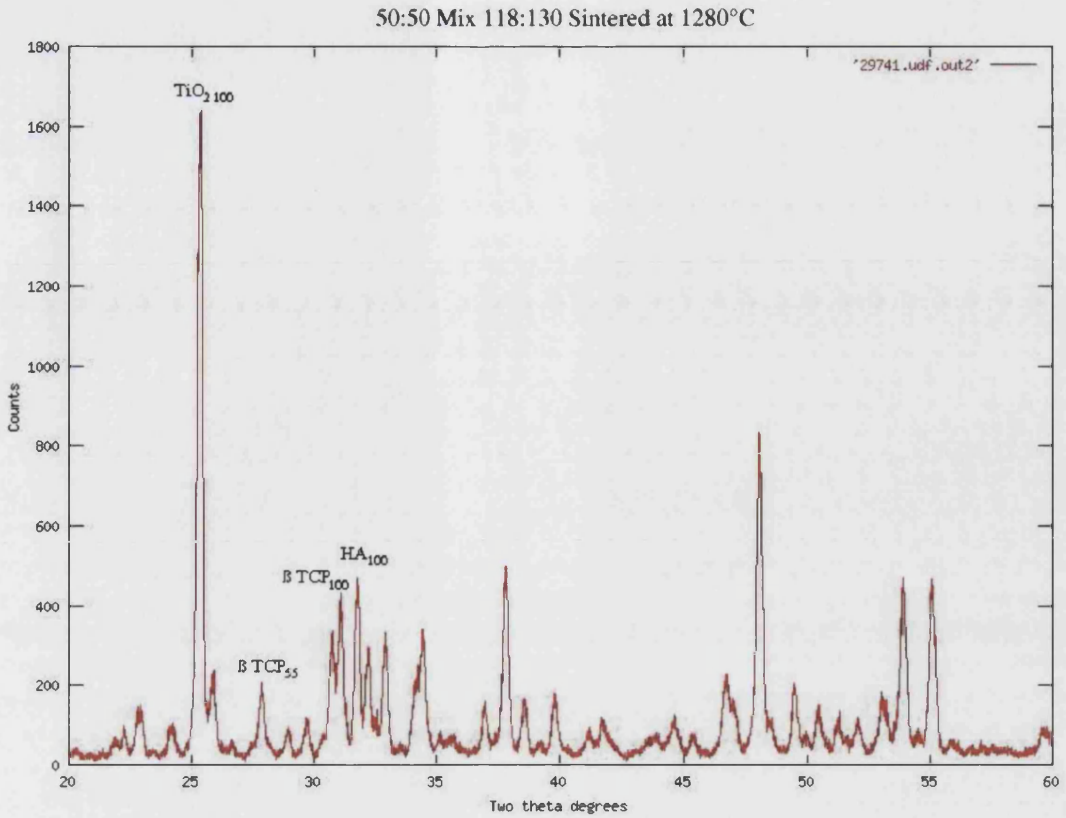

Figure 20 XRD trace from 1280°C sintered material with fixed addition of internal standard.

Figure 20 shows the XRD trace for sample sintered at 1280°C with a fixed addition of 0.5g of TiO_2 per 1g of sample. The peaks of interest for HA β–TCP and TiO_2 are marked. Again in this trace the HA and TCP response was far lower than predicted.

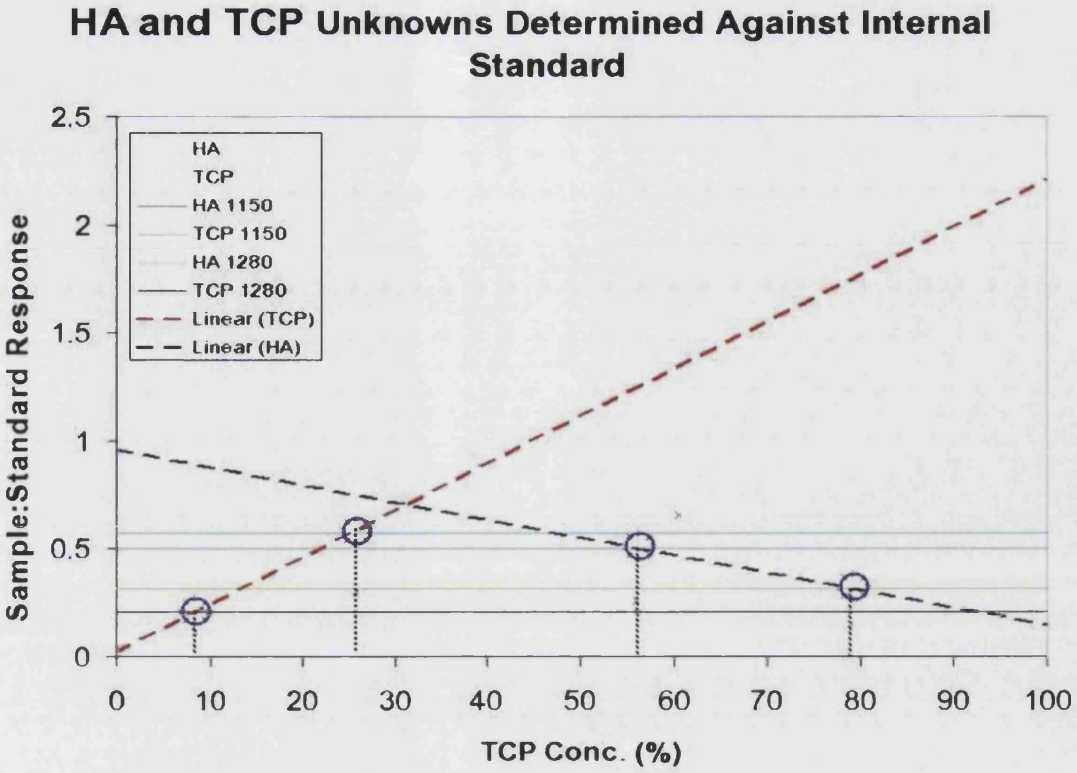

Figure 21 Peak intensities for 1150°C and 1280°C sintered material with extrapolated HA and β–TCP concentration.

Figure 21 shows the level of the integrated peak intensities for HA and β–TCP in the sample materials sintered at 1150° and 1280°C normalised against the internal standard. These levels are shown superimposed on the linear fit from the calibration run. The intersection of these levels and their respective fit line gives a graphical read off of the mass fraction of each component.

Sintering Temperature	*HA Mass Fraction*	*β–TCP*
1150°C	22%	26%
1280°C	44%	8%

Table 8 Phase composition of sintered materials as determined by internal standard method

From Table 8 it can be seen that the β–TCP and HA mass fractions in both materials are lower than the anticipated 50% HA and 50% β–TCP as would be predicted from the analysis of the input powders. The basis of the predicted composition and this anomalous result are discussed in section 3.3.

3.3 Discussion of Powder Characterisation

Results from the qualitative analysis show clearly the difference between the two main powders used, the Grade 130 and the Grade 118 materials.

The Grade 130 material was found to be a highly stable HA with a high degree of crystallinity in its received state. Thermal treatment of this material up 1280°C only had the effect of increasing the intensity of the HA peak, indicative of increased degree of crystallinity.

By contrast the Grade 118 material showed evidence of being of low stability in the as-received state. This was confirmed by the complete thermal transformation of the HA and CPH high crystallinity β–TCP. The XRD of the β–TCP thus produced showed a good match for that of the high purity β–TCP from Plasma Biotal demonstrating this thermal transformation process to be an effective method of generating high crystallinity β–TCP in the sintered material. Sintering the Grade 118 material to 1280°C resulted in the transformation of β–TCP to α–TCP. Therefore materials produced with powder blends containing the Grade 118 sintered at 1280°C will contain a significant portion of the highly soluble α–TCP.

The behaviour of the HA material provided by Howmedica was also found to be radically different to the HA Grade 130. This material was shown to not have the same stability as the Grade 130 material forming the α–TCP at temperatures as low as 1150°C. This suggests that the stoichiometry of the two HA's were subtly different.

The low response on the HA and β–TCP peaks in the samples run through quantitative analysis was anomalous as it was half that predicted by the qualitative analysis. This was initially though to be error due to a mistake in the amount of TiO_2 addition made to the unknown. However repeat analysis confirmed the result. Though the conversion of β–TCP to α–TCP would account for some of the reduced signal from the β–TCP there was no evidence that this would be sufficient to account for the missing mass fraction indicated by the quantitative analysis. This results remains inexplicable at this point.

3.4 Porosifiers Results

This section details the findings of the characterisation of the different fugitive agents used to create porosity in the sintered ceramic materials. The main aim of this characterisation was to establish the shape and size of the porosifiers so that a relationship between pore size and shape in the sintered materials and the porosifier could be established.

3.4.1 Powder Fillers for BurPS Production Method.

A number of organic filler materials in powder form were used in the production of porous ceramics by the BurPS method. Shown below are the SEM images of these powder fillers showing particle size and morphology.

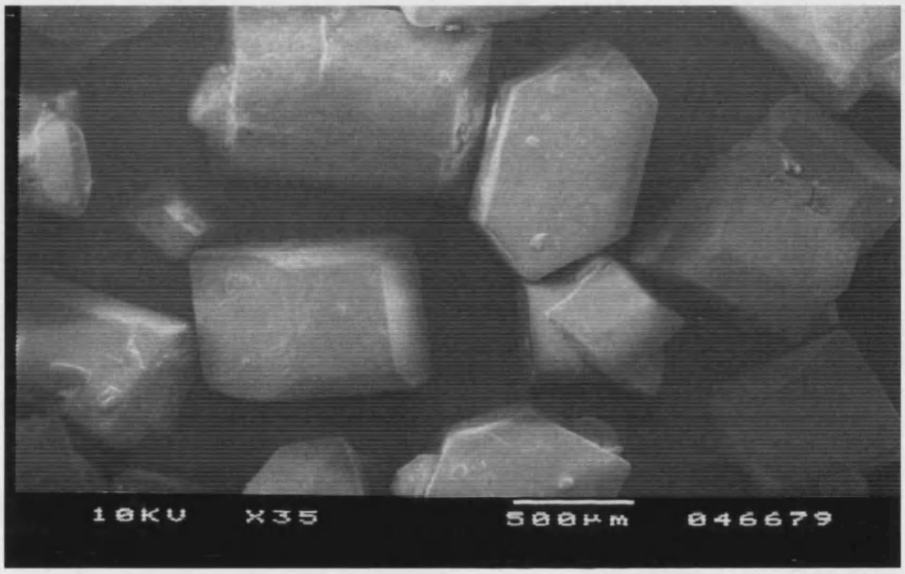

Figure 22 Low magnification SEM image of sugar granules.

Figure 22 shows an SEM image of the sugar granules typical of those used in the production of porous ceramic materials both by the conventional BurPS technique and via the processing route used by TCM . Points of note are the highly faceted particle shape and the particle size. The size of the sugar particles was found to be in the range of 200µm to 1000µm.

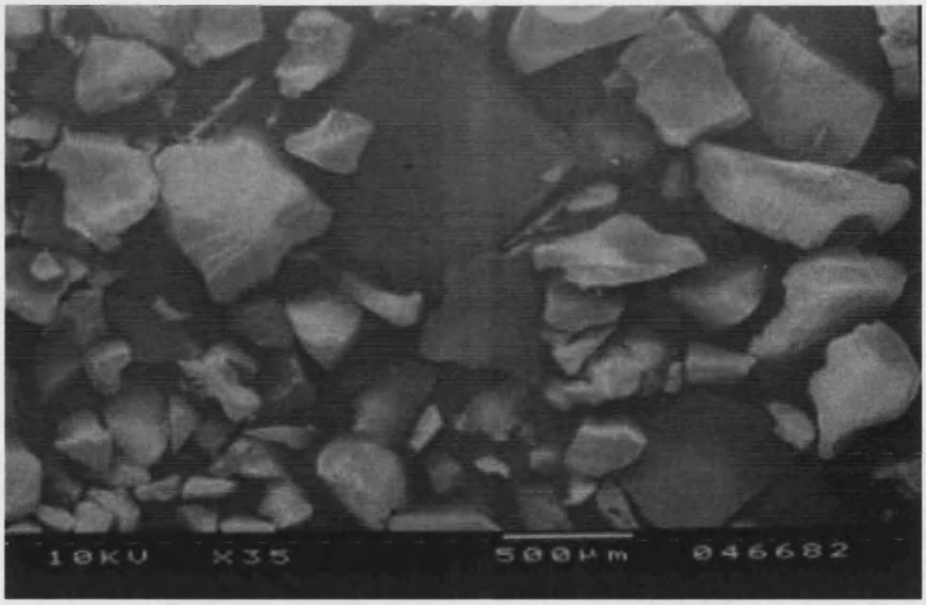

Figure 23 Low magnification SEM image polyethyleneoxide powder.

Figure 23 shows the polyethyleneoxide (PEO) powder, of note are the large distribution in the particle size and the irregular flake like morphology. Particles can be seen to range from 100µm to over 1mm across.

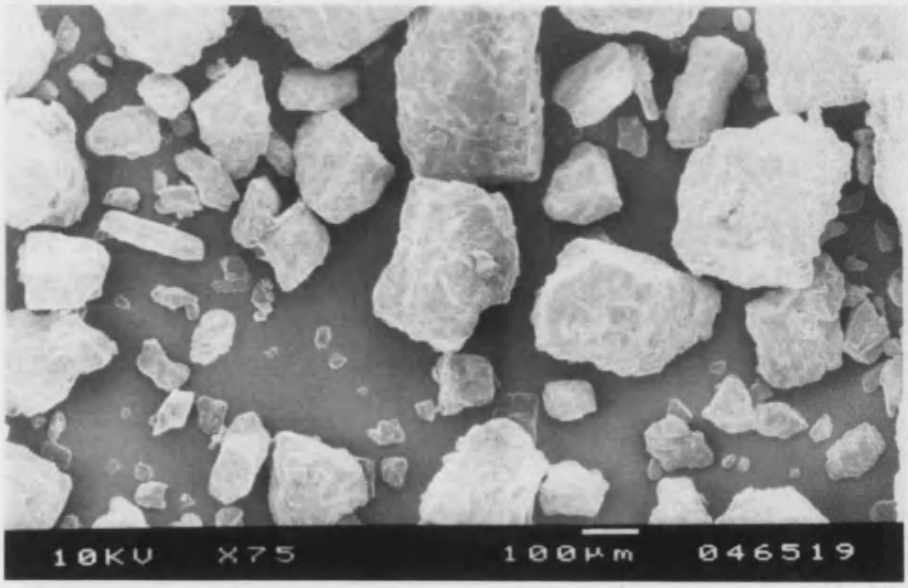

Figure 24 SEM image of polyethylene glycol powder.

Figure 24 shows the polyethylene glycol (PEG) powder particles. These were irregularly shaped and had a rough surface. Particles were seen to range from 10µm to 500µm.

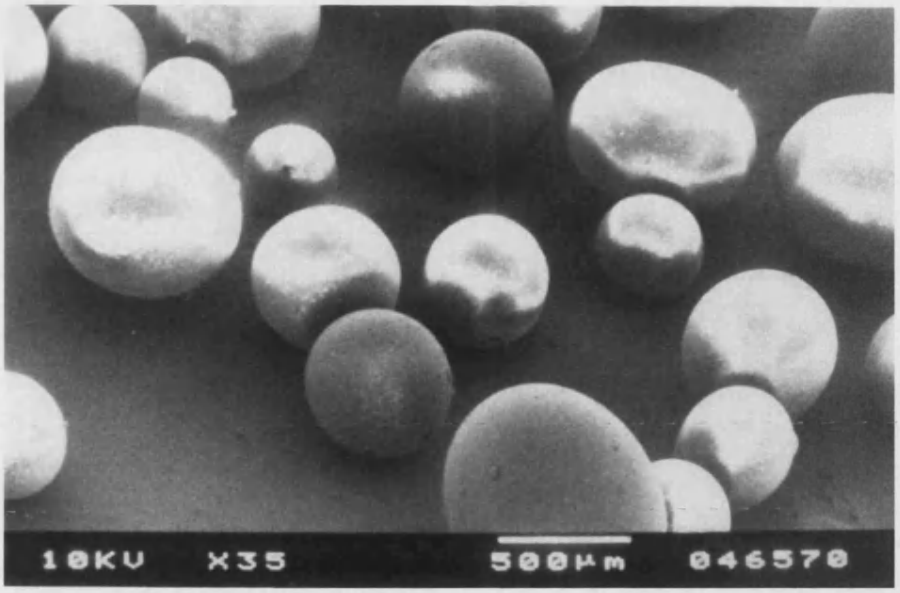

Figure 25 Low magnification SEM image of PMMA spheres.

Figure 25 shows the polymethylacrylate particles used in the production of BurPS materials. These particles were seen to be highly spherical and have a diameter in the range of 200µm to 600µm. As such they were the most uniform of the filler powders used.

3.4.2 Organic Foams.

Reticulated organic foams of various densities were used as both carriers for the ceramic slip and as porosifiers in the sintered materials. Characterisation of the structure of these foams was carried out, with particular attention being paid to the strut cross sections in the foams reticulated structure.

Macroscopic

From low magnification optical microscopy of reticulated organic foam the hexagonal foam cells and the coarse foam struts are clearly visible. Close examination of the struts revealed their concave cross-section. These shapes were found to be mirrored in the SEM of the foam cross sections and in the pore shapes of the ceramic materials produced with these foams as the main porosifer.

SEM

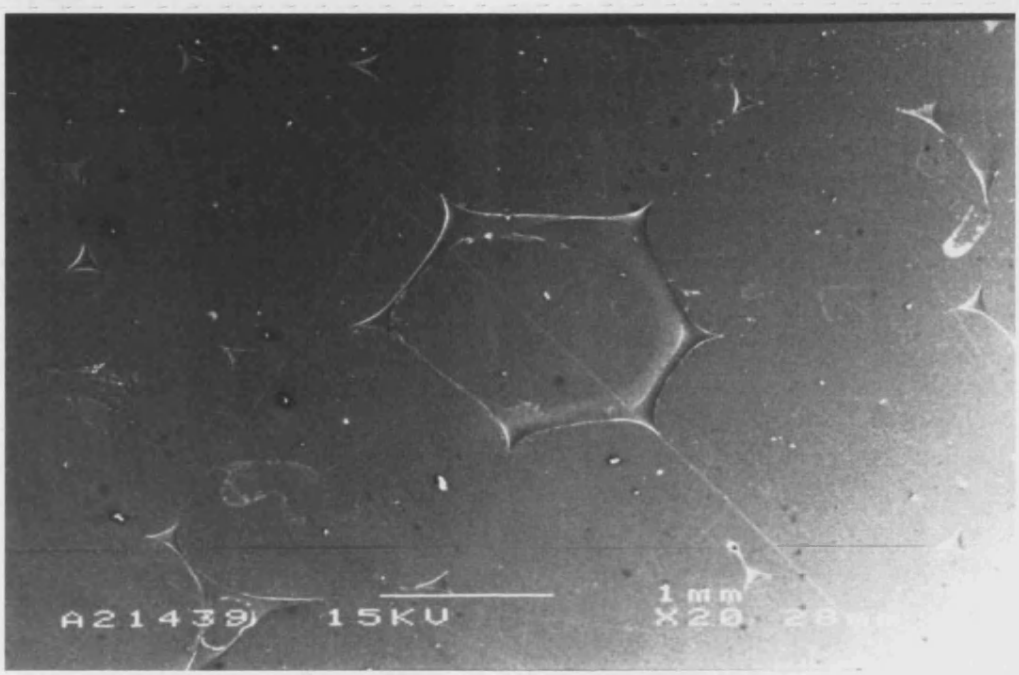

Figure 26 Cross section of foam cell showing strut shape in 30ppi foam

Figure 26 shows an SEM of mounted 30ppi foam in cross section showing a section through a foam cell. Of note were the distinctive shape of the strut cross section, this can be seen more clearly in the image below.

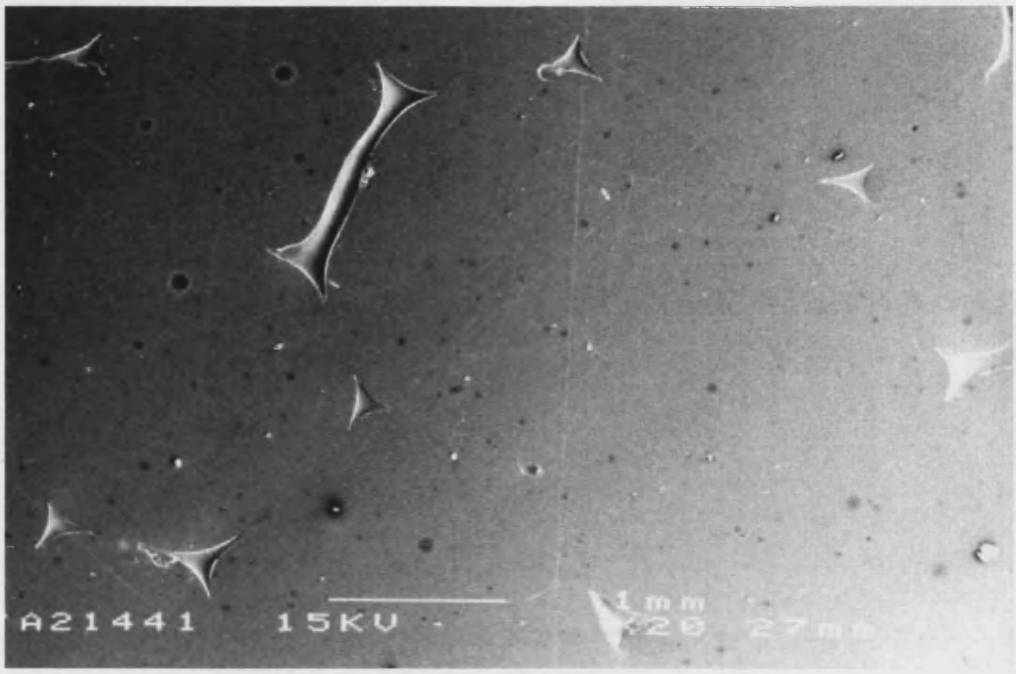

Figure 27 Typical foam strut cross section in 20ppi foam

Figure 27 shows the distinctive strut cross section found in all of the foams used. This specific example shows a typical strut in the 20ppi foam, note scale of strut to be over 1mm along its long axis.

3.5 EDAX

EDAX analysis of the foams was carried out to check for the presence of any additives that could survive the firing process to contaminate the sintered material.

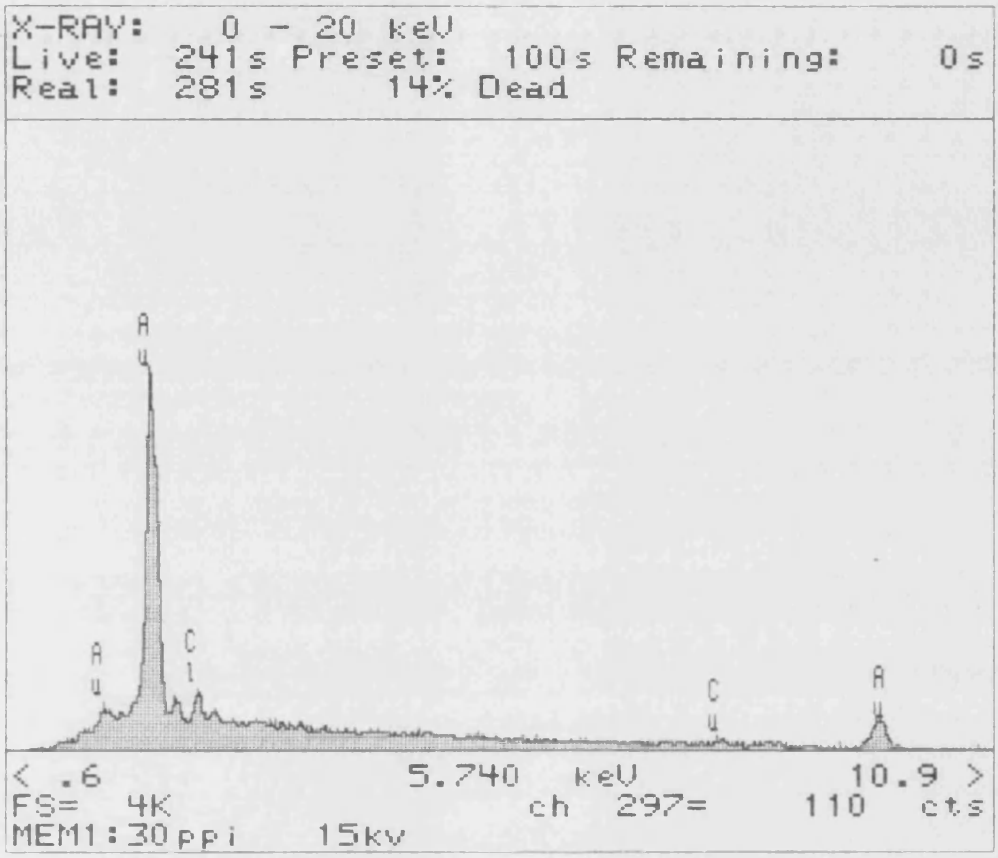

Figure 28 EDAX analysis of PU foam.

Figure 28 shows the results of the EDAX analysis of the PU foam. The important feature in this trace is the lack of aluminium and antimony peaks in the trace. The absences of these elements indicate the absence of fire retardants in the foam, eliminating the possibility of metal contamination of the sintered ceramics based on these foams. The presence of the gold and copper peaks was due to the gold plating of the samples for SEM examination.

3.6 Discussion of Organic Porosifiers Results.

The SEM images of the organic powders used in the BurPS method were shown to to differ radically in terms of scale and morphology. The particle shapes of the materials broke down into flakes, granular and spherical, with the PMMA spheres having the most uniform size and shape.

The uniform particle size and the relative hardness of the PMMA spheres raised concerns about how well this material would pack during the powder pressing stage of the BurPS process, this was later found to be a key issue with these materials.

The characterisation of the polyurethane foam showed them to have an open cell structure with hexagonal cells typical of reticulated materials. The struts forming the cell structure were shown to have a concave cross section. The mounted SEM images of the foam show these struts to produce a distinctive cross section with a bow-tie shape.

The size of these features in the coarse 20ppi and 30ppi foams was found to be in excess of 1mm along the longest axis. These structures were later found to be replicated in the large-scale porosity in the foam based ceramic materials.

3.7 Baseline Materials Results

3.7.1 Baseline materials

Materials produced in this part of the work were characterised so as to set a reference point for the further development work. Two material types were produced, high density pressed and sintered tablets and porous materials produced by the BurPS method.

Pressed Materials

High density materials were produced by uniaxial or isostatic pressing of the pure base powders and sintering to 1150°C and 1280°C.

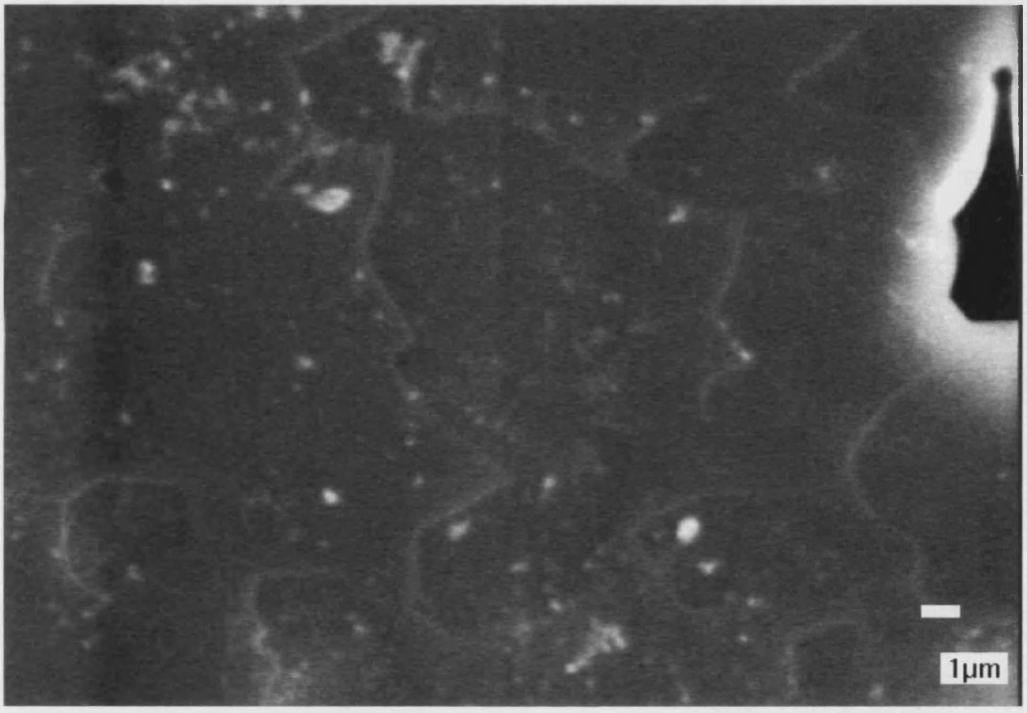

Figure 29 SEM of isostatically pressed Grade130 sintered at 1280°C.

Figure 29 shows the microstructure of material produced by isostatic pressing and sintering Grade 130 powder at 1280°C. The micrograph shows the material to be highly densified with no apparent intra-grain or inter-grain micro porosity. Grain size can be seen to range from 1µm to 6µm though grain boundaries are not distinct enough to allow accurate measurement of grain size distribution. The feature visible on the right side of this image is an example of a rare instance of voidage in this material. The microstructure of the uniaxially pressed and sintered material was found to be very similar to that of the isostatically pressed material. It was noted that the degree of shrinkage observed in the uniaxially pressed material was greater than that of the isostatically pressed material.

BurPS Materials

A range of samples were produced by the BurPS method as detailed in the materials and method section. The condition of the samples both prior to and subsequent to sintering was noted. The outcome of the sample production with the various powder:filler combinations are detailed below, with an "X" indicating that the resultant material did not remain as an intact solid or was not sufficiently robust to handle.

Filling Agent	Filling Agent(Vol%)	Pressing	Sintering
Sugar	16.7%	✓	✓
	37.5%	✓	✓
PEG	16.7%	✓	✓
	37.5%	✓	✓
	44.4%	✓	✓
PVA	16.7%	✓	✓
	28.6%	✓	X
	37.5%	✓	X
	44.4%	✓	X
PMMA	13%	✓	✓
	20%	X	X
	28.6%	X	X
	37.5%	X	X
Polyethylene Oxide	16.7%	✓	✓
	28.6%	✓	✓
	37.5%	✓	✓
	44.4%	✓	✓
	33%	✓	✓
	57%	✓	✓

Table 9 Outcome of pressing and sintering of BurPS materials

Scanning electron micrographs of materials produced from the highest successful additions of the various fillers are shown below.

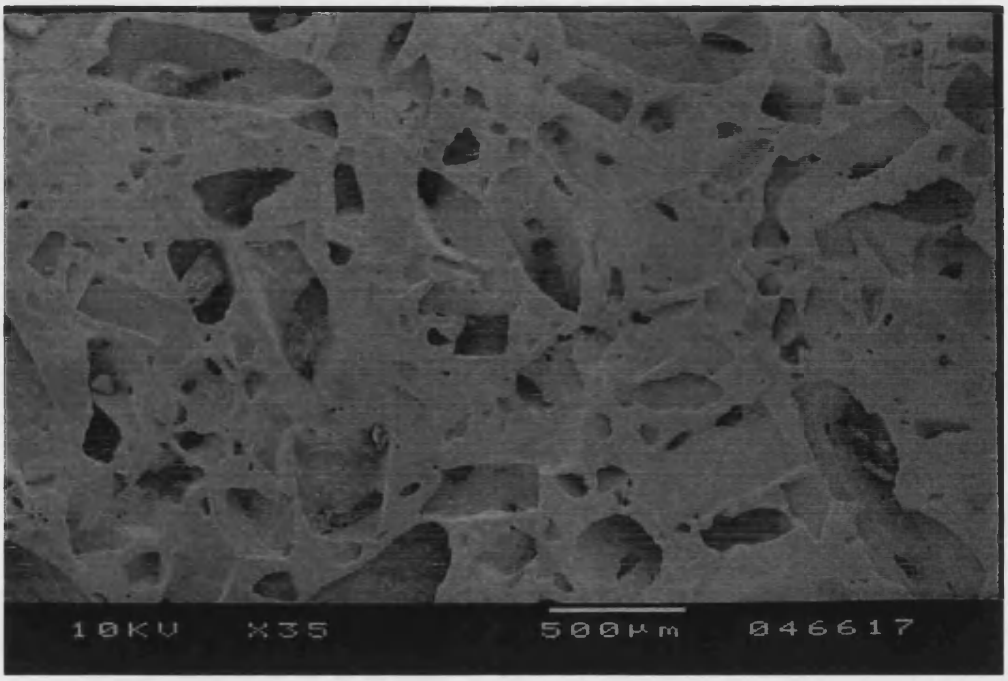

Figure 30 Material produced by BurPS method using 45% powder volume PEG filler.

Figure 30 shows the pore structure produced by BurPS method using 45% by volume addition of the PEG filler. The micrograph shows the porosity to be well dispersed through the bulk. The pore size generated can be seen to vary from less than 10µm up to 500µm. The interconnection of pores was observed in this material, due to the high pore volume.

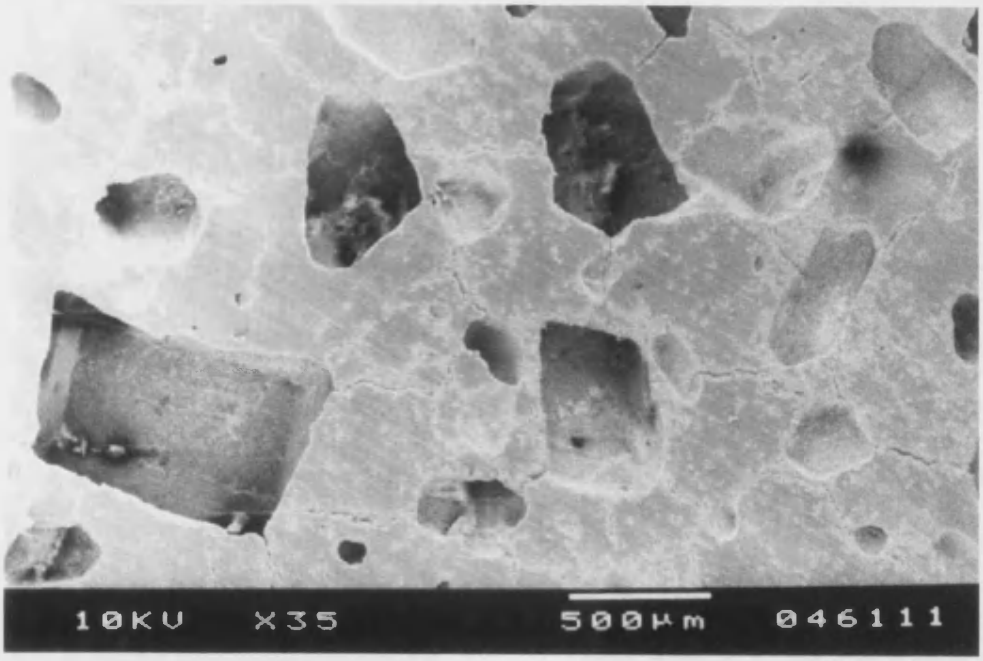

Figure 31 Material produced by BurPS method using 37.5% powder volume sugar filler.

Figure 31 shows a micrograph of the material produced with a 37.5% powder volume addition of sugar, using the BurPS method. The micrograph shows the distinctive rectangular pore cross-section produced by the burn out of the sugar. Very low levels of pore interconnection were observed in this material. Of note in the presented image are the

cracks radiating out from the corners of a number of the pores. This cracking at the pore corners was observed in all the sugar based BurPS materials. A further feature of the sugar-based materials was the uneven distribution of porosity.

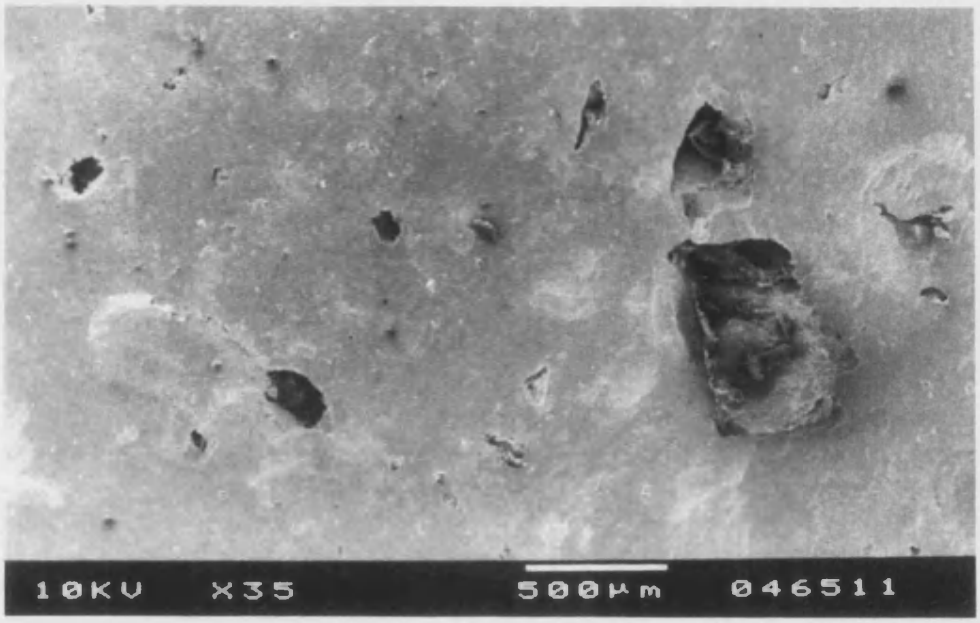

Figure 32 Material produced by BurPS method using 17% powder volume PVA filler

Figure 32 shows the porosity produced by use of BurPS method using 17% powder volume of PVA filler. Due to the low powder volume achievable with the PVA the porosity is dispersed and isolated. Though the pore size generated would appear to be in the useful size range, the low pore volume would indicate that the PVA was not a useful porosifier.

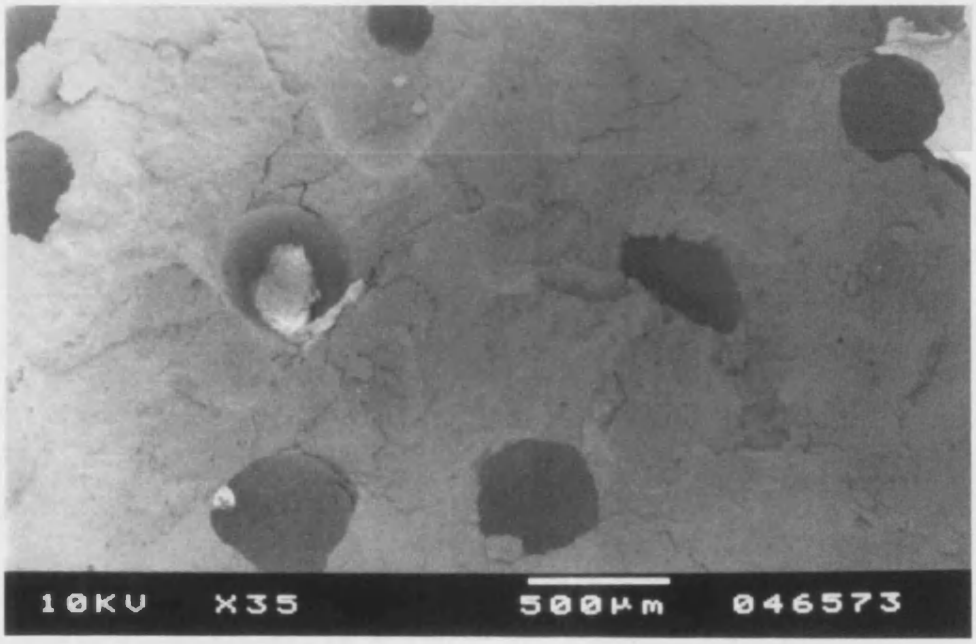

Figure 33 Material produced by BurPS method using 13% powder volume PMMA filler

Figure 33 shows the porosity produced by use of the BurPS method with the addition of 13% by volume PMMA filler. Porosity was found to be evenly dispersed throughout the bulk of the material. The pores can be seen to have a circular cross-section and a pore diameter in the range of 200μm to 500μm. The degree to which the porosity was isolated was typical of this material due to the low powder volume achievable.

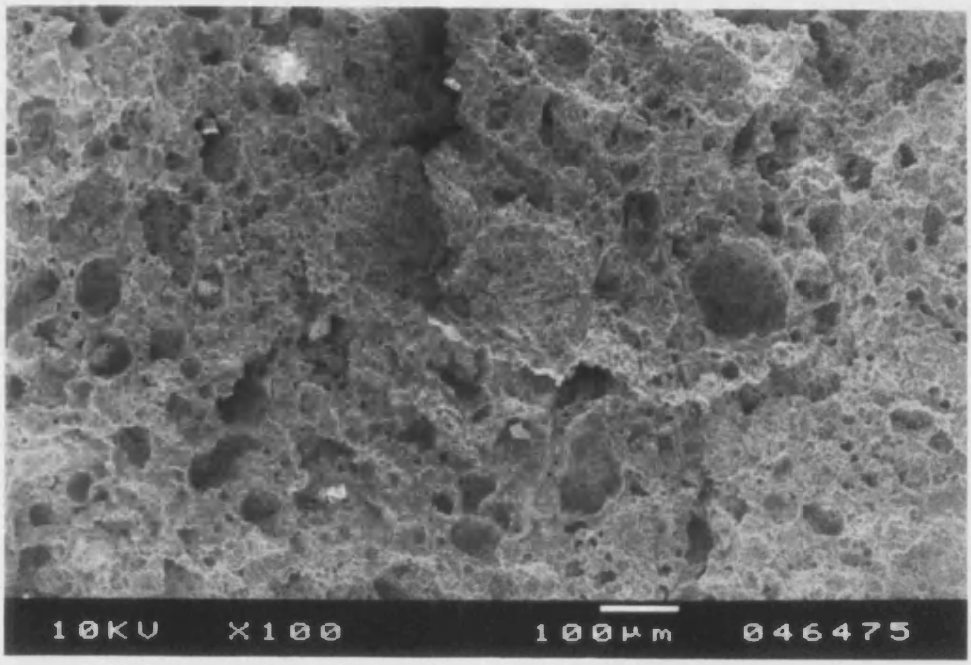

Figure 34 Material produced by BurPS method using 57% powder volume PEO filler.

Figure 34 shows the porosity produced by the BurPS method using a 57% PEO filler volume. The porosity can be seen to have a large size distribution from less than 10μm to 100μm. This porosity was found to be well distributed throughout the material. Due to the high filler volume achievable with this material a high pore volume was produced and as a result pore interconnections were found to be numerous.

Slip Characterisation.

With the exception of the BurPS materials all other processing routes used to produce porous materials in the project required the production of a ceramic slip precursor. Control of slip viscosity was a key element in the success of the impregnation methods. This was achieved by the addition of a dispersant as detailed in the materials and method section. Measurements of the effects of dispersant additions are detailed below.

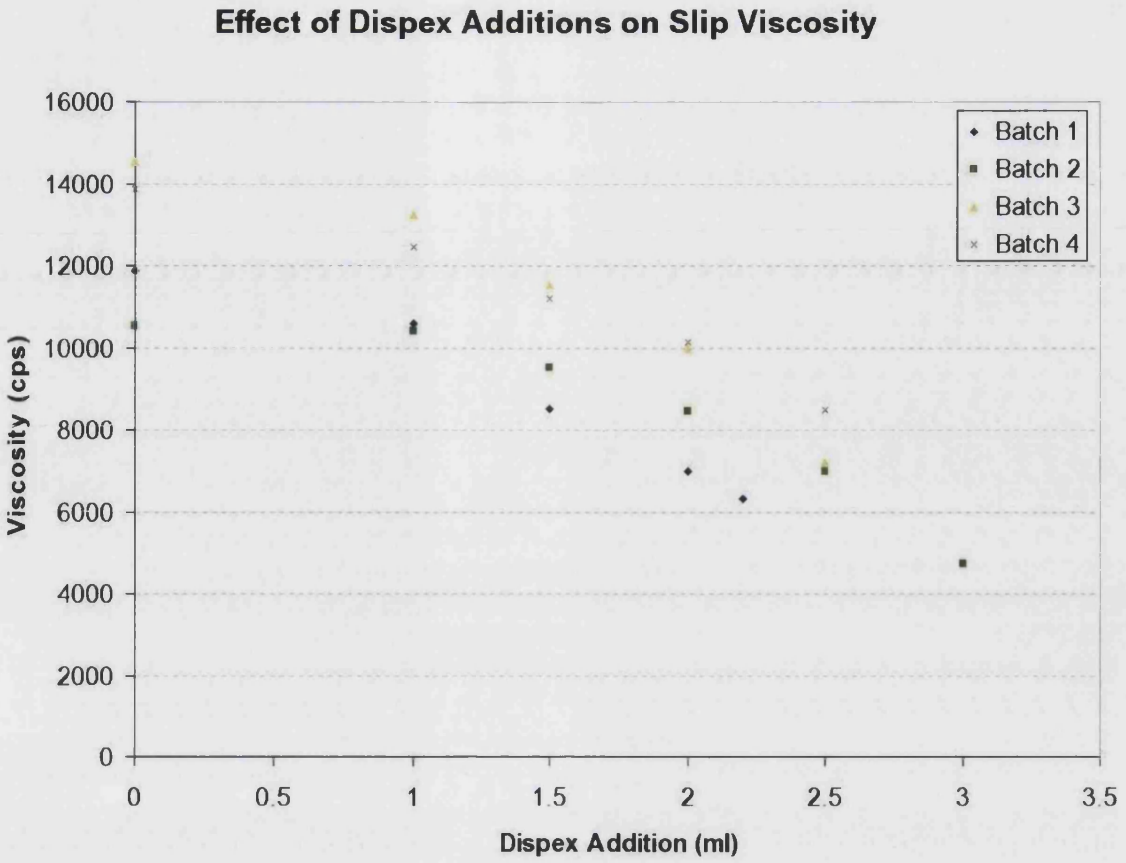

Figure 35 Shows the effect on slip viscosity of increasing additions of Dispex A40 dispersant.

Figure 35 above shows a typical dispersant vs. viscosity graph for the ceramic slips. In the diagram shown above the powder loadings in the for the slips marked Batch 1 and Batch 2 were 500g/l, the loadings for slips marked Batch 3 and Batch 4 were 600g/l. The curves shown were typical of the slips produced, with a strong linear region between 1ml and 3ml per litre addition of dispersant.

To determine the effect of the slip casting process, and dispersant addition on the microstructure of the sintered material, sintered materials were produced from a dispersed and a non-dispersed slip.

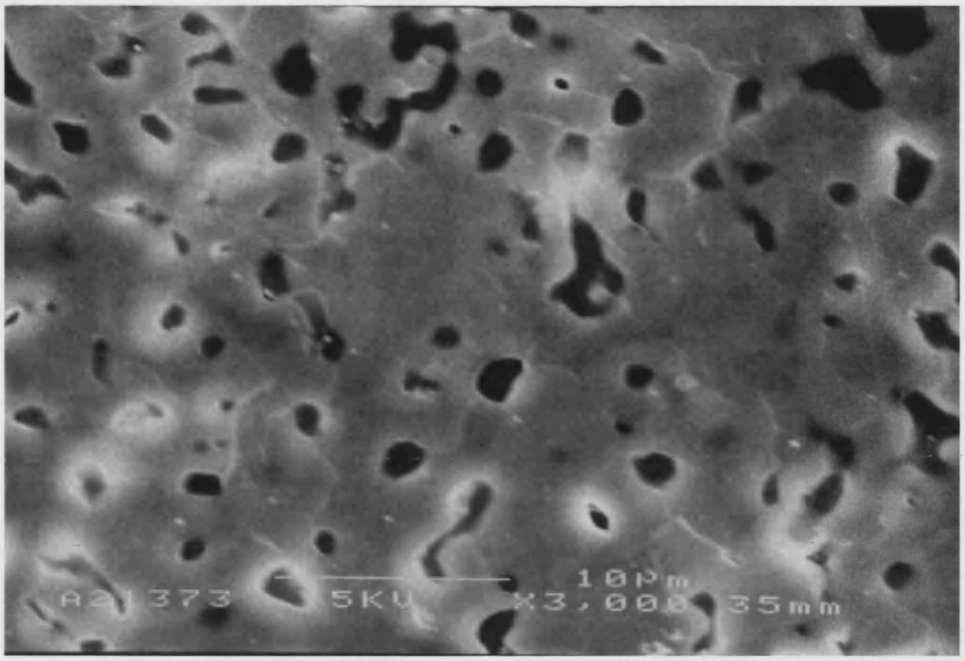

Figure 36 Slip casting based material. Non-dispersed slip, sintered at 1280°C.

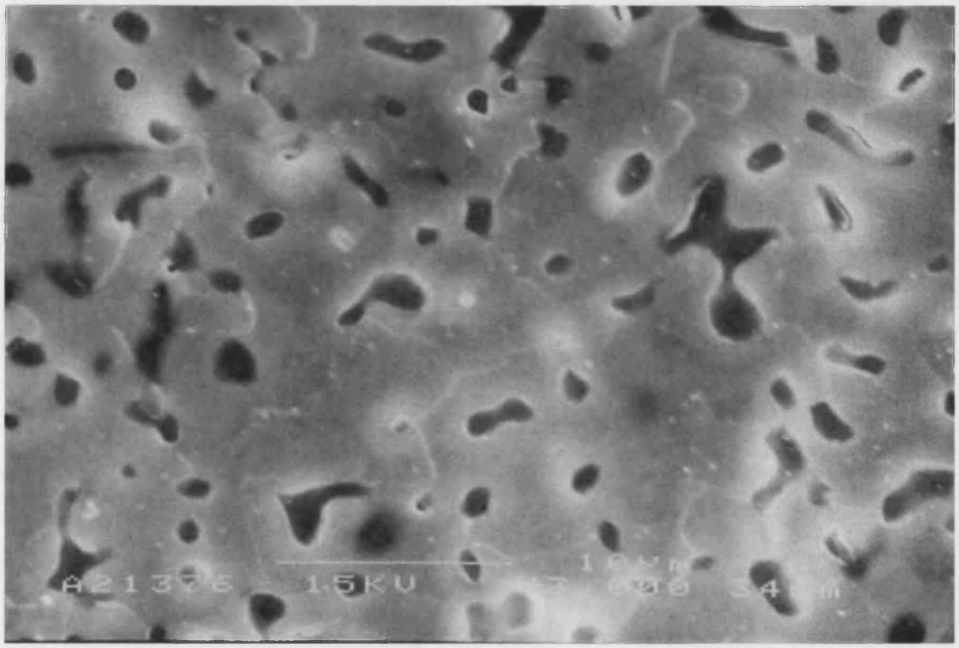

Figure 37 Slip casting based material. Dispersed slip, sintered at 1280°C.

Figure 36 and Figure 37 show the microstructure of the slip cast materials based on non-dispersed and dispersed slips respectively. The main feature of note was the high degree of micro porosity present in the materials. Grain structure can also be seen in both micrographs. The micro porosity and grain structure can be seen to be very similar in both materials, indicating the formation of this type of microstructure was not dependent on dispersant addition.

Image analysis of the micrographs of these materials yielded a pore size distribution for the microporosity in the material.

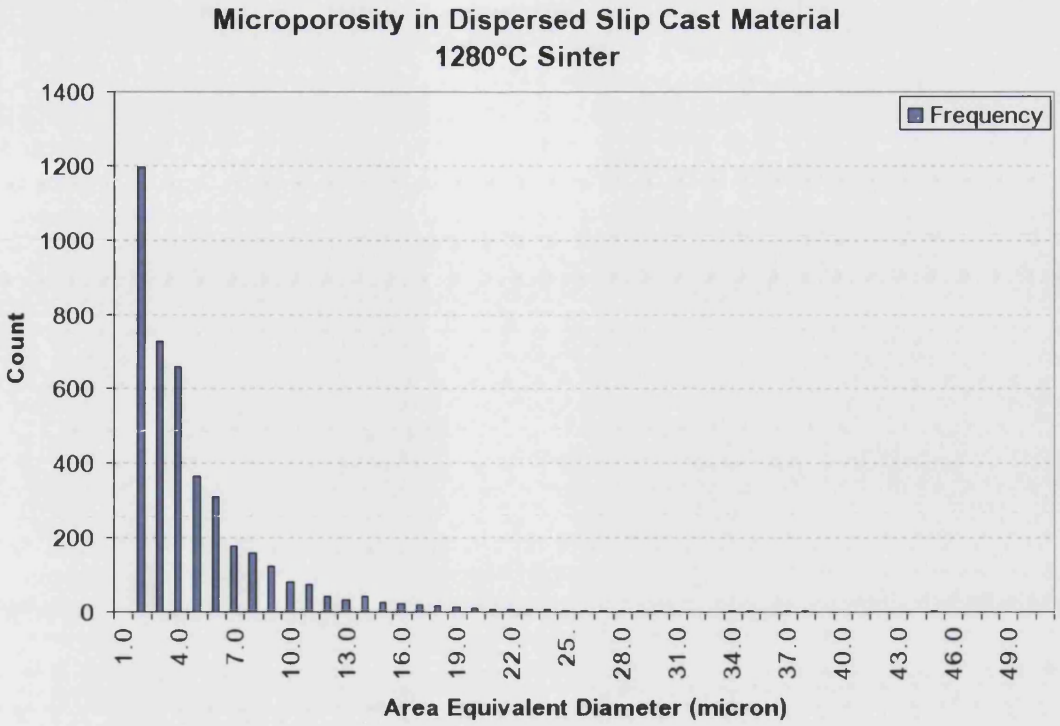

Figure 38 The pore size distribution of the porosity in the slip cast materials sintered at 1280°C

Figure 38 shows the pore size distribution for the slip cast materials sintered at 1280°C. From this frequency distribution it can be seen that the majority of the porosity is in the 1μm to 4μm range, though a significant number of pores are in excess of 10μm in their equivalent diameter.

3.8 Discussion of Baseline Materials Results.

The results from the baseline material characterisation established a starting point against which the development of the new materials was measured. The immediate usefulness of the exercise was demonstrated by the finding of marked differences between the micro structure of the high density pressed material and that produced by the slip casting route. In the pressed materials the grain size was found to be much larger than that of the slip cast material. However far more striking, and ultimately more significant , was the high level of micro porosity found in the slip cast material as compared with the almost complete absence of micro porosity in the pressed material. The presence of this micro porosity in the slip cast material was found not to be dependent on the addition of dispersant but rather that it was caused by the slip casting process itself. The presence of such high levels of microporosity may have important ramifications on the biocompatibility of the material and for its potential use as a drug delivery system, as discussed later.

The production of materials by the BurPS method was carried out to establish the limitations of this technique for the production of porous biomaterials. The results demonstrated that the production of interconnected porosity in the required size range by this method was difficult to achieve.

The high levels of filler loading required to generate interconnecting porosity precluded the use of the larger and more uniform PMMA filler as the packing density required to produce a viable green body could not be achieved. In the materials where high filler volume, and thus interconnected porosity, was achieved the resultant sintered material was delicate and unsuitable for machining or placement in a load bearing application.

The distribution of the porosity throughout the bulk of the material was also found to be variable as the large difference in both the size and density of the ceramic powder and organic filler allowed separation on settling. This problem was exacerbated in the sugar filled material by the tendency for the sugar granules to stick together, causing distinct areas of high porosity to form.

3.9 Foam Based Processing Routes Results

3.9.1 Coated Foams

Initial work with the production of porous materials based on PU foams used a slip coating technique. These efforts met with limited success as sample size was limited to small artifacts. Poor control of the slip distribution and difficulties in drying the materials without the production of widespread cracking meant that only samples produced with high coating levels based on the 45ppi foams survived drying and sintering intact.

SEM

Scanning electron micrographs were taken of fracture surfaces of the samples produced by the coated foam method. The samples shown were those produced using high slip coating levels on the 45ppi foam structures as all other materials produced were fragile to the point of being difficult to mount for SEM.

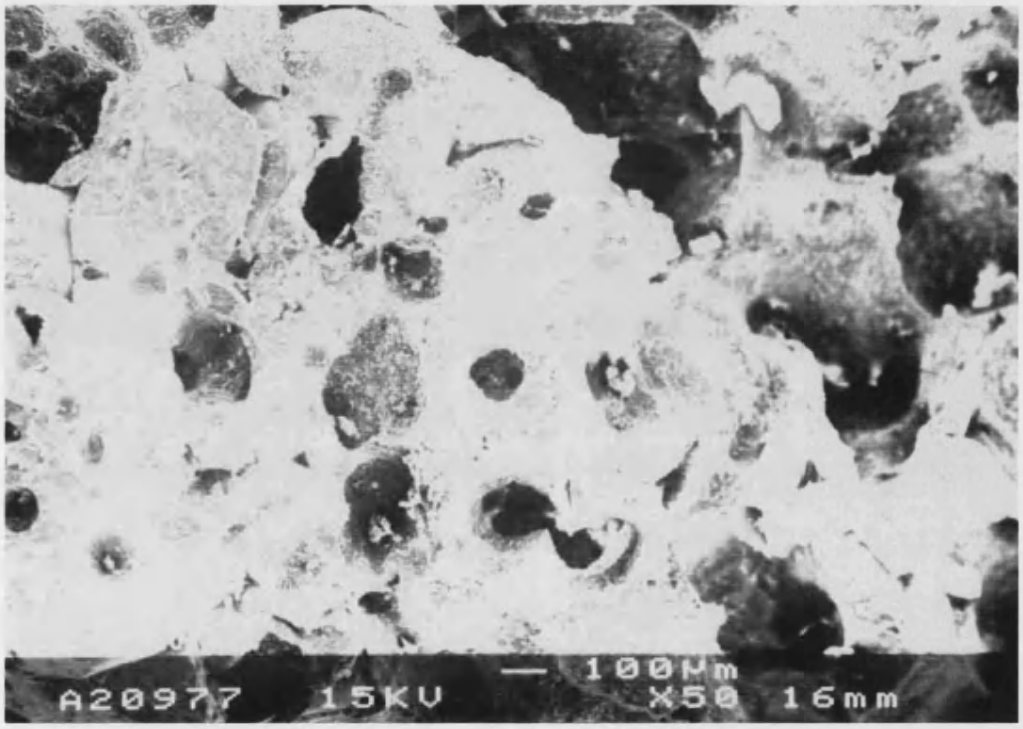

Figure 39 Material produced by coated method based on 45ppi 800g/l non-dispersed slip.

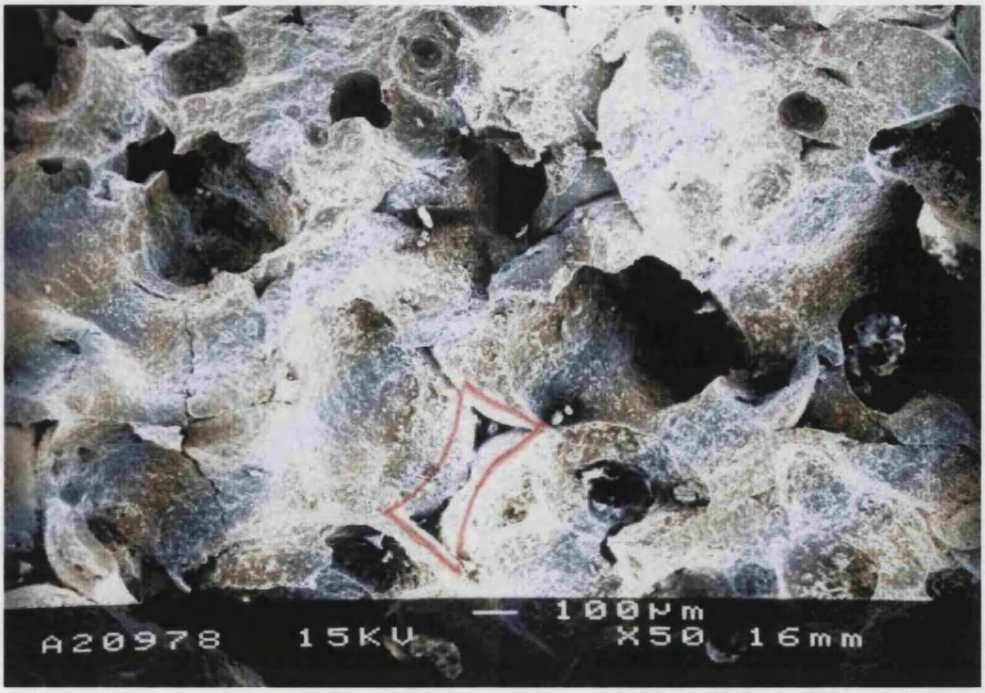

Figure 40 Material produced by coated method based on 45ppi 800g/l non-dispersed slip.

Figure 39 and Figure 40 show the pore structures observed at these fracture surfaces. The channels left as the slip was drained or blown out of the foam support dominate the pore structure . These channels were found to be highly interconnected and have a diameter of between 50µm-200µm. The presence of large voids in the structures was also common.

Further features of note in the image are the "bow-tie " found, an example can be seen in the bottom centre of Figure 40. This pore shape was found to be typical of foam strut burn-out.

3.9.2 Impact Impregnated Foams

Macroscopic

Initial work with impact impregnation successfully produced small artefacts with evenly distributed porosity using a non-dispersed slip. This process did not however scale well into producing larger samples.

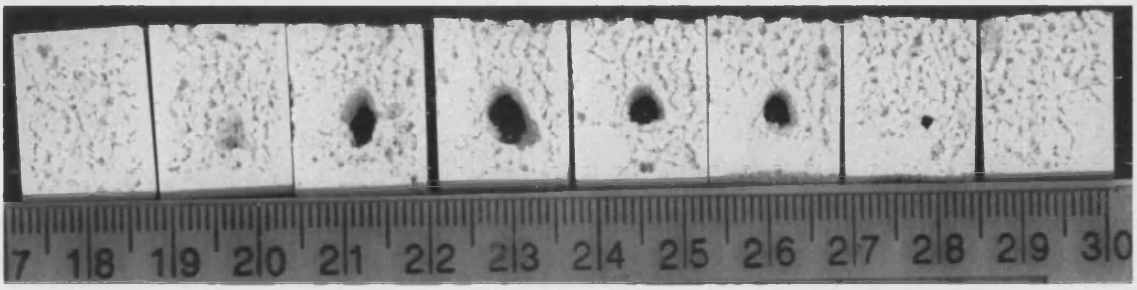

Figure 41 Coring effects due to incomplete impact impregnation using a non-dispersed slip and 45ppi foam

Figure 41 shows sections through sample produced using a 600g/l non-dispersed slip and a 45ppi foam via the impact impregnation route. This example demonstrates problems associated with production of large items using non-dispersed slips. In addition to the obvious coring effect, pore distribution through the material was not uniform with large areas of high porosity due to voidage, contrasted by areas where foam burn out was the main porosity source.

SEM

Scanning electron micrographs were taken of polished cross-sections of materials produced by impact impregnation. Images were taken of materials sintered at 1150°C and 1280°C. The images presented below are of those materials sintered at 1280°C as the quality of polish was found to be superior to that of the materials sintered at 1150°C, however the macropore structures shown below were found in both the 1280°C and 1150°C sintered materials.

30ppi base impact impregnated material

The following samples were produced with a 30ppi base foam using a dispersed slip with a powder loading of 650g/l

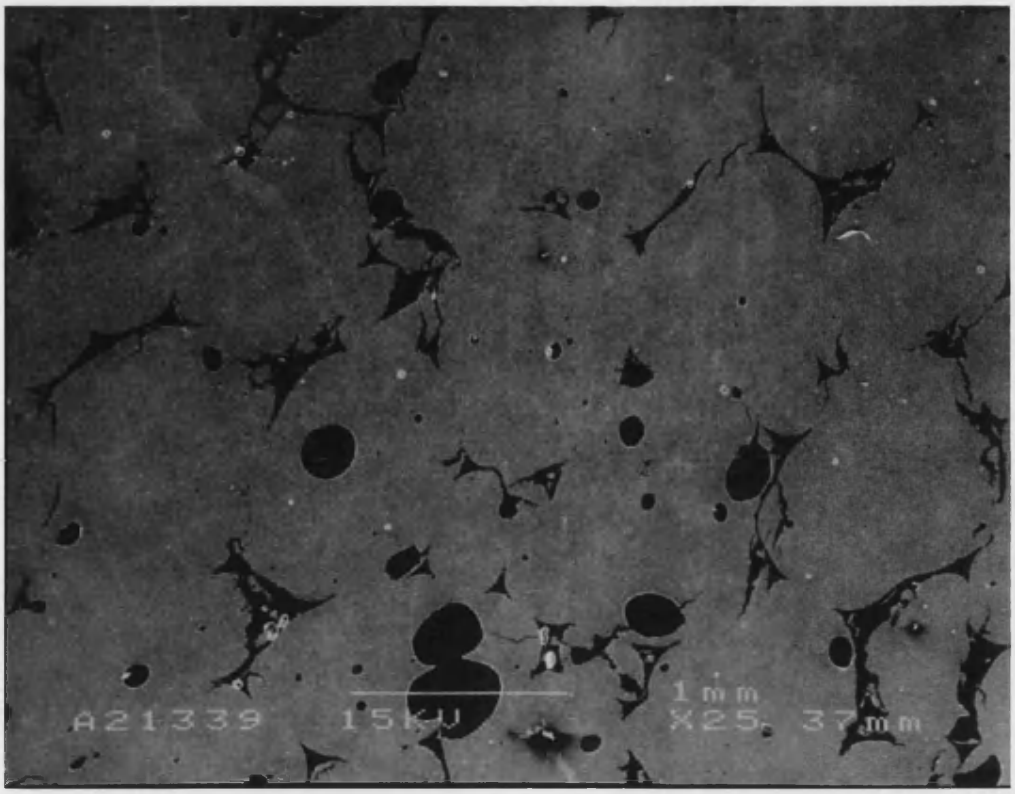

Figure 42 Pore structure in 30ppi based material produced by impact impregnation, tissue dried, sintered at 1280°C.

Figure 42 shows the pore structure of 30ppi based material produced by impact impregnation as dried on tissue. It can be seen that two distinct types of porosity exist within the material. The rounded pore cross sections that were associated with incomplete impregnation of the base foam. The distinctive bow tie shaped pore cross sections were associated with voidage created by the burn out of the struts of the base foam.

It was found that the pore structure in the mesh dried materials was dominated to a greater extent by the porosity associated with incomplete impregnation. This was common to both the 30ppi and 45ppi based materials.

45ppi based impact impregnated material

The following samples were produced with a 45ppi base foam using a dispersed slip with a powder loading of 600g/l

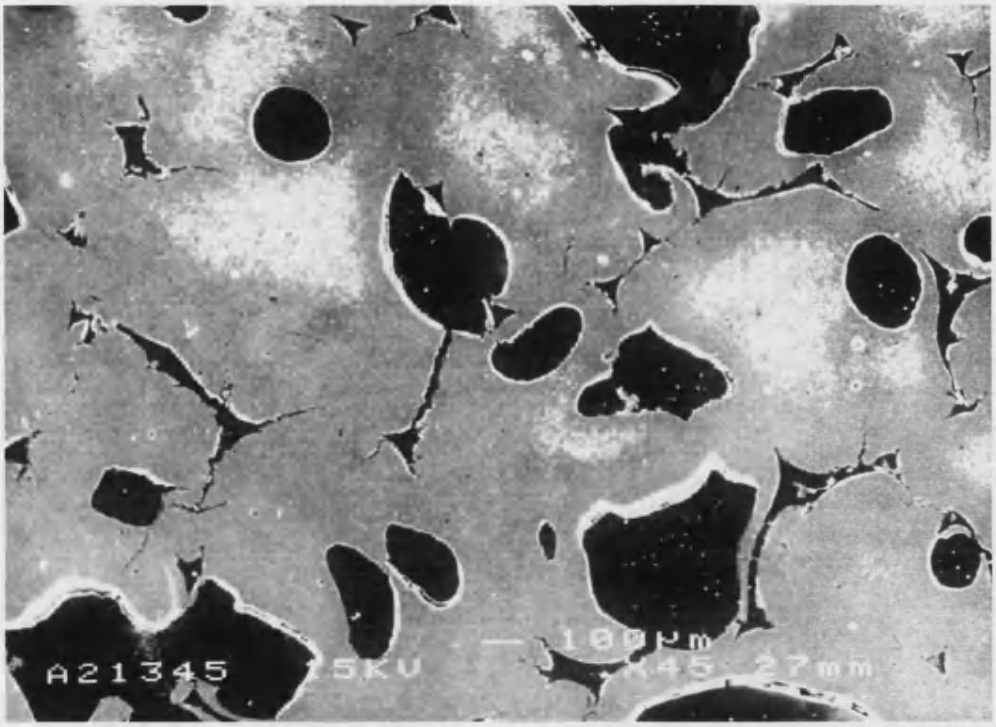

Figure 43 Pore structure in 45ppi based material produced by impact impregnation, tissue dried, sintered at 1280°C.

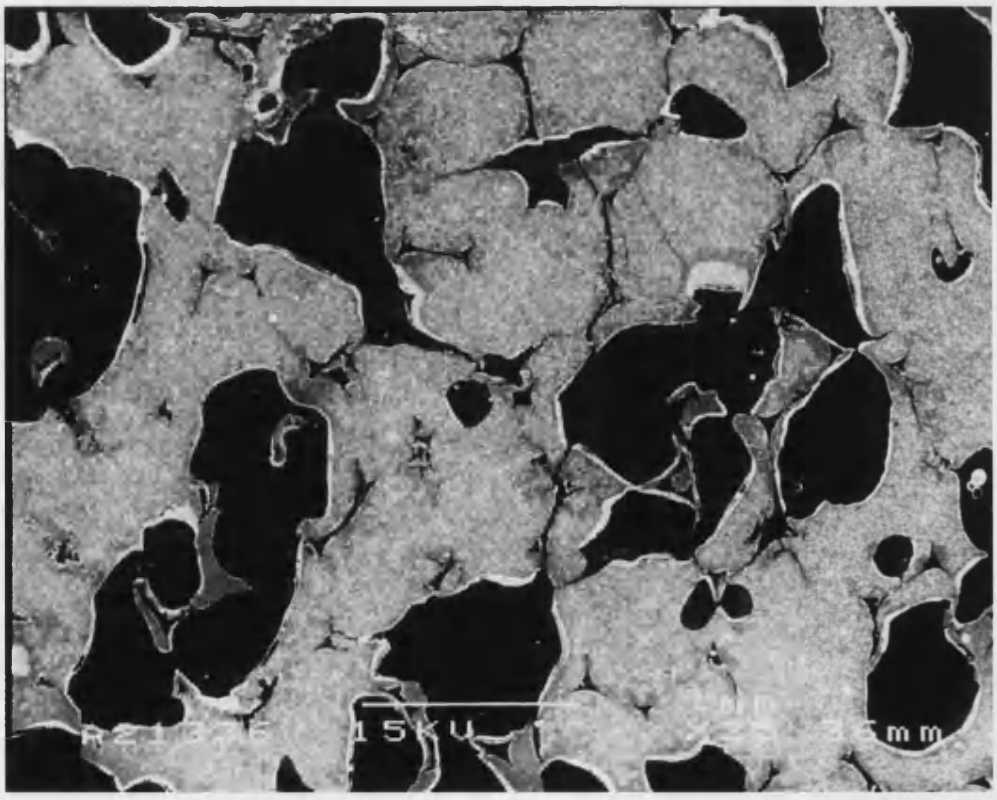

Figure 44 1280 Mesh Pore structure in 45ppi based material produced by impact impregnation, mesh dried, sintered at 1280°C.

Figure 43 and Figure 44 show the pore structure of 45ppi based material produced by impact impregnation as dried on tissue and on mesh respectively. Here too it can be seen that two distinct types of porosity exist within the materials. In the case of the mesh dried

material, the porosity associated with incomplete impregnation dominates the pore structure.

Image Analysis

Image analysis of the electron micrographs was used to quantity the difference in the pore structure of the various materials.

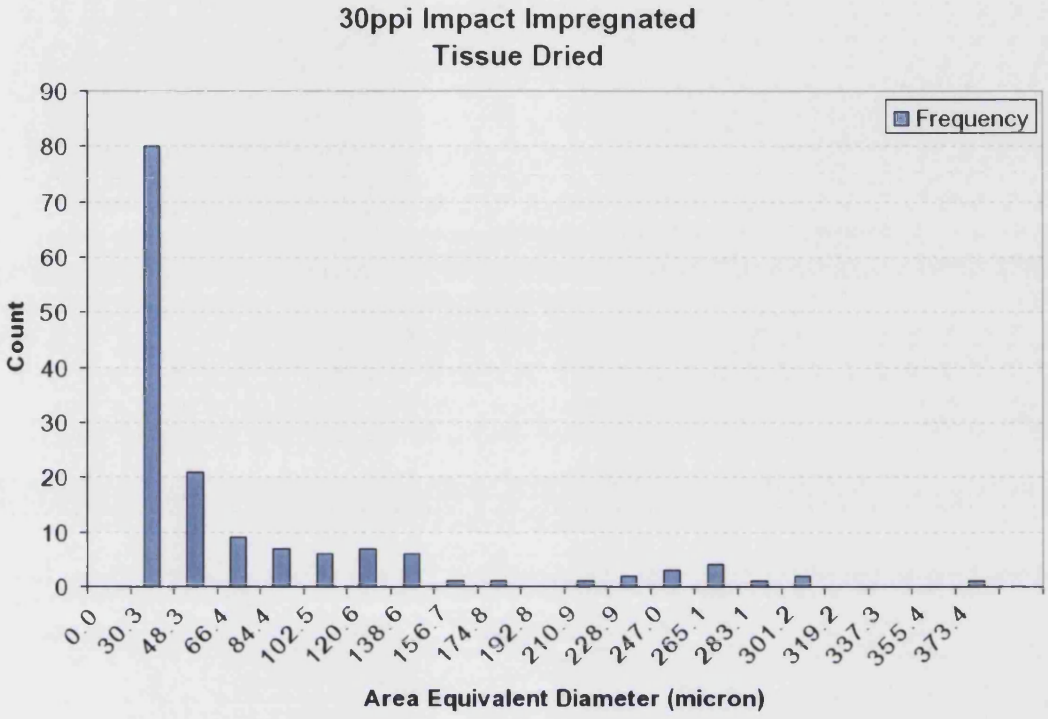

Figure 45 Pore size distribution of 30 ppi based materials produced by impact impregnation and tissue drying.

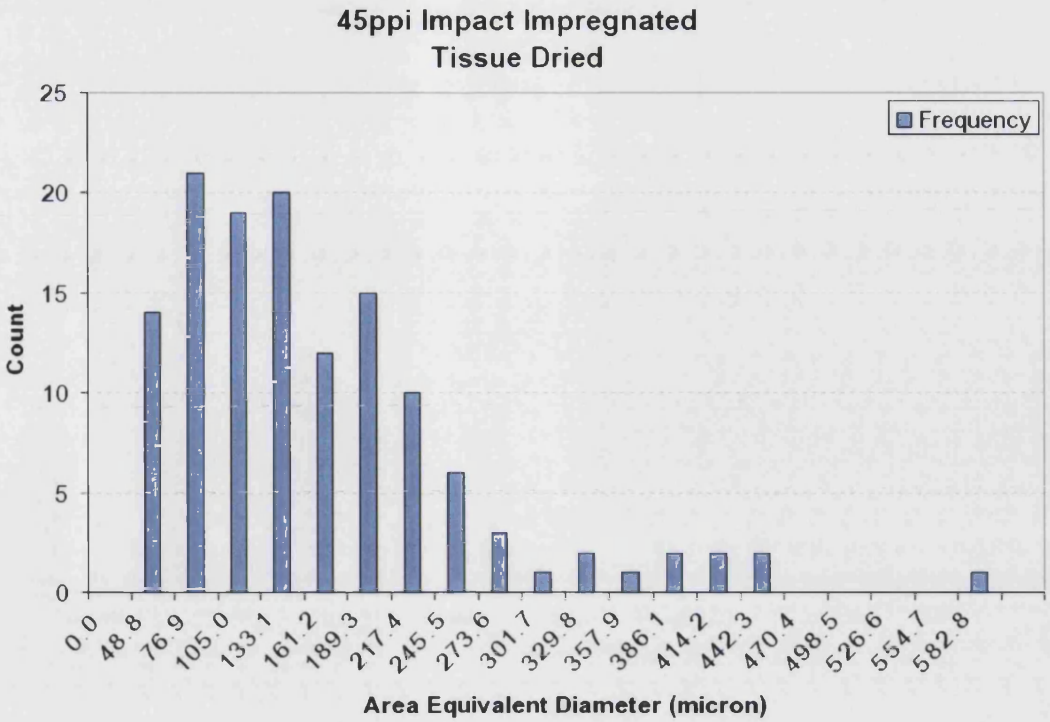

Figure 46 Pore size distribution of 45 ppi based materials produced by impact impregnation and tissue drying.

Figure 45 and Figure 46 show the pore size distributions in the impact-impregnated material based on 30ppi and 45ppi foams respectively. These distributions show a wider range and larger pore size in the 45ppi based materials. This was found to be due to the prevalence of large pores associated with incomplete impregnation in the 45ppi based material.

3.9.3 Vacuum/Pressure Impregnated Foams

Optical Microscopy

Characterisation of the pore structure in the vacuum/pressure impregnated materials by optical microscopy relied heavily on the use of darkfield imaging. Darkfield imaging produced a high contrast between the pore volume and the bulk ceramic and allowed the imaging of some of the translucent features within the material.

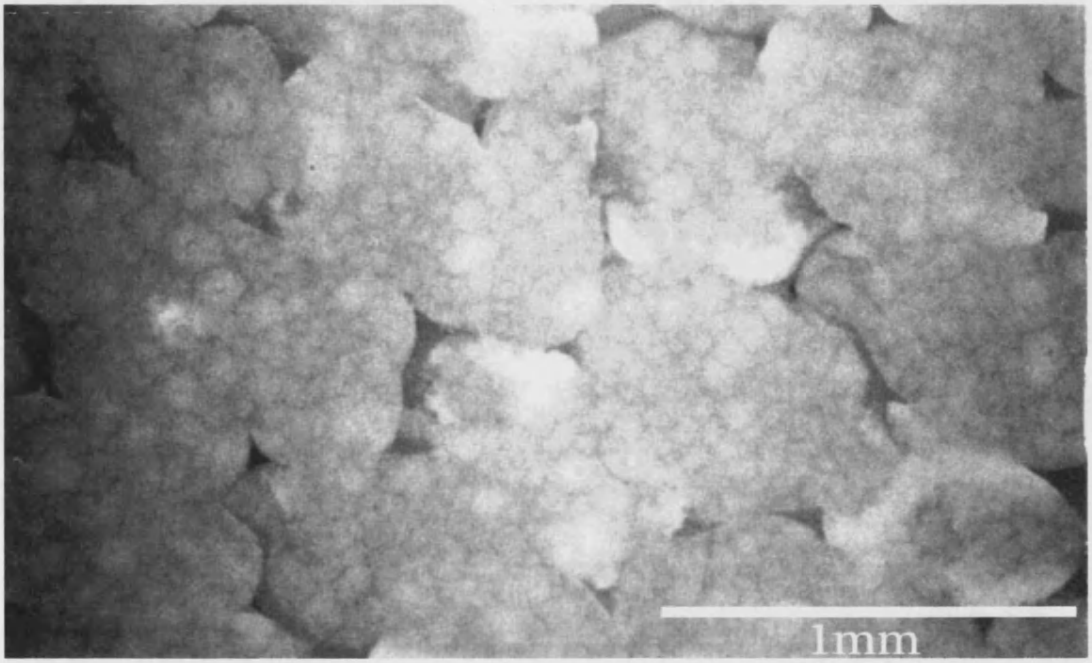

Figure 47 Darkfield image of 45ppi based material produced by vacuum/pressure impregnation, tissue dried, sintered at 1280°C.

Figure 47 shows the pore structure in material based on a 45ppi foam produced by vacuum/pressure impregnation. The distinctive bow tie shaped pore can be clearly seen to be present. The mottled appearance of the bulk ceramic was also noted. The area shown in the above image was selected as being representative of the high density regions of the material where all of the porosity was due to foam burn out.

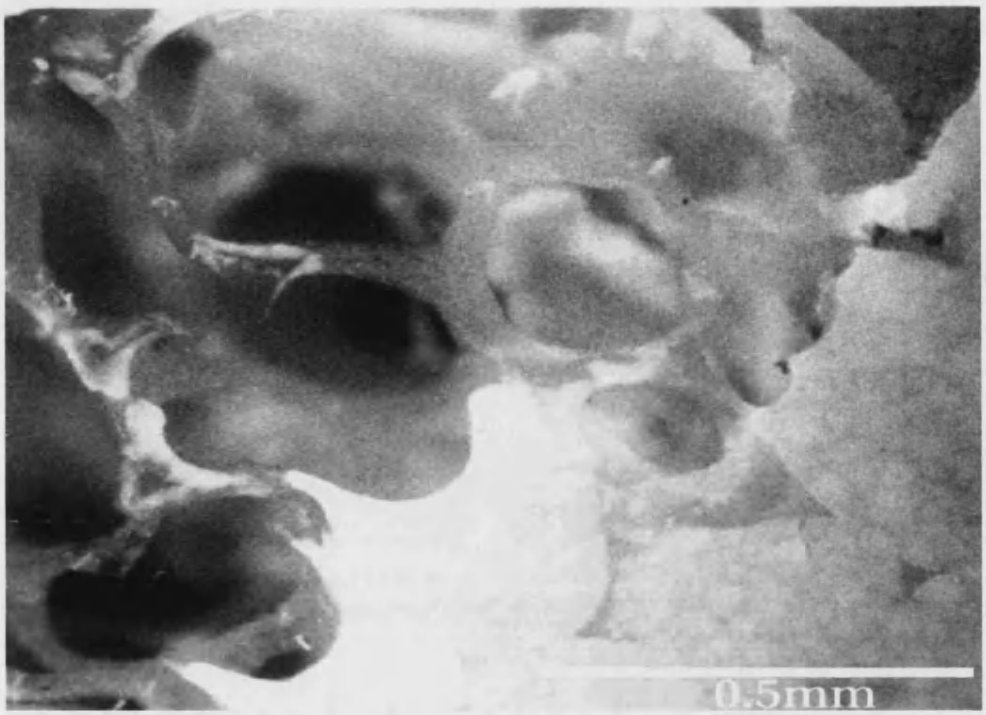

Figure 48 Hollow ceramic struts in 45ppi based material produced by vacuum/pressure impregnation, tissue dried, sintered at 1280°C.

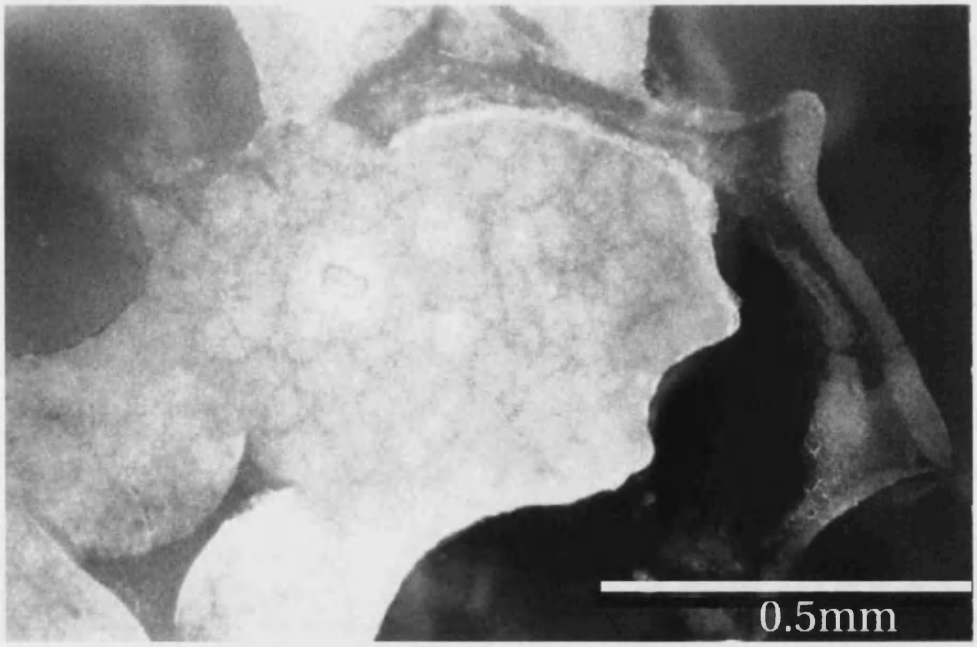

Figure 49 Hollow ceramic strut and bow tie pore in 45ppi based material produced by vacuum/pressure impregnation, tissue dried, sintered at 1280°C.

Figure 48 and Figure 49 show the cross-sections of hollow ceramic struts found in a low density region in a 45ppi based material produced by vacuum/pressure impregnation. The large-scale porosity in these regions was due to voidage as a result of incomplete impregnation, and as such was not representative of the structure typically produced.

However these images clearly illustrate the mechanism by which the burn out of the base foam generates the bow tie shaped porosity in these materials.

SEM

30 ppi based vacuum/pressure impregnated material

The following samples were produced with a 30ppi base foam using a dispersed slip with a powder loading of 600g/l

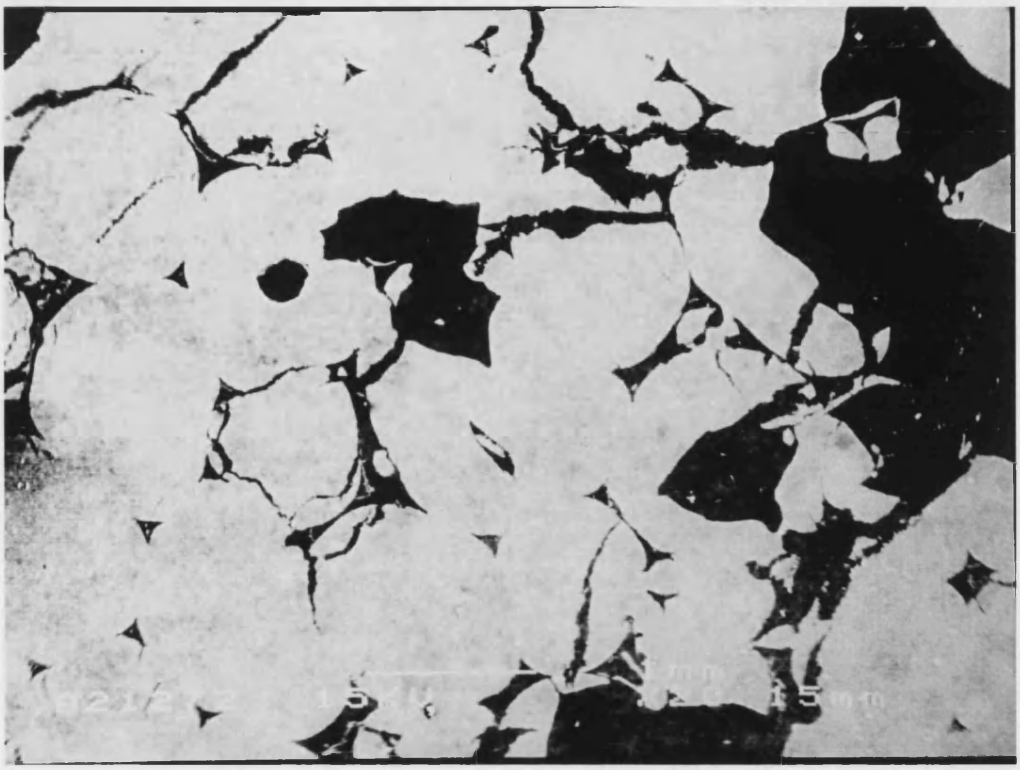

Figure 50 Pore structure in 30ppi based material produced by vacuum/pressure impregnation, tissue dried, sintered at 1280°C.

Figure 50 shows the pore structure of the 30 ppi based material produced by vacuum pressure impregnation. Though bow tie shaped pores can be seen, the pore structure was dominated by porosity associated with incomplete impregnation. Also of note was the widespread cracking in the material.

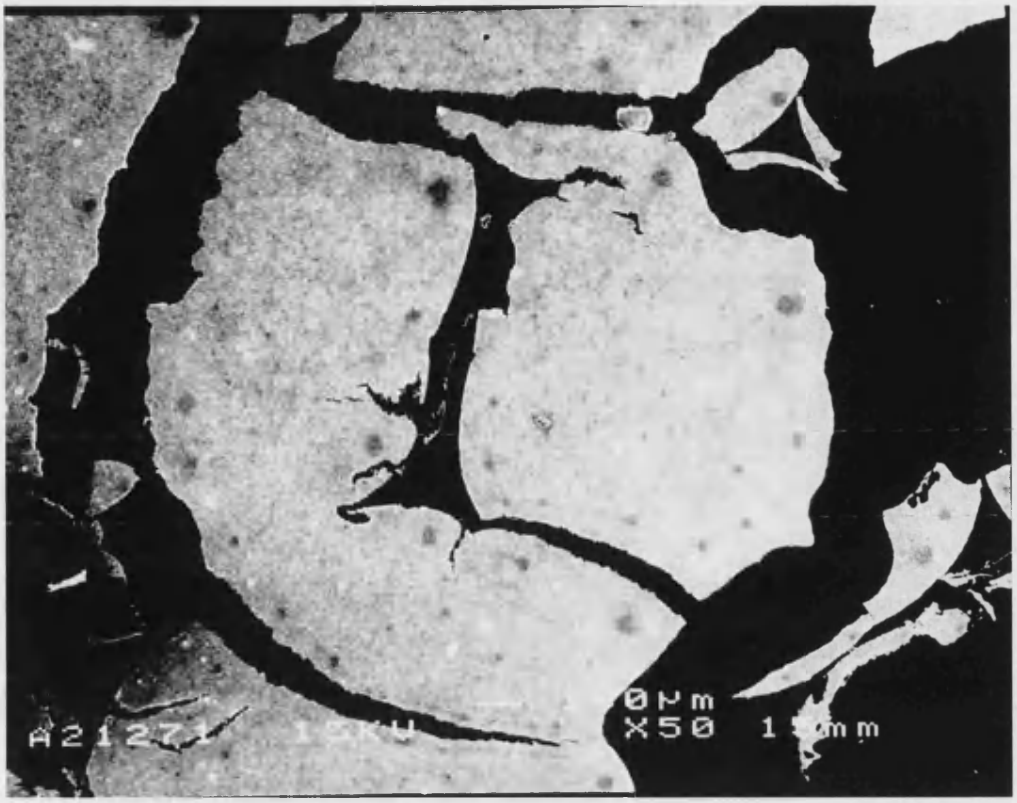

Figure 51 Distinctive bow tie pore in 30ppi based material produced by vacuum/pressure impregnation, tissue dried, sintered at 1280°C.

Figure 51 shows an example of porosity associated with burn out of the base foam strut. The size and aspect ratio of this pore was typical of many of those found in the 30ppi based material.

45ppi based vacuum/pressure impregnated material

The following samples were produced with a 45ppi base foam using a dispersed slip with a powder loading of 600g/l.

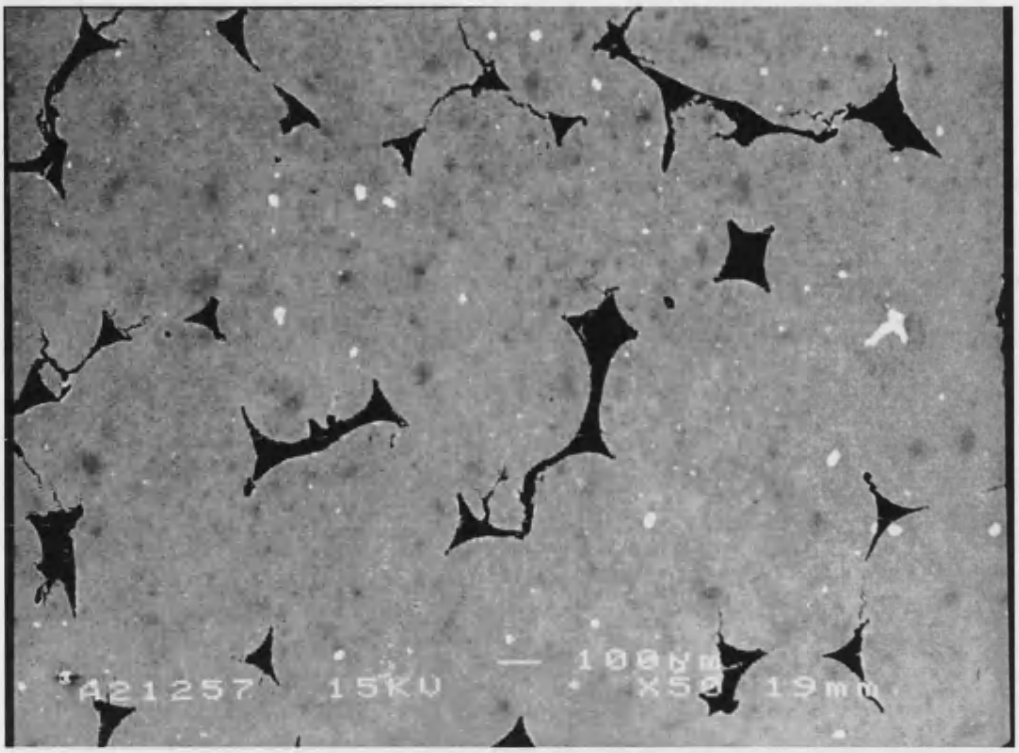

Figure 52 Pore structure in 45ppi based material produced by vacuum/pressure impregnation, tissue dried, sintered at 1280°C.

Figure 52 shows the pore structure in 45ppi based material produced by vacuum/pressure impregnation. The structure is dominated by porosity associated with the burn out of the organic base foam.

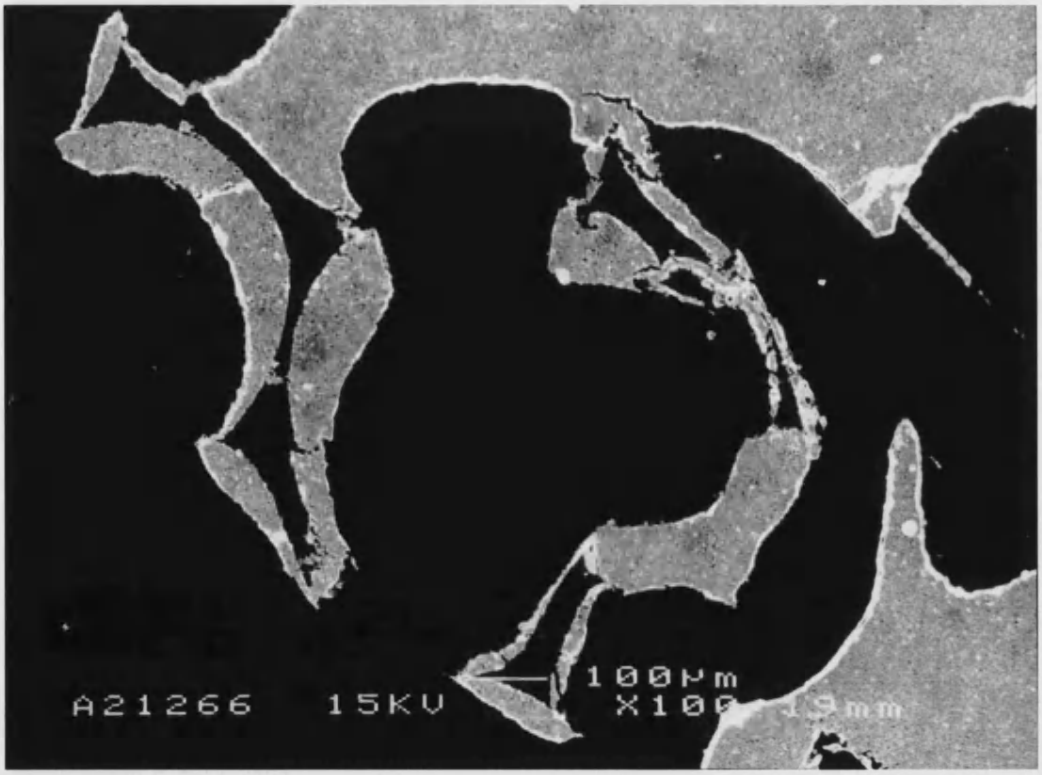

Figure 53 Pore formation in 45ppi based material produced by vacuum/pressure impregnation, tissue dried, sintered at 1280°C.

Figure 53 shows the cross-section of hollow strut in a low density region of a 45ppi based material produced by vacuum/pressure impregnation. The cross section of the strut can easily be related to the distinctive bow tie shaped porosity found in the material.

65ppi based vacuum/pressure impregnated material

The following samples were produced with a 65ppi base foam using a dispersed slip with a powder loading of 600g/l.

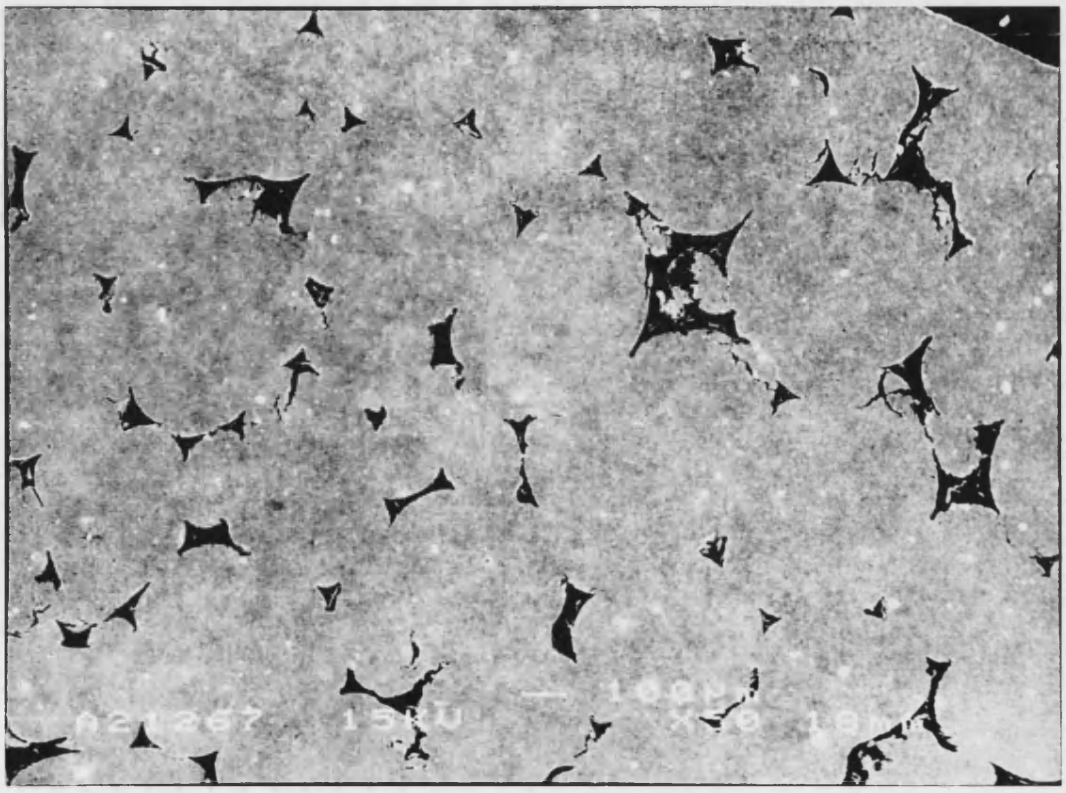

Figure 54 Pore structure in 65ppi based material produced by vacuum/pressure impregnation, tissue dried, sintered at 1280°C.

Figure 54 shows the pore structure found in the 65ppi based materials produced by vacuum/pressure impregnation. A high level of slip impregnation and retention has produced a pore structure dominated by pores from foam strut burn out. Pore structure was visibly finer than that produced by the 45ppi foam.

Image Analysis

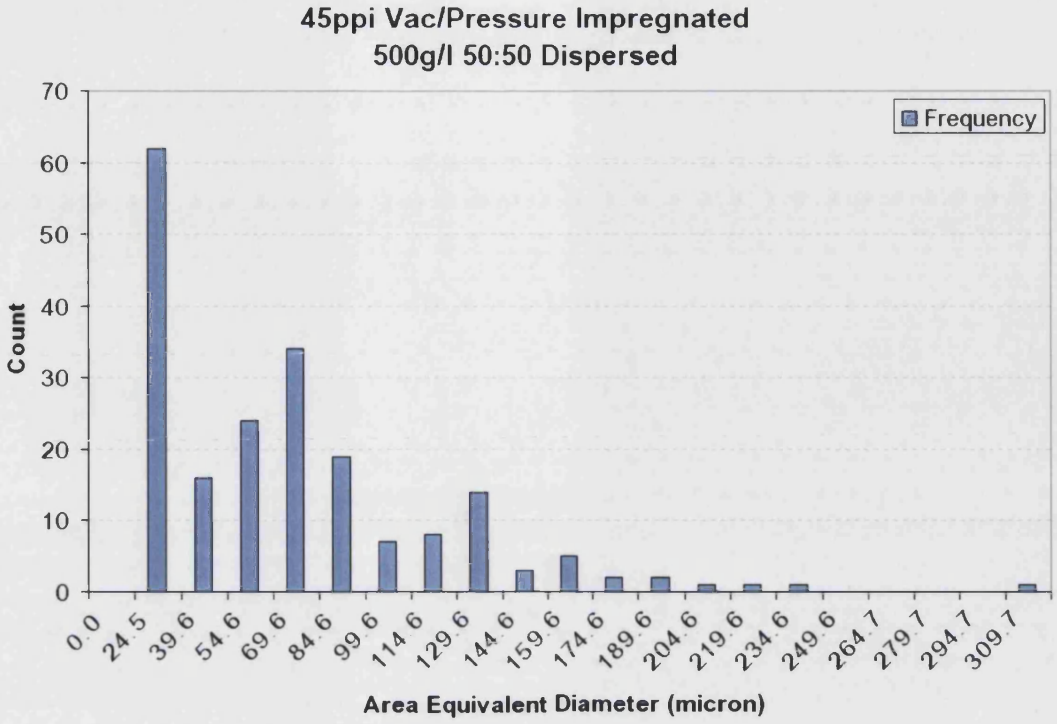

Figure 55 Pore size distribution in 45ppi based material produced by vacuum/pressure impregnation

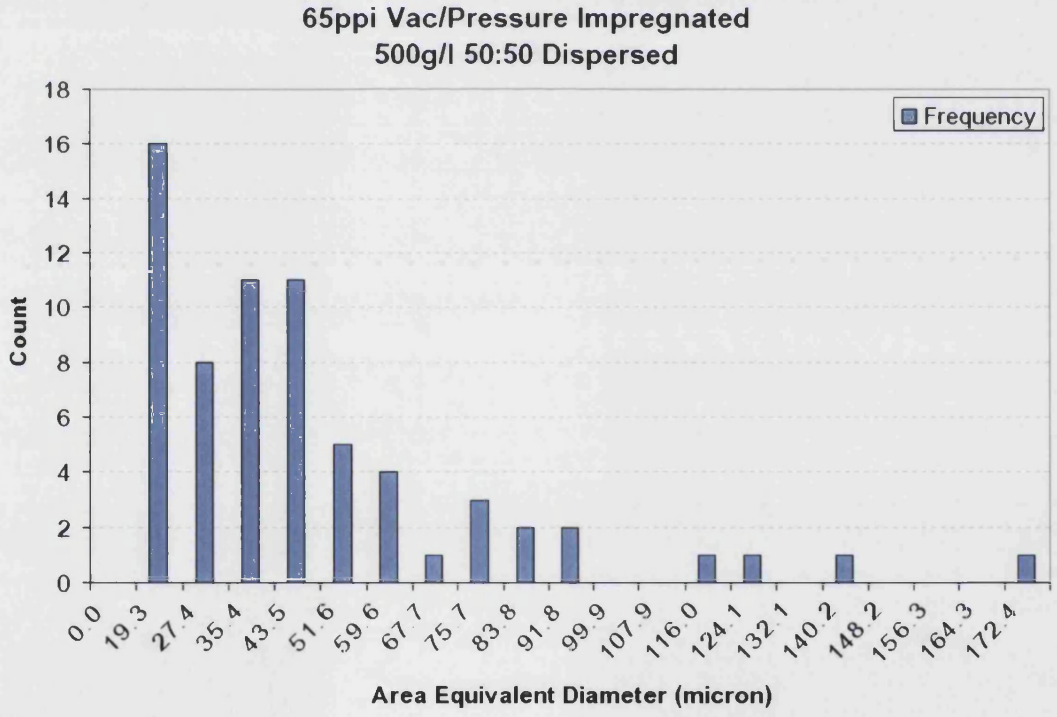

Figure 56 Pore size distribution in 65ppi based material produced by vacuum/pressure impregnation

Figure 55 and Figure 56 show the pore size distribution for the 45ppi based and the 65ppi based materials produced by vacuum pressure impregnation. The frequency distributions show the 65ppi based material to have a lower pore size than that of the 45ppi based material.

Microporosity

A high degree of microporosity was observed in all sintered materials based on a slip precursor. Earlier results from the slip cast materials demonstrated that this effect was not dependant on the addition of a dispersant in the slip or the use of an organic foam porosifer. The degree of microporosity and its size distribution was assessed for materials sintered at 1150°C and 1280°C.

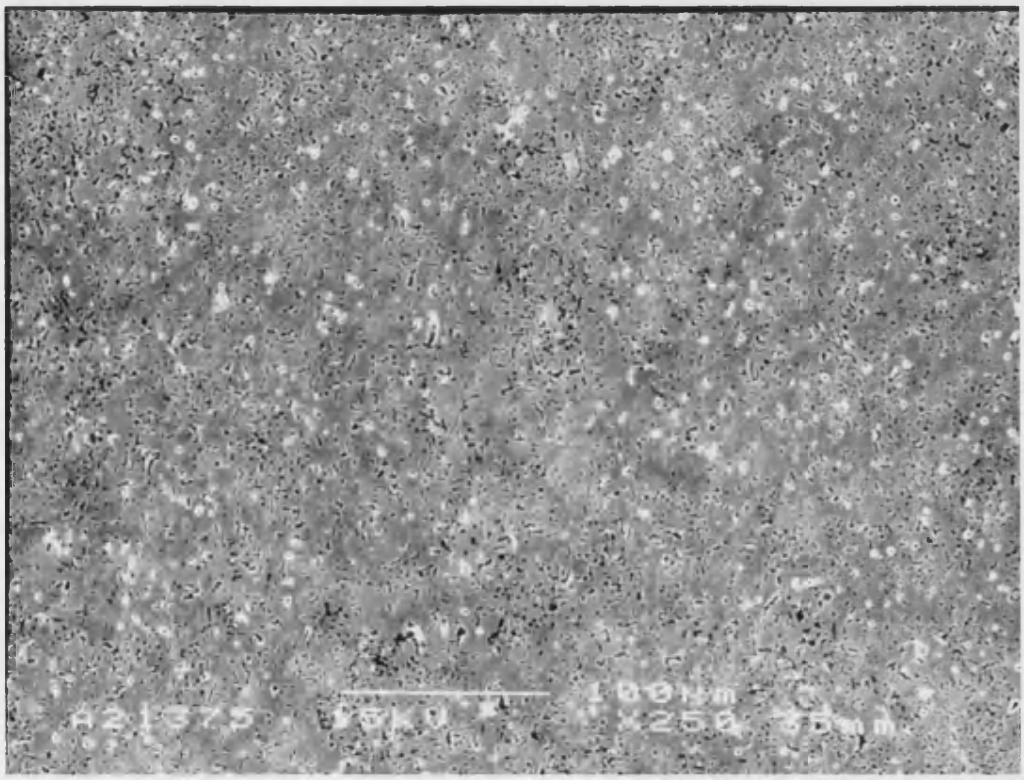

Figure 57 Micro porosity in material slip cast using dispersed slip, sintered at 1280°C

Figure 57 shows the microporosity present in material produced by slip casting using dispersed slip and sintered at 1280°C. Micro pores can be seen evenly distributed thought out the material and appear as discreet pores as opposed to surface texture.

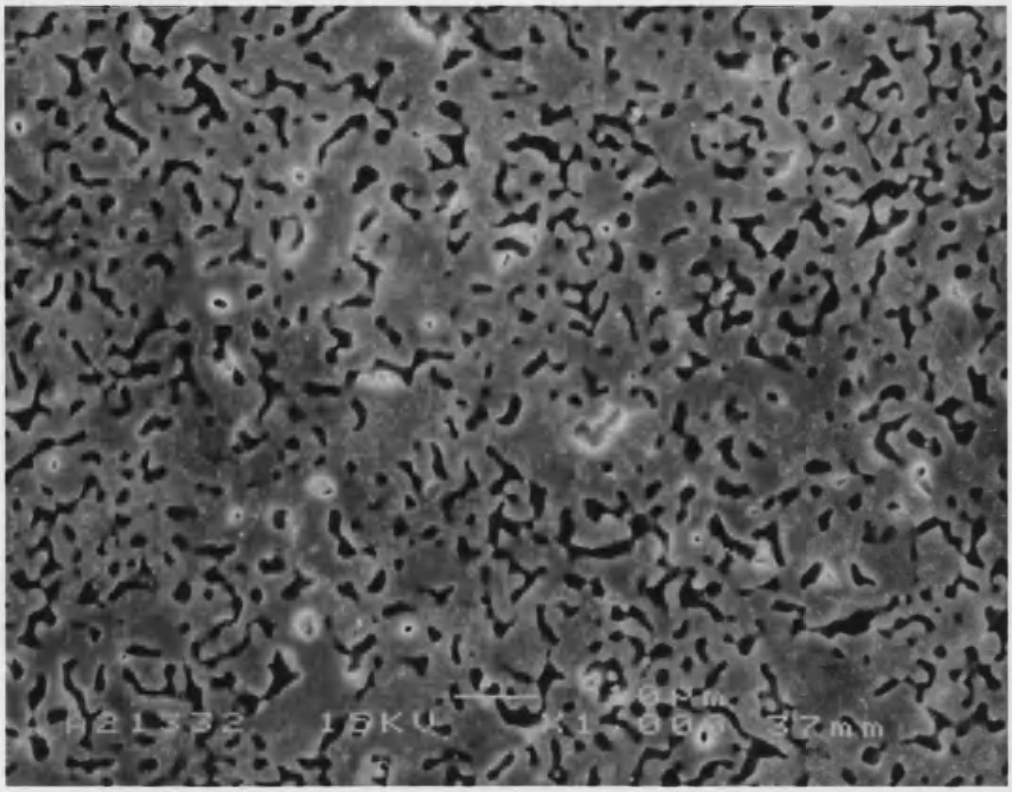

Figure 58 Micro porosity in material vacuum/pressure impregnated using dispersed slip, sintered at 1280°C

Figure 58 shows the micro porosity present in material produced by vacuum/pressure impregnation using dispersed slip and sintered at 1280°C. Again micro pores can be seen evenly distributed throughout the material and appear as discreet pores. Grain structure can also be seen in the areas of lower microporosity.

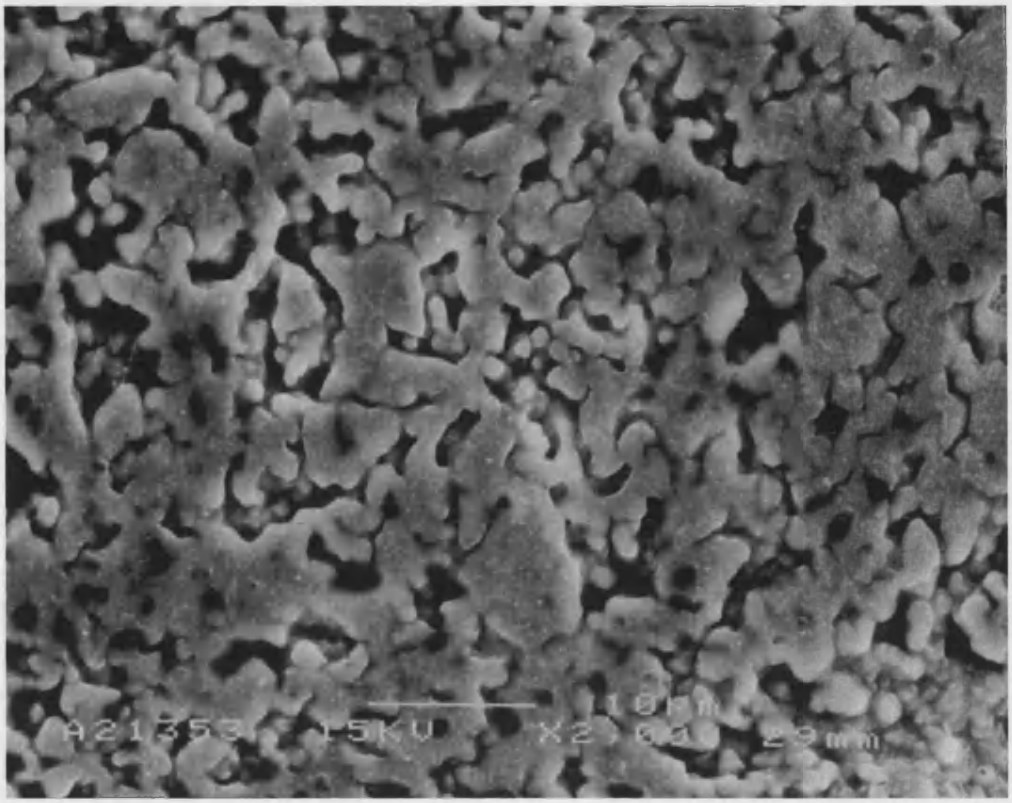

Figure 59 Microporosity in material vacuum/pressure impregnated using dispersed slip, sintered at 1150°C

Figure 59 shows the microporosity in material produced by vacuum/pressure impregnation using dispersed slip and sintering at 1150°C. The porosity does not in this case appear in discreet pores but rather as a network of channels giving an appearance of surface roughness. Well defined grain boundaries were not found in this material

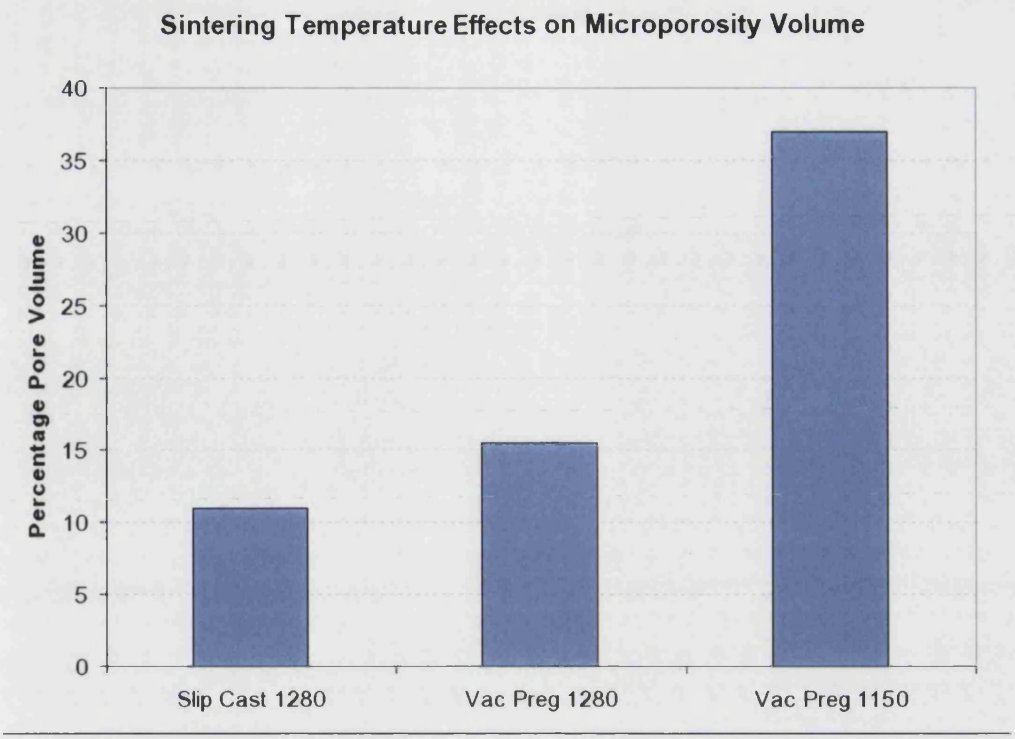

Figure 60 Effects of sintering temperature on micro porosity.

Figure 60 shows the effect of sintering temperature to strongly effect the overall micro pore volume in the material, while the effect of vacuum processing and burn out of organic inclusions are not as strong.

3.9.4 Double Vacuum/Pressure Impregnated Foams

The double vacuum impregnation technique was developed as a modification to the basic vacuum impregnation technique in an attempt to improve the reliability of the process and to allow the production of larger samples.

Macro observations

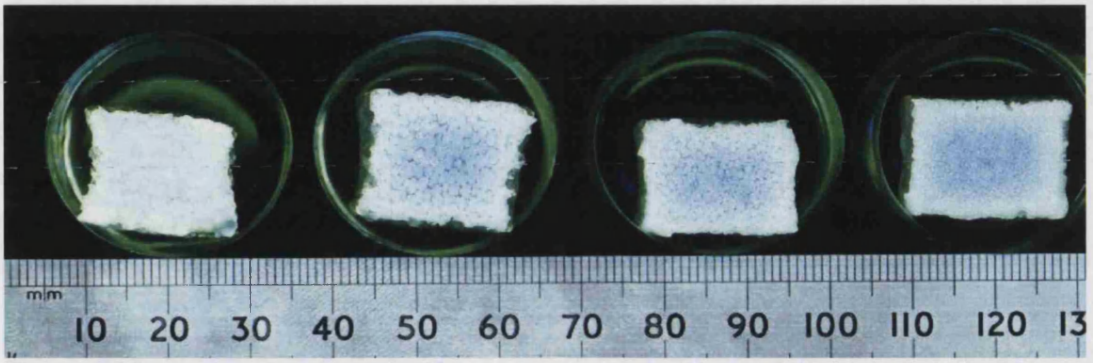

Figure 61 Mounted sections from double vacuum impregnated material with various base foams

Figure 61 shows a scan of the mounted and sectioned double vacuum impregnation samples prior to their being gold coated for SEM. The leftmost sample was produced using a 20ppi foam but with two slips which differed in their mix of Grade 118 and Grade 130 for the first and second impregnation. The remaining samples were produced using the same slip for the first and second impregnation. These were based on the 20ppi, 30ppi and 45ppi foams, shown from left to right above. What was most striking about these materials was the absence of any voidage due to the incomplete impregnation of the foam, as seen in Figure 41. The effect of the foam size on the pore size in the material can also be clearly seen.

SEM

SEM images of the 20ppi 30ppi and 45ppi based foams produced by the double vacuum impregnation method were made to characterise the macro and micro porosity and to facilitate the determination of pore size distribution by image analysis.

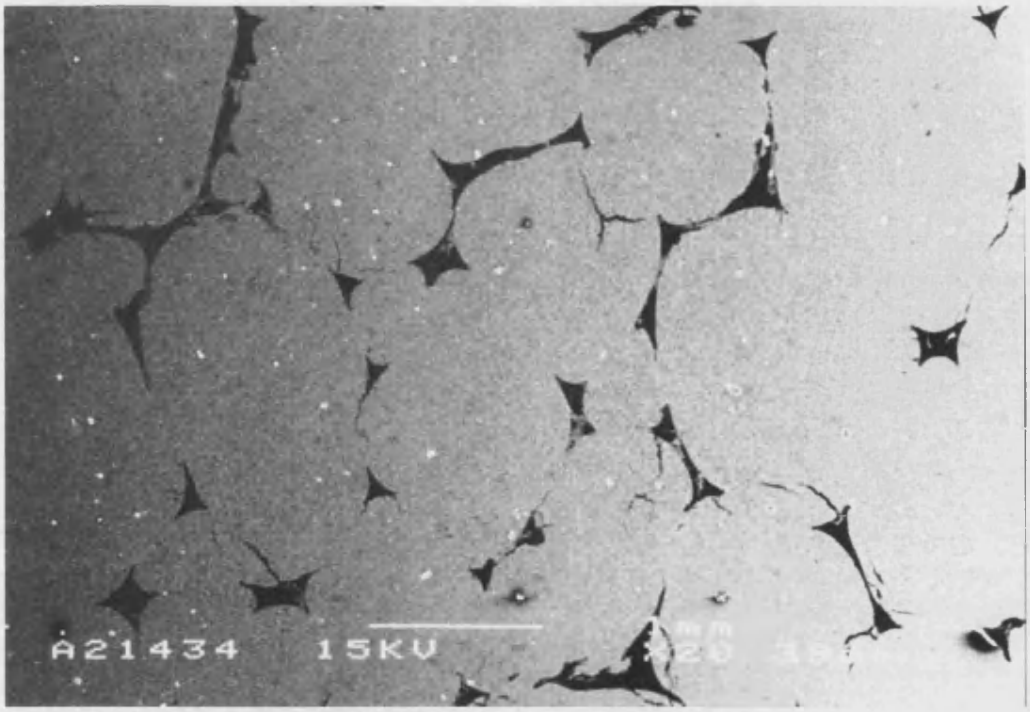

Figure 62 Material produced by double impregnated of 20ppi foam

Figure 62 shows the pore structure produced by double impregnation of a 20ppi base foam. In this structure all of the macro porosity was due to foam burn out, demonstrating that complete foam impregnation with the ceramic slip had been achieved. The section shown above was typical of all the materials produced using these conditions. The scale of the pores shown was also significant, as the production of these type large pores was only achieved by use of the 20ppi base foam. The double impregnation method was the only route by which an intact sample based on the 20ppi foam had been produced. There was evidence of cracking throughout all of the 20ppi based materials. This cracking was thought to occur during the drying stage.

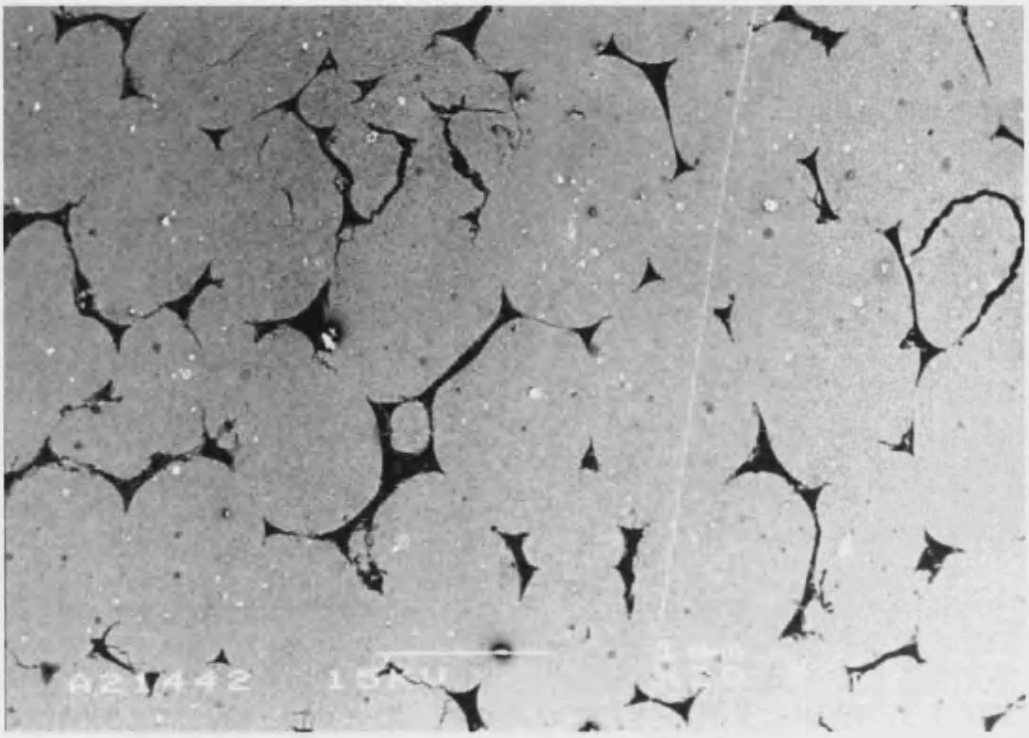

Figure 63 Material produced by double impregnated of 30ppi foam

Figure 63 shows the material produced by double vacuum impregnation of 30ppi foam. As in the 20ppi based material all of the macro porosity was due to the burnout of the organic foam. In this material there was less evidence of cracking than was found in the 20ppi material.

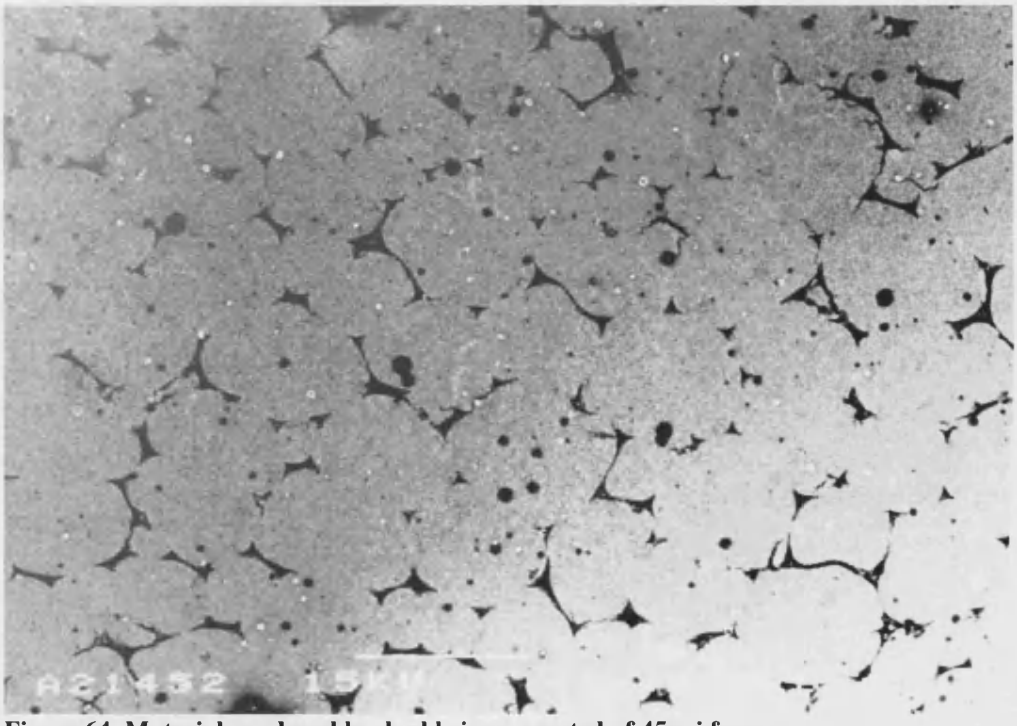

Figure 64 Material produced by double impregnated of 45ppi foam

Figure 64 shows the material produced by double impregnation of the 45ppi foam. As the magnification was the same for this and the two preceding images it can be clearly seen

that the porosity in this material was of a much finer scale than in the 20ppi and 30ppi materials. The black round features seen in this image were not pores as they may appear, but were found to be charging artefacts form the SEM imaging and not real features in the material.

Image Analysis

Image analysis of the micrographs from the double vacuum impregnation materials was carried out to quantify the differences in the macro pore structure produced.

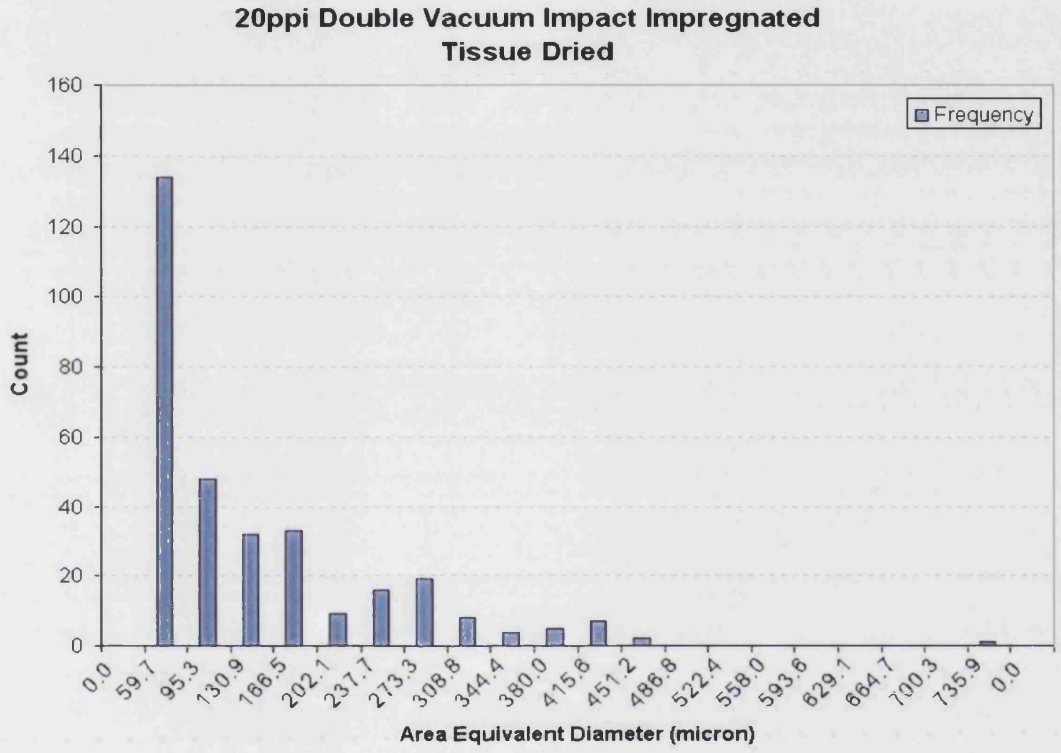

Figure 65 Pore size distribution in 20ppi based double impregnated material

Figure 65 shows the pore size distribution for the 20ppi foam based material produced by double vacuum pressure impregnation as determined by image analysis. This distribution shows that though the majority of pores are in the size range of 60µm to 200µm, there was a significant amount of porosity with an area equivalent diameter of 200µm to 450µm.

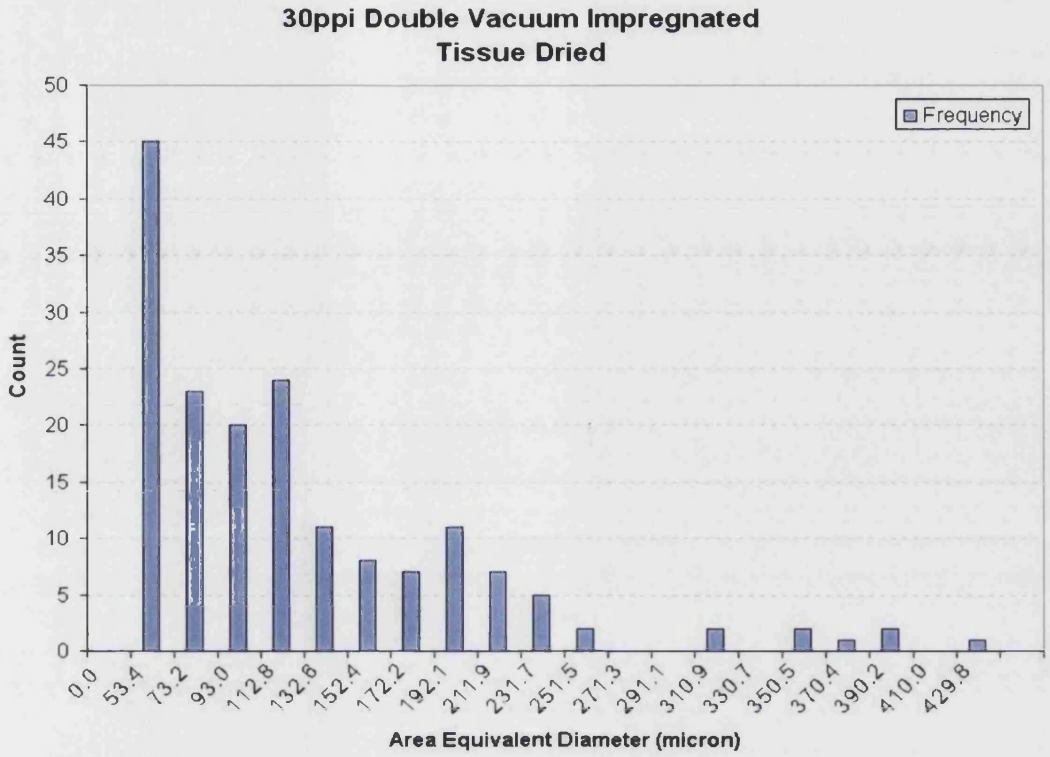

Figure 66 Pore size distribution in 30ppi based double impregnated material

Figure 66 shows the pores size distribution for the 30ppi foam based material produced by double vacuum impregnation. This shows a spread of pore size from 54μm to 270μm with the frequency decreasing with increased pore size. A small but significant number of larger pores were also found to be present in these materials.

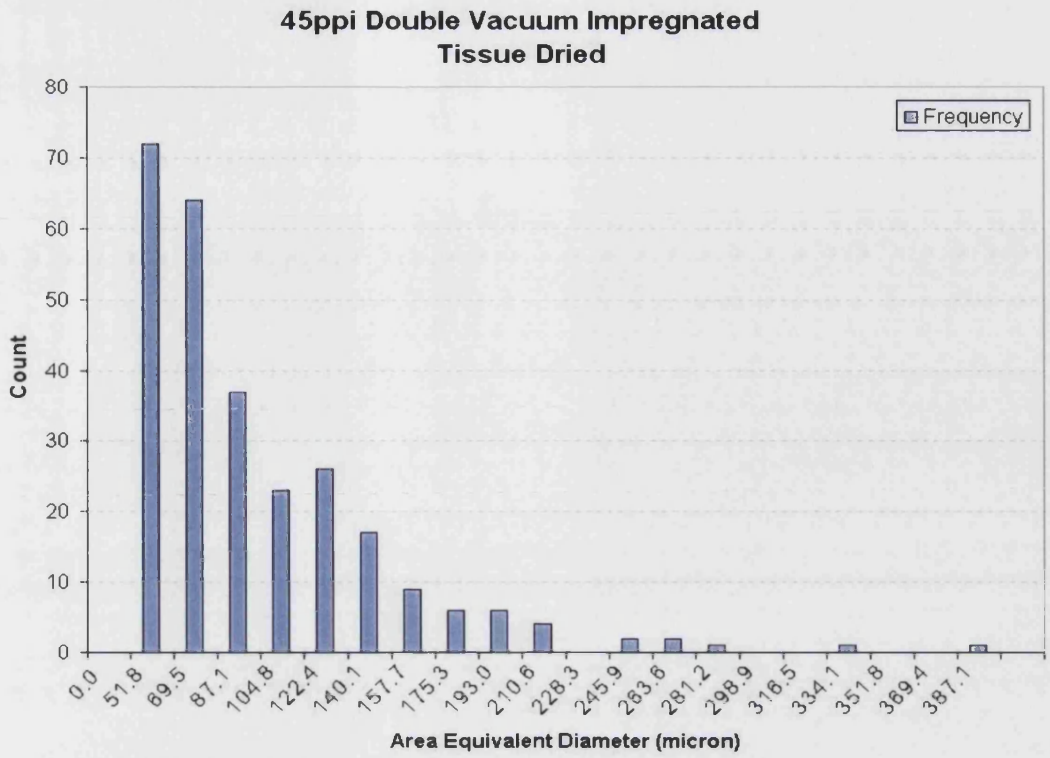

Figure 67 Pore size distribution in 45ppi based double impregnated material

Figure 67 shows the pore size distribution for the 45ppi foam based material produced by double vacuum impregnation. This distribution shows a decay in frequency of occurrence of pores as the size increases from 50μm to 210μm. The distribution shows the pore structure to be much finer in the 45ppi based material that the 20ppi and 30ppi based materials.

Measurement of the overall macro pore volume by image analysis showed the degree of macro porosity in all the double vacuum impregnation materials was in the range of 4.5% to 5%. This pore volume was found to be independent of the size of the input foam.

3.9.5 Physical Testing.

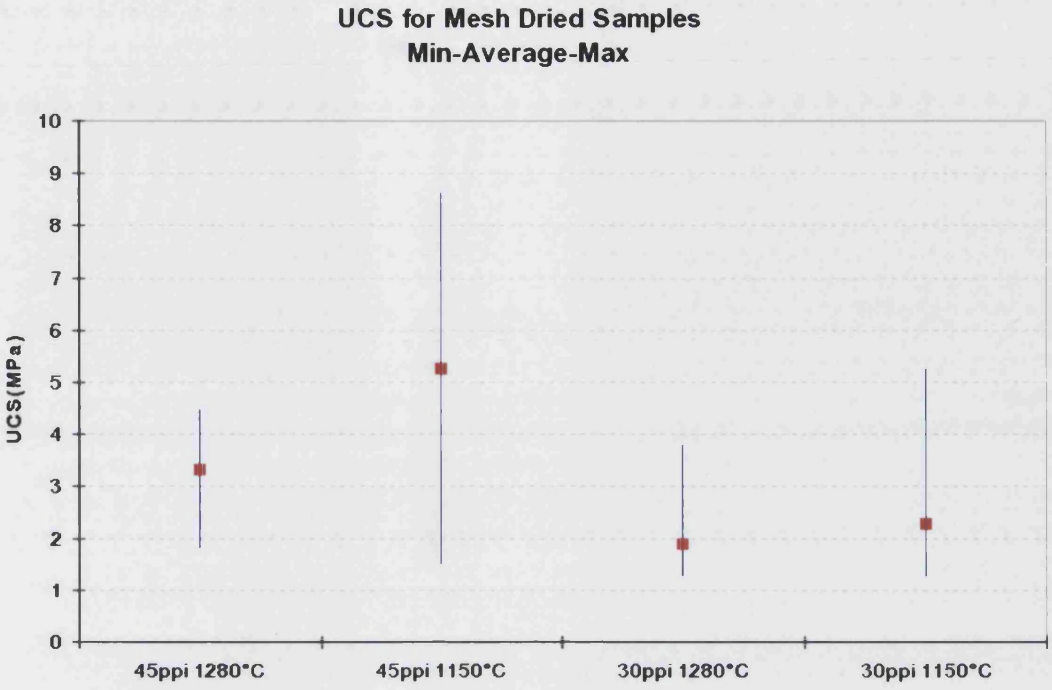

Figure 68 UCS for various mesh dried impact impregnated materials.

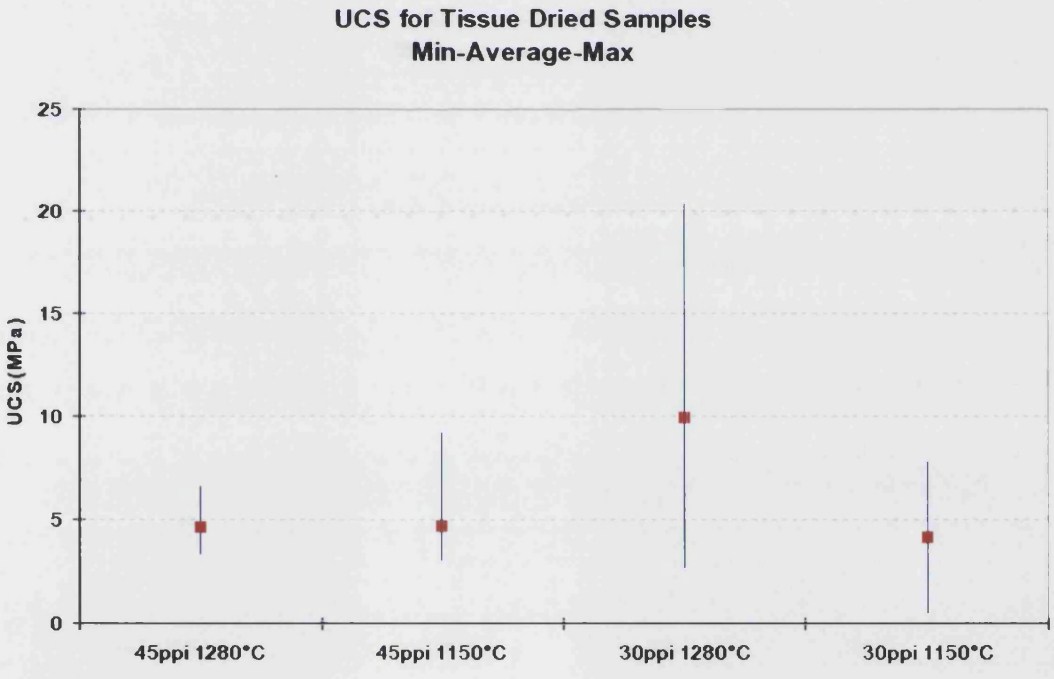

Figure 69 UCS for various tissue dried impact impregnated materials.

Figure 68 and Figure 69 above show the spread of ultimate compressive strengths (UCS) obtained from the mechanical testing of the various impact impregnated materials. These graphs clearly show a high variability in the loads withstood by materials produced under the same conditions. The average strengths for the tissue dried material was found to be

greater than the mesh dried materials. It was noted that the highest value achieved was over 20MPa for a tissue dried 30ppi based material sintered at 1280°C.

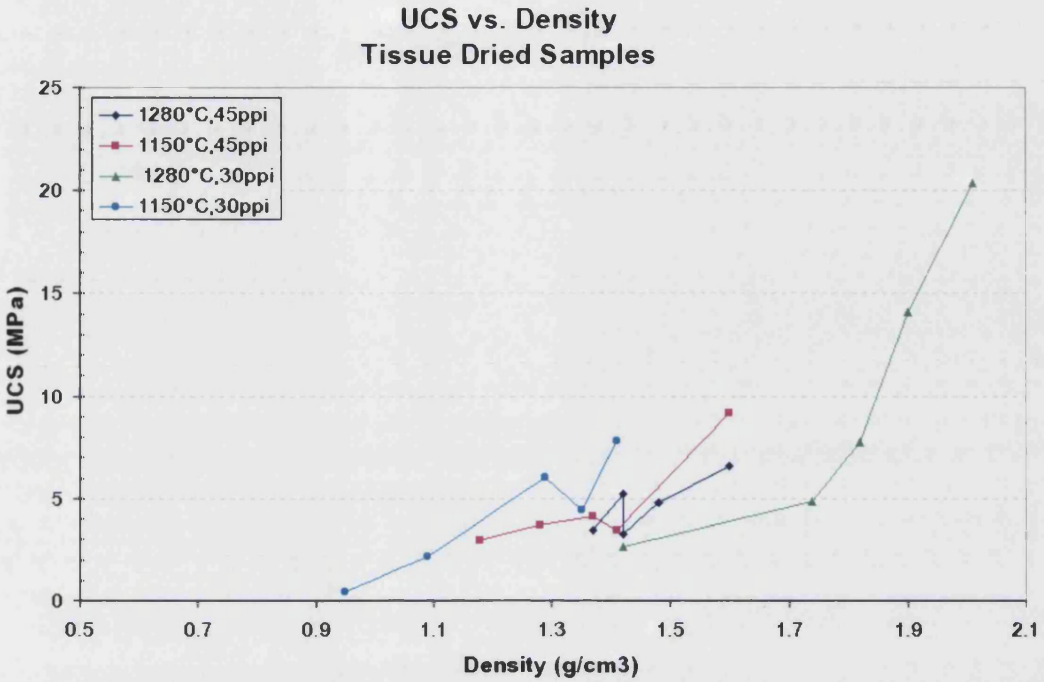

Figure 70 Effect of sample density on UCS in tissue dried impact impregnated materials

Figure 70 shows that the variation in strength of the materials within each batch was largely determined by the density of the individual sample.

Double vacuum impregnated materials: Compression results

Samples sintered at 1280°C based on the 30ppi foam produced by double vacuum impregnation method were tested in compression and found to have ultimate compressive strengths in the range of 15.8 MPa to 30.4 MPa with densities in the range of 2.06g cm^{-3} to 2.18g cm^{-3}.

3.10 Discussion of Foam Based Materials Results

The results of the characterisation of the foam based materials show the progressive improvement of the reliability of the product material with each successive refinement. The elimination of porosity due to incomplete impregnation was a key part of this improvement. The materials produced in the latter stages of the work by means of the double vacuum impregnation process show a complete absence of porosity due to incomplete impregnation as all of the porosity seen in these materials has the distinctive bow tie shape demonstrated to be associated with foam burn out.

Process refinements, such as the use of dispersed slips and vacuum impregnation, allowed total impregnation of the organic foam with ceramic slip to be achieved and allowed control of the pore size as this was then strongly dependent on the structure of the input foam. The porosity generated in this manner was shown to be inherently interconnected. This was clearly illustrated by the darkfield images showing the hollow channels running through the materials. These darkfield images also clearly illustrated the pore formation mechanism in the impregnated foam production method.

Increasing levels of refinement also allowed the reliable production of materials based on larger pore size. The impact impregnation method was limited to the production of 45ppi based materials whereas the double vacuum impregnation method allowed the reliable production of 20ppi based materials. This increase in maximum usable foam openness was accompanied by an increase in the size of sample which could be produced. The impact impregnation method was severely limited by this restraint. With the double vacuum impregnation method the limiting factor was the size of the containment vessel in the impregnation rig.

The results show that the vacuum impregnation method, and later the double vacuum impregnation methods reduce the occurrence of coring in the samples, to the point of absence in the latter case. These improvements were as a result of both improving the degree to which the ceramic slip was forced into the foam and ensuring the slip stayed in place during the drying process. It was seen throughout the foam impregnation work that the conditions of drying had a profound effect on the pore structure of the resultant material.

The results of the image analysis show that where high levels of impregnation had been achieved the pore size distribution depended on the input foam. The shape of these pore

size distributions largely resemble exponential decay patterns, with large numbers of small pores and a decreasing number of pores as the pore size increases.

It should be noted that the 30ppi and 20ppi foam based materials showed a significant number of pores with an area equivalent diameter of over 200 micron which is very much in the useful range for osseoconduction in bone substitute materials. Image analysis of the porosity of the materials also demonstrated that where good impregnation had been achieved the overall pore volume was between 4.5% and 5% independent of the structure of the input foam. This result should hold true when the density of the input foams is constant across the range of pores per inch.

The results of the mechanical testing on the impact impregnated foams showed that the strength of the materials was dependant on the porosity, which in turn had been found to be solely effected by the degree of impregnation achieved. It was interesting that this crude process nonetheless yielded samples that showed an ultimate compressive strength of up to 20MPa. From the results of the compression testing of the double vacuum impregnated materials it was seen that the reliability and strengths achieved in mechanical testing were in line with the improvements in impregnation reliability observed in the optical and SEM work on these double vacuum impregnated materials.

The results of the mechanical testing also showed a difference in the properties of the materials sintered at 1150°C and those sintered at 1280°C. These differences were reflected in the differences in the microstructure of materials sintered at these temperatures. The microporosity of the 1150°C sintered material was found to be higher than that of the 1280°C material. The texture of this microstructure was also seen to be radically different. These factors suggest that the 1150°C material had a very high surface area. This could have important effects on the material's dissolution rates and cell interactions as well as its performance as an effective drug delivery system.

4 Discussion

4.1 Overview

As outlined in the introduction the aim of the project was to develop a methodology for the production of a ceramic synthetic bone substitute material to fulfil the growing demand for a wholly synthetically derived material. To measure the success of the developed process and the resultant material, a number of criteria were laid out in the introduction. These criteria were set with consideration for both the biological and clinical requirements of the material.

The aim therefore was the development of a process to manufacture a porous HA/TCP material in which the pore size and distribution could be carefully controlled and in which the porosity was interconnected. The size distribution of the interconnected porosity should be in the ranges optimal for the promotion of bone ingrowth, as outlined in the introduction.

The process should also be such that it allows the phase composition of the material to be optimised in terms of the HA, β-TCP and α-TCP so as to gain maximum benefit from the osteoconductive and bioactive properties of these phases.

To meet the clinical requirements of a bone substitute material the developed process had to be capable of producing mechanically robust material so that it could be machined to a desired shape, to allow easy handling in theatre and to allow its use in applications where it is likely to see loading. It was also deemed desirable that the process be capable of producing large shaped components in addition to granular materials. The final requirement of the process was that it should be scalable, to allow a large volume of product to be manufactured in a reproducible manner.

4.2 Development of Project Goals

To achieve the goals as set out above a progressive series of refinements took place, from gaining experience of the current processes through to the development of the impregnated foam method. The first step in this process was the characterisation of the input materials. In terms of the ceramic powders this focused on understanding the changes in phase composition occurring during the heat treatment of the powders. With regard to the organic porosifer materials, the characterisation work focused on examining the morphology of these materials, as this would strongly effect the porosity in the end materials.

The next step in the development process involved the production of sintered artefacts from the two base powders. These materials were produced by pressing or slip casting to produce a green body to be subsequently sintered, with no introduced macroporosity. This stage was important to establish a reference for future materials with introduced macroporosity so that effects due to pressing, casting or sintering could be isolated from those due the introduction of macroporosity. This stage also demonstrated the successful sintering of the materials at 1150°C and 1280°C using the sintering regime laid out in section 2.3.1 of materials and methods.

To establish a base line against which the materials could be compared it was necessary to reproduce some of the materials produced by the more established methods of BurPS and coated foams. At this stage it was also important to replicate TCM materials, the characterisation of which formed the basis of the initial stages of the project. This stage was also important for reasons other then establishing a baseline for development. It was useful in identifying the limitations of these processes and allowed the first hand experience of using these processes, essential to enable informed decisions in the development of a novel fabrication method, to be made.

The impregnated foam method was developed to overcome the limitations in the existing methods, identified in the previous step and to achieve the design goals as set out above. The development of this new method was not without difficulties and therefore an iterative development cycle was required to overcome these problems. Key stages in this learning cycle were the refinement of slip processing techniques, developing an understanding of the effects of various drying techniques and the development of more sophisticated and controllable methods for the impregnation of the ceramic slip into the foam structure.

4.3 Overview of Baseline Materials Produced

In this section the materials produced as a baseline for development will be reviewed. The important results arising from their characterisation will be placed in the context of the development cycle. In addition the limitations of these materials for use as a bone substitute will be outlined.

4.3.1 High Density Materials

The characterisation of the materials produced with no introduced macroporosity raised a number of interesting issues, most notably the difference in the microstructure produced by slipcasting the material against pressing the material to generate a green body.

In the case of the materials produced via the pressing route it was found that there was no appreciable difference in the microstructure of the materials produced via isostatic pressing as opposed to those produced via uniaxial pressing. The large degree of shrinkage observed in the uniaxially pressed materials indicates that the greater degree of initial consolidation in the isostatically pressed material was largely offset by the densification during sintering. Similarly very little difference could be found between pressed materials sintered at 1150°C and those sintered at 1280°C with both showing a well developed grain structure and very low incidence of voidage. This demonstrated that in the case of the pressed materials at least, the sintering regime was sufficient to effect good consolidation.

In contrast to the pressed materials, the slip cast materials possessed a high degree of microporosity. The shape and size of the porosity was also found to be effected to a great degree by the sintering temperature used. This was evident in the material sintered at 1150°C which had a highly porous microstructure with evidence of low densification, indicative of incomplete sintering.

This effect was initially attributed to the presence of dispersant in the slip, however further investigation showed the same microstructure was produced using non-dispersed slips. It is proposed that the green body density in the slip cast materials was sufficiently low such that the mass transfer required for complete densification was greater than that achievable with the sintering time and temperatures used and thus was more evident in the low temperature material.

The consequences of this higher degree of microporosity on the materials' effectiveness are largely positive. The high surface area in such a microporous material greatly increases its wettability *in vivo*. This will allow a greater penetration of physiological fluid into implanted material which should serve to enhance the degree of interaction between the implant and the adjacent tissue. The potential benefits of this microporosity in allowing cell ingress and transport through the implant have been given by Lu *et al*[39]. In addition to these factors, the high wettability and large surface area greatly increase the potential of this material as a drug carrier and delivery system.

The finding that the microporosity was an artefact of the slip casting route was important as this microporosity was found to be a major feature of the materials produced by the impregnated foam method. Identifying the source of the effect to be inherent in all of the slip based methods was a key finding of this stage of work.

4.3.2 Fabrication by BurPS Method

The purpose of this section of the work was to explore the limitations of the BurPS method and also to replicate the material as produced by TCM "in house". The results of this work clearly demonstrated the limitations of the BurPS method.

The pore structure generated by this method was inherently isolated porosity generated by the burnout of the individual polymeric particles, with pore interconnections only occurring where impingement of these particles occurs. The formation of an interconnected network of pores therefore relies on a large number of these impingements and thus a high volume fraction of organic filler.

With the exception of the materials based on the TCM method the porosity generated was uniformly distributed through the bulk of the BurPS based materials. Suitably high volume fractions of filler to create an apparently interconnected porosity were only achieved with the PEG and PEO fillers. This result was to be expected as both of these materials are used extensively as pressing aids in ceramic processing. In both cases there was a large particle size distribution which allowed for efficient packing, thereby adding to the strength of the green body. The packing efficiency of the powder/filler mix was a crucial factor in the process, with the manufacture of a robust green body becoming progressively more difficult as the particle size of the filler material increased.

A further drawback of the method was that the size of the interconnections was inherently small as it depended on the impingement of the two filler particles. The harder and more spherical the particle therefore, the smaller the size of the interconnections. Though many of the materials produced by this method were mechanically robust, those with the higher filler volumes were quite fragile, and thus unsuitable for applications where any loading would be encountered. Manufacture of a robust material with an interconnected pore structure in the required size range in HA/TCP by this method would therefore not seem feasible.

Coated Foams

The work carried out using the reticulated foam, or coated foam method met with limited success. This may have been due, in part, to the fact that the methods utilised in slip processing at this early point in the project were not fully developed.

A range of materials were produced using this method with various coating levels and using a number of foam substrates. It was found that the materials that replicated the

structure of the base foam were very fragile. The yield on these sample production runs was also very low as large numbers of samples failed due to cracking during the drying stages while others disintegrated during sintering.

The fragility of these materials was due to the thin ceramic struts which were also found to be hollow, as demonstrated by later work on the impregnated foams (see Figure 49). This inherent weakness was compounded by internal cracking due to drying. Robust material was only produced where little effort was made to expel excess slip from the foam carrier. This created the type of partially impregnated structure seen in Figure 40 which were not in fact true coated foam structures.

The structures produced by this method were in the main low density structures, with high levels of interconnected porosity. Even in the samples produced with the highest density foam an interconnected pore size in excess of 350μm was observed. In terms of appearance these low density structures had some structural similarity to cancellous bone.

Though of limited success in this project, refinements in the composition of the HA to include glass reinforcement[68] and careful control of slip production and coating application[61] can allow the production of highly porous materials sufficiently robust for use in low load applications. Further investigation of the reticulated foam method utilising the slip refinements and application techniques developed in the latter stages of the project is proposed in the section on future work.

4.4 Development of Filled Foam Method

The development of the impregnated foam method arose out of the work on the coated foam method. As stated above, robust materials were produced using the coated foam method only where the amount of slip retained in the foam structure was high. Observations of these samples showed that two distinct types of porosity were present. The majority of the macroporosity was present as voids between the coated foam struts. However a small amount of the macroporosity was seen to be formed by the burnout of the organic foam itself. The presence of this second source of macroporosity became increasingly apparent as the slip loadings into the reticulated foam increased.

The basis of the impregnated foams therefore represents a move away from use of foam as a support and instead utilising the burnout of the foam to create an interconnected network of pores. At its inception, this method was seen as a way to guarantee interconnected porosity and control of pore size and pore volume.

4.4.1 Slip Processing.

The first process improvement required to implement the impregnated foam method was the improvement of slip production method. The requirements of the slip were that it maintain stability while carrying a high powder loading. It was found that a further requirement of the slip was that it should flow well enough to impregnate the foam structure, while being viscous enough not to flow back out.

Initial slips were manufactured on a small scale, with the largest batches being 200g. This small scale in itself presented problems as the mobility of the milling media in the containers was restricted. Improvement in the quality and repeatability of the slip production was seen on scaling the process up to larger batch sizes and larger milling vessels. From the outset it was clear that the non-dispersed slips with binder additions were not suitable for the impregnated foam method. Early impact impregnation work was carried out with non-dispersed slips. Though the results of this work were promising, the samples shown in the results section are all of materials produced with dispersed slips.

Experimentation with the use of high shear dispersion mixing to replace ball milling in the preparation of slips was found to be unsuccessful. The suspension of powder in these slips was found to be less stable than with those produced by ball milling. Sample materials produced with high shear mixer did not sinter well with the resultant material being friable. The combination of these effects points to the high shear mixed material retaining a larger particle size than those produced by ball milling. For these reasons high shear mixing was abandoned as a method of slip preparation.

With the introduction of the use of dispersant in slip preparation, the viscosity of the slips was not determined solely by powder loading. This allowed the preparation of slips with high powder loadings which still retained a sufficiently low viscosity to allow impregnation into the foam support. It was noted that slip stability was also improved with the addition of dispersant. The choice of dispersant used was dictated by the requirement that it leave no residuals after sintering. This requirement eliminated a large range of sodium based surfactants and dispersants.

The dispersant used was Dispex A40 which is an ammonia based dispersant designed to be fugitive at 40°C. Therefore it is likely the the large part of this dispersant was removed during the drying process. No detrimental effects of dispersion additions were observed in the sintering behaviour of the slip cast material as indicated by the similarity in the microstructures of the dispersed and non-dispersed slip cast material.

The viscosity vs. dispersant addition graph (see Figure 35) demonstrated that for the slips with the required powder loading the viscosity could be reproducibly set at a specific value. The combinations of viscosity and powder loading shown in Figure 35 encompassed the full working range found useful in this project.

4.4.2 Impregnation Methods

The impregnation methods themselves are presented as progressive degrees of refinement. With each iteration greater degrees of control of pore structure and reproducibility were achieved.

Mechanical Working/Impaction

As indicated above, the initial trials of the impact impregnation method utilised a non-dispersed slip, with limited success. As demonstrated by the image of the cored sample (see Figure 41) the process was limited by the degree to which impregnation could be achieved.

The SEM images of impact impregnated materials presented in the results section were of materials produced using a dispersed slip, the viscosity and powder loading of which had been arrived at by extensive trial and error. From these images, and the later work with mechanical testing, it can be seen that pore distribution and pore size in the materials varied radically. This variation was found to be dependent to a large degree on operator skill.

An attempt was made to reduce the effect of operator skill on the variations in the material by using a vibration table to standardise the amount of agitation used to effect slip ingress into the foam structure. These attempts were unsuccessful in producing any intact materials.

It can be seen from the SEM images and the mechanical testing work that the best results were achieved with this method using the 30ppi foam. This was due to the ease of impregnating the more open pored structure of this foam.

This effect highlights the key issue in the impregnated foam method, that of ease of slip impregnation must be traded off against the tendency for low viscosity to flow back out of the foam carrier. This effect of slip run-out was referred to as slumping.

Drying Effects

Drying was shown to be a key issue with all the impregnation based methods and indeed with the coated foam method. The radical effect drying conditions can have on the outcome was clearly demonstrated by the image analysis and compression testing of the

impact impregnated materials. It was clear from the work on drying that the tissue method was the superior method as it produced a stronger and more uniform material, with less void based porosity than the mesh drying method.

The poor performance of mesh drying technique was attributable to two main effects. The first of these was excessive slumping due to the slow extraction of the excess water in the system by comparison with the fast wicking tissue method. This allowed the slip a greater degree of mobility for a longer period resulting in migration of the slip out of the foam. The second effect was that of the contraction of the drying green body being restricted by the base of the material adhering to the support mesh. This effect was compounded by the protrusion of the migrating slip through the support mesh. These effects combined to produce the poorly impregnated structures shown in Figure 44.

Vacuum Impregnation

The move from impact impregnation to vacuum pressure impregnation represented an attempt to improve the reproducibility of the process, and to increase the overall degree of impregnation achieved. The first requirement with the process change was the need to adapt a vacuum impregnation chamber for the purpose. The use of a mesh stand and retaining clip were the main adaption put in place for the method to work. These features allowed slip ingress into the foam from all directions.

Maximising the ease with which the slip could penetrate into the foam carrier was the main problem associated with the vacuum impregnation methods. This was the case as slip viscosity was found to be dictated by the need to avoid slumping of the green body in drying offset against the tendency for the foam to crush under the pressure of the slip ingress. This crushing occurred where the evacuated foam was not stiff enough to resist the pressure of the inflowing slip on the reintroduction of atmospheric pressure. Once the core of the foam had buckled in this manner it was held in place by the viscosity of the slip. This lead to the formation of foam rich veins in the centre of the green body, which on burnout resulted in a region of high porosity.

When a lower viscosity slip was used, slumping of the green body was problematic. Therefore control of slip viscosity and rapid removal of excess water were critical in the process. Ultimately the effectiveness and reproducibility of this method were limited by the sensitivity of the process to these factors.

Double impregnation

The double impregnation method was developed to reduce the sensitivity of the process to the crushing and slumping effects discussed above. The stage of tissue drying after the first impregnation removes the excess water from the foam/slip body. This has the effect of concentrating the powder loading of slip and reducing its mobility. Therefore on the introduction of the second stage slip the total water fraction combined impregnations is reduced and with it the overall slip mobility. This effect reduces the tendency of the slip to slump without increasing the viscosity of the slip and thereby the tendency to crush the foam.

Re-evacuation for the second impregnation step assists in removing any crushing introduced in the first impregnation. Further to this effect, the presence of partially dried slip within the foam may act to stiffen the structure, leading to a reduction or elimination of crushing in the second stage.

Resultant material

The materials produced by the double impregnation method differed from previous materials in two noticeable ways. Firstly the consistency with which these materials could be produced was far superior to any materials previously produced or characterised in the project. This consistency manifested itself in the uniformity of macroporosity distribution within the sample and also across a batch of samples produced with the same input materials. This consistency of behaviour and uniformity of macroporosity distribution was also reproducible from batch to batch.

One of the main reasons for this reproducibility was that the macroporosity in the structure was produced solely by the burnout of the organic foam. As the foam content and structure could be fixed this allowed greater levels of control than were previously possible. One of the ramifications of the elimination of voidage due to incomplete impregnation was the generated structure was of a higher density than those previously produced, with a macropore volume of 4.5-5%.

As the pore structure was generated entirely by the burnout of the foam a completely interconnected network of pores can be assured. Also as the size and volume of the porosity was dictated by the input foam this presents the possibility of selecting or creating foams to produce a specific pore size and pore volume tailored for specific applications. The structural variations possible through foam choice and manipulation of the organic foam prior to impregnation will be discussed in more detail in the section on future work.

As a result of the high levels of impregnation achieved the compressive strength was found to be far greater than those previously achieved in the project. This capacity for load bearing opens up potential applications for the material in loaded environments where, in accordance with Wolff's law, the rate of osteoblast and osteoclast activity is know to be higher[22]. The robust nature of the materials produced by this method facilitated cutting and grinding of the material to form shaped components.

4.5 XRD Results

X-ray analysis was utilised in the project to establish the phase composition of the input powders and also to demonstrate the thermal transformation of the unstable materials so as to establish a basis on which input powder mixes could be selected to produce a sintered material in which the phase composition was conducive to osteoconduction. By understanding the relationship between input powders, sintering temperatures and resultant phase compositions, materials could be designed to exhibit widely differing resorption rates.

4.5.1 Qualitative

The qualitative analysis of the input powders demonstrated the difference between the two main powder grades used in the work. The grade 130 material was shown to be a highly stable HA which did not undergo any detectable change in phase composition on thermal treatment at 1280°C. This was an unusual degree of stability as some degradation of the HA to α–TCP would be expected at this temperature. The only significant change noted in the material on heat treatment was the apparent increase in crystallinity observed as an increase in the intensity of the HA reflections with regard to the level of background radiation.

The grade 118 powder was shown to be a low stability material, primarily HA, which underwent complete thermal transformation to a high crystallinity β–TCP on heating to 1150°C. Further heating to 1280°C resulted in the transformation of a fraction of this β–TCP to α–TCP. This behaviour would indicate that the grade 118 material as-received was a calcium deficient HA (Ca-def HA). These materials are know to transform at temperatures above 900°C to produce β–TCP and water[77].

From the results of the qualitative analysis the HA/β–TCP composition of any final sintered materials can be largely predetermined by the appropriate selection of the starting powder blend and sintering temperature. From the XRD analysis of the grade 118 and grade 130 input powders it can be seen that, on heating, these materials form high

crystallinity β–TCP and HA respectively. Therefore the HA/β–TCP composition of a sintered product will be roughly equal to the grade130/grade 118 composition of the starting powder blend. This relationship holds true until the formation of α–TCP from the degradation of the β–TCP at the higher sintering temperatures. From Figure 18 it can be seen that in the grade 118 material sintered for four hours at 1280°C, the generation of α–TCP was not accompanied by a marked decrease in the β–TCP peak height. This indicates that the quantities of α–TCP produced under these sintering conditions were low.

Should significant quantities of α–TCP be required in the material this could be generated by sintering the grade 118 material at higher temperatures for an extended period. The limitation on the amount of α–TCP which could feasibly introduced in this manner would appear to be the stability of the HA at high temperature and the sintering times required to produce significant quantities of α–TCP.

4.5.2 Quantitative

The use of the internal standard method was instigated in an attempt to directly establish the HA/TCP composition of the final sintered materials rather than by inference from a knowledge of the mix of input powders combined with their established behaviour on heating. This ability to directly establish composition would have been useful in the analysis of other related materials for purposes of comparison.

The construction of a calibration curve was carried out to quantify the mass adsorption effects as discussed in the introduction. There are a number of commonly used internal standard materials, anatase TiO_2 was chosen in this case as it possessed small number of clear peaks which occur in the scan range most useful in chacterisation of HA and TCP. These peaks did not overlap with any of the significant peaks from HA or β–TCP. A further advantage of TiO_2 as an internal standard was its availability in a high purity form. To construct the calibration curve a pure HA ex- Howmedica was used and a high purity β–TCP supplied by Plasma Biotal as external reference powders.

The β–TCP behaved as expected showing a great deal of similarity with the β–TCP produced by heat treatment of the grade 118 material at 1150°C. The behaviour of the HA ex-Howmedica however was found to be radically different to the HA Grade 130. As this sintering behaviour differed from that seen in the grade 130 material it was prudent to assume there to be structural differences between these two powders. It was therefore only valid to consider the HA component of the calibration materials as a standard dilutant for

the β–TCP in the construction of the calibration curve. Given this, the internal standard as used could only give meaningful data on the β–TCP concentration in the unknown samples.

It was found that the mass fraction of β–TCP in the unknown materials, as determined by the internal standard method, was in conflict with composition predicted from the composition of the input powders. The low response of both the HA and β–TCP peaks in the samples sintered at 1150°C were anomalous, being less than half that predicted by the qualitative analysis. In the material sintered at 1280°C, generation of α–TCP would account for a reduction in the amount of β–TCP present though, from the qualitative assessment of the β–TCP, it would not appear likely to have as dramatic an effect as indicated by the quantitative XRD.

One possible explanation for the apparent low β–TCP response in the material produced at 1280°C was the possible overlap of one of the α–TCP peaks with the main marker peak of the TiO_2 . This would have resulted in an amplification of the marker peak strength thus skewing the apparent ratio of marker to sample.

At this point no definitive explanation is available to account for the large discrepancy between the predicted values for β–TCP mass fraction, and those measured by the internal standard method. Some error may have been introduced by a disparity in the particle size of the marker powder and the ground unknown. This may have been compounded by poor mixing of the unknown and the internal standard. To overcome these effects ball milling of the powders in a suitable media may have been effective.

Further inaccuracy may have been introduced due to the approximations made in fitting a line on the calibration curve. These errors can be reduced by constructing a calibration curve with a greater number of standard dilutions and running XRD a number of times on these dilutions to build a more statistically valid curve.

As XRD is a statistical method based on collection of a large number of emitted X-rays, the greater the number of counts recorded, the better the validity of the pattern acquired. Therefore to improve accuracy and resolution a larger number of counts should be collected at each scan step and the scan step reduced. This translates to longer scanning times per degree of scan arc covered. Realistically therefore to improve the accuracy of each sample scan a smaller area of interest can be selected and scanned with greater resolution. This was carried out on the standard dilutions, but it would also have been

valuable to do the same for the determination of the phase composition in the unknown materials.

4.6 Assessment of Materials' Potential as a Bone Substitute

To judge the success of the developed process it was necessary to assess the likely suitability of the double impregnation material for use as a bone substitute material. As the use of *in vivo* trials and *in vitro* cell work were beyond the scope of this work, assessment of suitability was limited to comparison of the properties of this candidate material to those of successful materials reported in the literature.

Factors likely to effect the materials performance as a bone substitute material were pore structure, phase composition and mechanical properties.

4.6.1 Porosity

To assess the likely effectiveness of the porosity of the material in encouraging bone ingrowth a comparison was made between the pore structure present and those reported to be effective in other materials.

In the work reported by Lu *et al*[39] into the effect of pore interconnection size on bone ingrowth into porous osteoconductive materials it was suggested that a range of pore sizes were important for effective osteoconduction. These pore size ranges were; 1-10μm to allow ingrowth of cells, 15-50μm to allow fibrous ingrowth and vascularisation , 150-300μm to allow ingrowth of bone. Though interconnected pores as small as 50μm were found to allow bone ingrowth. Interconnections of porosity were found to be critical with an interconnection size of 50μm shown to allow minerialised bone formation in the connected macropores.

It can be seen from the image analysis of the 20ppi based double vacuum impregnated foam that almost half of the porosity in the material has an area equivalent diameter in the range 150-500μm. This porosity was 100% interconnected due to the nature of the burnout process which created it. The size of the interconnections can be assumed to be in excess of 50μm as none of the macropore features found in the material were below this size. This large scale interconnection of pores was an artefact of the foam burnout process and as a result was dependent solely on the structure of the base foam.

The 30ppi based material also shows an interconnected porosity in the required size range. However with this material there are fewer numbers of the larger pores present, as would be expected.

From the SEM images of these materials it was clear that the pore shape was not spherical and therefore the sizes quoted were area equivalent diameters. It is therefore probable that the effective pore diameter as regards bone ingrowth will be smaller than this figure. The effect of the distinctive pore shape on the osteoconductive properties of the material has yet to be assessed.

The drawback of the material was its low macropore volume fraction, being in the range of 4.5-5%. The effect of such a low overall porosity in a bone substitute material has not been established where the macroporosity is so highly interconnected. In all previous studies of low porosity materials the pore volume has been largely isolated. *In vivo* trials may be required to establish if overall macropore volume or macropore interconnection is the key requirement for bone ingrowth.

4.6.2 Phase Composition

In looking at the possible effects of phase composition on the *in vivo* performance of the new material consideration must be given to the work by Oonshi *et al*[27] and by Hench[41] on the osteoconductive effectiveness of HA discussed in the introduction. This work demonstrated the ability of new bone to bond directly to implanted HA material and the ability of HA to form a bioactive surface layer *in vivo*. Also, as part of this work, the long term stability of HA has been established, with resorption being shown to occur as a slow, cell mediated, process. In contrast to relatively stable HA, the bioactive effects of TCP are characterised by dissolution *in vivo* resulting in localised concentrations of Ca and P ions which were found to stimulate new bone growth[38][27]. This may in some instances lead to a situation where implant material is resorbed before substantive bone ingrowth can be established[31].

The biphasic composition of the new material attempts to provide the stimulation of osteoclastic activity by the production of a Ca and P rich region, caused by the TCP dissolution, while providing a stable HA scaffold onto which new bone can grow. This approach has been shown[45] to produce an enhanced biological response as compared with single phase HA material or TCP. The proposed mechanism for this enhanced response comprises the dissolution of the β-TCP which reprecipitates onto the stable HA as carbonatehydroxyapatite, bringing with it proteins from the biological fluid. This reprecipitated material has been shown to enhance the formation of new bone. The combination of the stable HA substrate with the carbonatehydroxyapatite precipitate coupled with the increased osteoblast activity due to the high concentration of Ca and P in the microenviornment lead to an enhanced osteoconductive response[45][44].

In addition to its biochemical effects, the dissolution of the TCP will result in an increase in the pore and interconnection size of a porous biphasic material, the result of which is a porous HA structure with high local concentrations of Ca and P[46]. The increased interconnection size should promote bone ingrowth as detailed in the discussion on porosity above. The dissolution rate of biphasic HA/β-TCP has been shown to be lower than that of single phase β-TCP material. In the study by Ke *et al*[45] the biphasic material showed a steady state dissolution of Ca and P, more akin to that of HA than of β-TCP. In a 50:50 HA/β-TCP material the dissolution rate was found to be approximately twice as high as that of the single phase HA. The dissolution rate of the biphasic material will depend heavily on the ratio of HA and β-TCP present. This steady state dissolution and dependence on phase composition will allow predictable response minimising the risk of implant adsorption prior to the establishment of viable bone ingrowth[31].

In the animal work reported by Blom *et al*[40] the *in vivo* performance of a material with a markedly similar phase composition to that being discussed here was shown to promote extensive bone ingrowth. This demonstrated the usefulness of biphasic HA/β-TCP materials in a bone graft extender applications. In related work consideration was given to the possible effect of the materials phase composition on dissolution rate *in vivo*, and thus mechanical stability of the impacted graft[73].

It should be noted however that the process developed in this project is capable of producing a full range of HA/β-TCP materials from single phase HA through to single phase β-TCP by the selection of the appropriate input powders and sintering conditions. Selection of the required composition should be based on the proposed application to achieve the optimum balance of enhanced osteogeneic potential and resorption against the requirements for long term stability.

4.6.3 Physical Properties

From the results of the compression testing it can be seen that double vacuum impregnation method produced far stronger materials than those produced by the impact impregnation method. This increase in strength was expected as the density of the material was greatly increased. This strong dependence of the material strength on density is consistent with the work by Le Huec *et al*[78] and Hing *et al*[35] on porous calcium phosphate materials. With the improved reproducibility of impregnation noted using the double

vacuum impregnation technique the scatter in the compressive strength due to variations in density should be minimised.

The impact impregnated materials were found to have compressive strengths in the range of 1-20 MPa, with a strong correlation between compressive strength and density, as shown in Figure 70. These results show a marked similarity to those obtained by Hing, Best and Bonfield[35] in their study of the compression testing of denatured bovine cancellous bone in the form of Endobon. In this case they found that material to show compressive strengths in the range of 2-10 MPa depending of material density, varying over a range of densities similar to those produced in the impact impregnated materials.

The strengths obtained from the impact impregnated materials also compares favourably with the values quoted for human cancellous bone from the distal femur of 1.8-9.4 MPa[20]. With the exception of some of the poorly produced samples, the compressive strengths exceed the requirements placed on coralline material of 2.2 MPa for use in spinal fusion applications[62].

These strengths compare favourably with the results obtained from other methods used to produce HA structures with an interconnected porosity. The mixed materials method outlined by Li *et al* [79] produced materials with a strength of approximately 6 MPa and the Sol-Gel route of Sepulveda *et al*[58] resulted in materials with strengths of 1.5-5 MPa. Early reticulated foam methods of producing porous HA resulted in similarly low values of compressive strength[59], though later improvements in the method have produced materials with strengths comparable to those produced in the impaction impregnated materials[61].

The compressive strengths achieved by the double vacuum impregnated materials were far in excess of those seen in cancellous bone, but fell far short of the 133-295 MPa typical of the UCS of human cortical bone[20]. The double vacuum impregnation route can be seen to have greatly improved the strength and reliability over the impact impregnated material while maintaining the interconnected pore structure. Of the materials currently available, the most direct comparison could be made with the materials produced by Richart *et al*[53][54] utilising pressed polymer spheres to generate an interconnected pore structure in sintered HA. This material had compressive strengths in the range of 9-25 MPa depending on macropore size.

The mechanical response of both the impact and double vacuum impregnated materials was radically different from that found in cancellous or cortical bone as the synthetic material lacked the viscoelastic elements present in the form of collagen in the natural bone. The testing in this instance was limited to compression testing but given the brittle

nature of the synthetic material it is likely that it would not compare as well to natural bone when tested in bending. The brittle nature of the synthetic material was obvious from its failure mode and fracture surfaces, however due to issues of machine softness associated with the compression testing rig no useful data of strain at failure or energy to fracture could be obtained.

The comparative strength of the double vacuum impregnated material allowed easy handling and machining of the material. With the use of standard ceramic cutting and grinding equipment the manufacture of simple geometric shapes from this material was easily achieved. In addition to the large number of cubic samples produced for compression testing a number of wedges and disc shapes were produced from these materials to demonstrate the kind of components that could be produced.

As the overall shape of the samples produced by this method was strongly dependent on the shape of the input foam it is envisaged that, with due consideration for shrinkage, near net forming of some components could be achieved by pre-cutting of the base foam. Cutting of the foam was easily achieved with hot blades or hot wires during the project. The material could also be produced in a granular form by either crushing larger blocks of the sintered materials or by impregnating small irregular pieces of base foam in the first instance. Investigation of the feasibility of both of these methods for the production of a granular material is proposed in the section on future work.

4.7 Potential Applications

The potential applications for this material as a bone substitute material are numerous. As outlined in the introduction a large number of orthopaedic procedures rely on the use of graft material for their success. The current material may provide an alternative to the allograft and autograft currently used in the majority of these applications.

In a crushed or granulated form the material could see application in impaction grafting, supplementing or replacing allograft as is currently the case with the BoneSave material. The mechanical strength of the material would be a benefit in this application as the security of the initial fixation is a key issue in recovery of function.

In its bulk form the ability of the material to be machined to shape presents the possibility of its use in corrective orthopaedic procedures, such as spinal fusions, where the use of a shaped component could greatly simplify the procedure. This would also be true in the case of large bone defect filling, or in such support structures as scarps, which are currently produced using allograft in conjunction with elaborate mesh structures[10]. The current

material presents the potential to replace these constructions with a shaped ostoeconductive implant.

In a similar vein, the use of a shaped implant in maxillofacial and crainofacial reconstruction or correction could greatly reduce the current dependence on allograft and autograft and greatly simplify the procedures used[8]. In the case of maxillofacial usage the load bearing capacity of the material could be useful promoting the rapid return of function limiting the discomfort to the patient often imposed by the necessity to wire the jaw.

The material also demonstrates a potential for use as a drug delivery system as the high surface area produced by the microporosity coupled with calcium phosphates affinity to binding with proteins should allow effective drug loading into the material, with the β-TCP dissolution presenting a control mechanism for drug release rate[80][48]. The drugs delivered by this system could be bone morphogenic proteins (BMP's) for stimulation of bone regeneration, or in the case of the work by Landi *et al* [80], anti-cancer drugs for targeted chemotherapy.

5 Conclusion

5.1 Effectiveness of process

In evaluating the success of the process in the production of a synthetic bone substitute material the following outcomes were considered:

- The process allows the control of pore size and pore interconnection by the selection of the base foam used.
- The pore structure and pore volume were dependent solely on the burnout of the organic foam and were thus reproducible in a reliable manner.
- Pore size distribution produced by the 30ppi and 20ppi base foams compared favourably to those reported to promote bone ingrowth in HA/TCP materials.
- Generation of a high degree of microporosity in the product material improves bioactive potential and increases the potential usefulness of the material as a drug delivery system.
- The phase composition of the resultant material can be controlled by selection of input powder ratios and sintering temperatures to maximise the bioactive potential of the HA/TCP materials.
- The materials produced were mechanically robust allowing their use in loaded environments. This mechanical strength also allowed easy handling and machining of the product materials.
- Due to the interconnected structure of porosity and slow heating rate used in sintering, the burnout of the organic foam was assured. Selection of the foam and dispersant used ensured that no metal impurities were residual in the sintered material.

5.2 Limitations of process

The limitations of the method as carried out in this work were seen to be as follows:

- The overall macropore volume was low by comparison with other available bone substitute materials.
- The pore shape produced by the burnout of the reticulated foam was not circular and therefore may not perform as effectively as circular porosity of the equivalent area.

These limitations of the method were associated with the foam used as a porosifer in this study. Selection of other foam structures may result in achieving a higher pore volume fraction and a more circular pore cross-section. However changing the base used will have dramatic effects on the other variables required to successfully produce the material. The potential use of alternative base foams is examined in the section on further work.

5.3 Overall outcome

The project was successful in developing a method whereby mechanically biphasic calcium phosphate ceramic materials could be produced with an interconnected pore structure suitable for use as a synthetic bone graft substitute. Additionally the flexibility and scalability of the process should allow manufacture of implant materials with a pore structure and phase composition tailored to their specific application.

6 Future Work

From the points raised in the discussion section it is clear that a great deal of further work can be carried out in this area of research before it is exhausted. In the first instance there are issues of further characterisation of the existing material to better understand its phase composition and better predict its performance in use.

The flexibility of the process allows for a large number of modifications. In particular the reliance of the materials' form on the shape and pore structure of the organic foam allows a large number of variations to be explored

6.1 Further characterisation work

6.1.1 Re-run XRD internal standard

From the comparison between the results of the quantitative XRD and the expected outcome from the qualitative XRD it can be seen that the use of the internal standard method produced some anomalous results. Therefore it is proposed that the construction of the calibration curve by standard dilution be repeated.

To improve the reliability of the repeat calibration curve the HA for use in the standard dilutions should be produced by heat treating the grade 130 material at 1150°C for four hours as this has been shown to produce a high purity and high crystalinity HA. To minimise errors arising from variations in particle size and non-homogeneous mixing of the powders it is proposed that all the standard dilutions be ball milled after weighing.

To greatly improve the statistical validity of the calibration curve it is proposed that a greater number of standard dilution compositions be made up, and the number of scans of each dilution increased. To improve the validity of each scan, the scan range should be confined to the specific areas of interest, with more counts being taken for these areas.

Additionally, to eliminate the possibility interference between the internal standard and transformation products in the sintered materials the choice of internal standard should be re-examined.

6.1.2 *In vitro* dissolution studies

To determine the dissolution behaviour, and its effect on material porosity with time, *in vitro* studies in simulated physiological fluid could be performed. To best ascertain the dissolution behaviour the calcium and phosphate ion concentration in the system should be monitored over time for materials sintered at both 1150°C and 1280°C. In addition to a

measure of the dissolution rate, careful analysis of the pore structure of the materials should be made before and after long term exposure to simulated physiological fluid, to determine whether the predicted increase in porosity does occur.

6.1.3 Drug release

In a related area, the potential for the materials' application as a drug delivery system should be assessed. A study similar to that carried out by Landi *et al*[80] should be performed to assess the drug carrying capability of the material and its release rate in simulated physiological fluid to evaluate the materials usefulness as a drug delivery system.

6.1.4 *In vivo* studies

Ultimately any proposed bone substitute material must have demonstrated its ability to perform its stated function *in vivo*. Therefore a number of the most promising potential applications should be identified for trial in animal studies.

6.2 Process modifications

6.2.1 Functional gradient

By impregnating, drying and sintering two or more differing base foams, held in intimate contact through the process, it should be possible to produce a sintered article in which the pore structure varies radically across the junction of the base foams. Ensuring intimate contact between the different base foams will require mechanical fixation or that one foam is press fit into the other.

Gradual variation in porosity through the ceramic material can be similarly achieved by heat setting foam wedges where the higher density of foam struts will produce a higher porosity.

6.2.2 Anisotropy

Anisotropy could be introduced into the sintered materials by stretching and heat setting the base foam. This should introduce directionality in the macropore structure of the sintered materials. This ability to influence the directionality of the macroporosity in the structure will produce a more anisotropic mechanical, more analogous to that of natural bone.

6.2.3 Change of input foam morphology

As the pore structure and pore shape in the sintered material is inherently linked to the shape and distribution of the polymer struts in the base foam, changing the base foam will allow different structures to be produced. Work should be carried out to establish the effects of using other organic foam structures with this technique to produce a variety of materials. It should be noted that changing the base foam may have subsequent effects on, for example, the drying and sintering process, so that the process may have to be significantly altered to accommodate these new support structures.

6.2.4 Shaped components by near net forming

The production of shaped components by near net forming could be established by pre-cutting base foam to shape prior to impregnation and sintering. This would require the quantification of the shrinkage in the process so that the size of the foam pre-cut could be established. One of the simplest applications of this type of process would be the production of granular materials by pre-cutting small irregular pieces of foam, prior to impregnation and sintering to produce a granular material with a highly interconnected macroporosity.

7 References

1: G. A. Gie, L. Linder, R. S. M. Ling, J-P. Simon, T. J. J. Slooff, A. J. Timperly. (1993). Impacted cancellous allografts and cement for total hip arthoplasty. *J. Bone Jt. Surg.* ,75-B No. 1, pp. 14-21.

2: G. Galea, D. Kopman, B. J. M. Graham. (1998). Supply and demand of bone allograft for revision hip surgery in Scotland. *J. Bone Jt. Surg.* ,80-B No. 4, pp. 595-599.

3: J. O. Hollinger, J. Brekke, E. Gruskin, D. Lee. (1996). Role of bone substitutes. *Clin. Orthop. Relat. Res.* , No. 324, pp. 55-65.

4: J. K. Kelly. (1973). Maxillofacial missile wounds: Evaluation of longterm results of rehabilitation and reconstruction. *J. Oral Surg.* ,31 , pp. 438-445.

5: L. F. Peltier. (1961). The use of plaster of paris to fill defects in bone. *Clin. Orthop. Relat. Res.* , No. 21, pp. 1-31.

6: K. H. Karlson, H. Ylanen, H. Aro. (2000). Porous bone implants. *Ceram. Int.* , No. 26, pp. 897-900.

7: F. J. Hornicek, W. Mnaymneh, R. D. Lackman, G. U. Exner. (1998). Limb salvage with osteoarticular allografts after resection of proximal tibia bone tumors. *Clin. Orthop. Relat. Res.* , No. 352, pp. 179-186.

8: A. Nataloni, R. Martinetti, G. Staffa, F. Servadei, C. Piconi. (2001). Porous hydroxyapatite custom made implants for cranioplasty: Two years of clinical experience. *Bioceramics* ,13 , pp. 881-884.

9: A. O. Ransford, T. Morley, M. A. Edgar, P. Webb. (1998). Synthetic porous ceramic compared with autograft in scoliosis surgery. *J. Bone Jt. Surg.* ,80-B No. 1, pp. 13-18.

10: H. Oonishi. (1991). Orthopaedic applications of hydroxyapatite. *Biomaterials* ,12 No. 2, pp. 32-40.

11: J. J. Callaghan. (1992). Total hip arthoplasty; Clinical perspective. *Clin. Orthop. Relat. Res.* , No. 276, pp. 33-40.

12: H. Malchau, P. Herberts. (1998). Prognosis of total hip replacement 1998. *65th Meet. Amer. Acad. Ortho. Surg.* .

13: G. A. Gie, R. S. M. Ling, A. J. Timperley, T. J. J. H. Slooff, J. W. M. Gardeniers, B.

W. Scheurs. (1999). *X-change revision instruments system: Operative technique.* Stryker Howmedica Osteonics .

14: S. S. Leopold, A. G. Rosenberg. (1999). Current status of impaction allografting for revision of a femoral component. *J. Bone Jt. Surg.* ,81-A No. 9, pp. 1337-1345.

15: R. P. Pitto. (2001). Bone graft substitutes for acetabular reconstruction in revision total hip arthoplasty. *Bioceramics* ,13 , pp. 947-950.

16: R. Fitzpatrick, E. Shortall, M.Sculpher, D. Murray, R. Morris, M. Lodge, et al. (1998). Primary total hip replacement surgery: A systematic review of outcomes and modelling of cost effectiveness. *Health Technology Assessment* , 2 No. 20.

17: J. Black. (1988). *Orthopaedic Biomaterials in Research and Practice.* Churchill Livingstone .

18: SEER's training web site. (15/01/03). *illu_compact_spongy_bone.jpg [online image].* http://training.seer.cancer.gov/module_anatomy/

19: A. Spence. (1990). *Basic Human Anatomy.* Benjamin/Cummings.

20: S.C. Cowin. (2001). *Bone Mechanics Handbook.* 2nd Ed. CRC Press.

21: L. J. Gibson, M. F. Ashby. (1999). *Cellular Solids : Structure and properties.* 2nd Ed. Cambridge University Press.

22: S. J. Hall. (1991). *Basic Biomechanics.* 1st Ed. McGraw & Hill.

23: K. A. Hing, S. M. Best, K. E. Tanner, W. Bonfield, P. A. Revell. (1999). Quantification of bone ingrowth within bone-derived porous hydroxyapatite implants of varying density. *J. Mater. Sci. : Mater. Med.* , 10, pp. 663-670.

24: D. C. Fredericks, J. A. Bobst, E. B. Petersen, J. V. Nepola, B. Heckendorf, B. Norberg, Y. Ko. (2002). Segmental bone defect repair using sintered porous ceramics. *Bioceramics* ,14 , pp. 409-412.

25: K. A. Hing, S. M. Best, K. E. Tanner, W. Bonfield, P. A. Revell. (1997). Biomechanical assesment of bone ingrowth in porous hydroxyapatite. *J. Mater. Sci. Mater. Med.* , 8, pp. 731-736.

26: J. Black. (1999). *Biological Performance of Materials - Fundamentals of Biocompatibility.* 3rd Ed. Marcel Dekker

27: H. Oonishi, L. L. Hench, J. Wilson, F. Sugihara, E. Tsuji, S. Kushitani, H. Iwaki. (1999). Comparative bone growth behaviour in granules of bioceramic materials of

various sizes. *J. Biomed. Mater. Res.* ,44 No. 1, pp. 31-43.

28: T. W. Bauer, S. T. Smith. (2002). Bioactive materials in orthopaedic surgery: Overview and regulatory considerations. *Clin. Orthop. Relat. Res* , No. 395, pp. 11-22.

29: E. D. Arrington, W. J. Smith, H. G. Chambers, A. L. Bucknell, N. A. Davino. (1996). Complications of illiac crest bone graft harvesting. *Clin. Orthop. Relat. Res.* , No. 329, pp. 300-309.

30: B. E. Buck, T. I. Malinin. (1994). Human bone and tissue allograft, preparation and saftey. *Clin. Orthop. Relat. Res.* , No. 303, pp. 8-17.

31: K. J. L. Burg, S. Porter, J. F. Kellam. (2000). Biomaterial developments for bone tissue engineering. *Biomaterials* ,21 , pp. 2347-2359.

32: G. Guillemin, J. Foutnie, J. Patat, M. Chetail. (1987). The use of coral as a bone graft substitute. *J. Biomed.Mater. Res.* ,21 , pp. 557-567.

33: H. Ohgushi, M. Okumura, T Yoshikawa, K. Inoue, N. Senpuku, S. Tamai. (1992). Bone formation process in calcium carbonate and hydroxyapatite. *J. Biomed. Mater. Res.* ,26 , pp. 885-895.

34: G. S. Johnson, M. R. Mucalo, M. A. Lorier. (2000). The processing and characterization of animal derived bone to yield materials with biomedical applications. *J. Mater. Sci. : Mater. Med.* , 11, pp. 427-441.

35: K. A. Hing, S. M. Best, W. Bonfield. (1999). Characterisation of porous hydroxyapatite. *J. Mater. Sci. Mater. Med.* , 10, pp. 135-145.

36: A. Uchida, S. Nade, E. McCartney, W. Ching. (1987). Growth of bone marrow cells on porous ceramics in vitro. *J. Biomed. Mater. Res.* ,21 , pp. 1-10.

37: C. A. van Bitterswijk, S.C. Hesseling, J. J. Grote, H. K. Koerten, K. de Groot. (1990). The biocompatibility of hydroxyapatite ceramics: A study of retrieved human middle ear implants. *J. Biomed. Mater. Res.* ,24 , pp. 433-453.

38: C. P. A. T. Klein, A. A. Driessen, K. de Groot. (1983). Biodegradation behaviour of various calcium phosphate materials in bone tissue. *J. Biomed. Mater. Res.* ,17 , pp. 769-784.

39: J. X. Lu, B. Flautre, K. Anselme, P. Hardouin, A. Gallur, M. Descamps, B. Thierry. (1999). Role of interconnections in porous bioceramics on bone recolonisation in vitro and in vivo. *J. Mater. Sci. Mater. Med* , 10, pp.111-120.

40: A. Blom, J. Cunningham, T. Lawes, G. Hughes, A. Goodship, I. Learmont. (2000). TCP/HA mixtures as bone allograft expanders in revision THA of the femur: An ovine study. *Bioceramics* ,13 , pp. 377-382.

41: L. L. Hench. (27/11/02). *Bioactice glasses: Mechanisim of bioactive bonding.* www.bg.ic.ac.uk/Lectures/Hench/Bioglass /cal3.html

42: S. Kotani, Y. Fujita, T. Kitsugi, T. Nakamura, T. Yammamuro, C. Ohtsuki, T. Kokubo. (1991). Bone bonding mechanisim of beta-tricalcium phosphate. *J. Biomed. Mater. Res.* ,25 , pp. 1303-1315.

43: Li Yubao, Zhang Xingdong, K. de Groot. (1997). Hydrolysis and phase transformation of alpha-tricalcium phosphate. *Biomaterials* ,18 No. 10, pp. 737-741.

44: R. Z. LeGeros. (2002). Properties of osteoconductive biomaterials: Calcium phosphates. *Clin. Orthop. Relat. Res.* , No. 395, pp. 81-98.

45: S. Ke, I. R. Gibson, K. A. Hing. (2002). Characterisation of mono- and biphasic calcium phosphates granules. *Bioceramics* ,14 , pp. 625-628.

46: C. N. Cornell, J. M. Lane. (1998). Current understanding of osteoconduction in bone regeneration. *Clin. Orthop. Relat. Res.* , No. 355s, pp. s267-s273.

47: S.F. Hulbert, J.S. Morrison, J. J. Klawitter. (1972). *J. Biomed. Mater. Res.* , No. 6, 347-358.

48: H. Yuan, J. D. de Bruijn, X. Zhang, C. A. van Blitterswijk, K. de Groot. (2001). Use of an osteoinductive biomaterial as a bone morphogenetic protein carrier. *J. Mater. Sci. Mater. Med.* , 12, pp. 761-766.

49: T. R. Shrout, W. A. Schulze, J. V. Biggers. (1979). Simplified fabrication of PZT/polymer composites. *Mater. Res. Bull.* ,14 , pp. 1553-1559.

50: Dean-Mo Lui. (1996). Fabrication and characterization of porous hydroxyapatite granules. *Biomaterials* ,17 No. 20, pp. 1955-1957.

51: Dean-Mo Lui. (1997). Fabrication of hydroxyapatite ceramic with controlled porosity. *J. Mater. Sci. Mater. Med.* , 8, pp. 227-232.

52: K. O'Kelly, D. Tancred, B. McCormack. (1996). A quantative technique for comparing synthetic porous hydroxyapatite structures and cancellous bone. *J. Mater. Sci. Mater. Med.* , 7, pp. 207-213.

53: O. Richart, M. Descamps, A. Liebetrau. (2001). Macroporous calcium phoshpate

ceramics : Optimization of the porous structure and its effects on the bone ingrowth in a sheep model. *Bioceramics* , 13 , pp. 425-428.

54: O. Richart, M. Descamps, A. Liebetrau. (2002). Preparation and mechanical characterization of hydroxyapatite monodispersed macroporous structure.. *Bioceramics*, 14 , pp. 9-12.

55: J. G. Binner, J. Reichert. (1996). Processing of hydroxyapatite ceramic foams. *J. Mater. Sci.* , 31 , pp. 5717-5723.

56: J. G. Binner. (1997). Production and properties of low density engineering ceramic foams. *British Ceramic Transactions* , 96 No. 6, pp. 247-249.

57: M. Fabbri, G. C. Celotti, A. Ravaglioli. (1994). Granulates based on calcium phosphate with controlled morphology for medical applications: Physico-chemical parameters and production technique. *Biomaterials* , 15 No. 6, pp. 474-477.

58: P. Sepulveda, A. H. Bressiani, J. C. Bressiani, L. Meseguer, B. Konig Jr.. (2002). Synthesis and properties of ceramic foams for hard tissue repair. *Bioceramics* ,14 , pp. 413-416.

59: M. Fabbri, G. C. Celotti, A. Ravaglioli. (1995). Hydroxyapatite-based porous aggregates: physico-chemical nature, structure, texture and architecture. *Biomaterials* ,16 No. 3, pp. 225-228.

60: F. R. Cichocki, K. P. Trumble. (1998). Tailored porosity gradients via colloidal infiltration of compression-moulded sponges. *J. Am. Ceram. Soc.* ,81 No. 6, pp. 1661-1664.

61: Jintao Tian, Jiemo Tian. (2001). Preparation of porous hydroxyapatite. *J. Mater. Sci.* ,36 , pp. 3061-3066.

62: D.C. Tancred, A. J. Carr, B. A. O. McCormack. (1998). Development of a new synthetic bone graft. *J. Mater. Sci. Mater. Med.* , 9, pp. 819-823.

63: G. de With, H. J. A. van Dijk, N. Hattu, K. Prijs. (1991). Preparation, microstructure and mechanical porperties of dense polycrystalline hydroxyapatite. *J. Mater. Sci.* ,16 , pp. 1592-1598.

64: M. Akao, H. Aoki, K. Kato. (1981). Mechanical properties of sintered hydroxyapatite for prosthetic applications. *J. Mater. Sci.* ,16 , pp. 809-812.

65: P. Wang, T. K. Chaki. (1994). Sintering behaviour and mechanical properties of hydroxyapatite and dicalcium phosphate. *J. Mater. Sci. Mater. Med.* , 5, pp. 150-158.

66: P. van Landuyt, F. Li, P. Keustermans, J. M. Streydio, F. Delannay, E. Munting. (1995). The influence of high sintering temperatures on the mechanical properties of hydroxyapatite. *J. Mater. Sci. : Mater. Med.* , No. 6, pp. 8-13.

67: J. D. Santos, P. L. Silva, J. C. Knowles, S. Talal, F. J. Monteiro. (1996). Reinforcement of hydroxyapatite by adding P_2O_5-Ca glasses with Na_2O, $K_2O$and MgO. *J. Mater. Sci. Mater. Med.* , 7, pp. 138-143.

68: J. C. Knowles, S. Talal, J. D. Santos. (1996). Sintering effects in a glass reinforced hydroxyapatite. *Biomaterials* ,17 No. 14, pp. 1437-1442.

69: A. Royer, J.C. Vinguie, M. Heughebaert, J. C. Heugebaert. (1993). Stoichiometry of hydroxyapatite : Influence on flexural strength. *J. Mater. Sci. Mater. Med.* , 4, pp. 76-82.

70: L. Hong, X. Hengchang, K. de Groot. (1992). Tensile strength of the interface between hydroxyapatite and bone. *J. Biomed. Mater. Res.* , 26 , pp. 7-18.

71: B. D. Cullity, S. R. Stock. (2001). *Elements of X-Ray diffraction.* 3rd Ed. Prentice Hall.

72: H. P. Klug, L.E. Alexander. (1974). *X-ray diffraction procedures for polycrystaline and amorphous materials.* 2nd Ed. John Wiley.

73: B. Grimm, A. W. Miles, I. G. Turner. (2001). Optimisation of HA/TCP ceramics as a bone graft extender for impaction grafting. *J. Mater. Sci. Mater. Med.* , 12, pp. 929-934.

74: B. Grimm, A.W. Blom, A. W. Miles, I. G. Turner. (2002). *In vitro* endurance testing of bone graft materials for impaction grafting. *Bioceramics* ,14 , pp. 375-378.

75: A. W. Blom, B. Grimm, J. Cunningham, A. W. Miles, I. D. Learmonth. (2002). In-vitro testing of BoneSave , a ceramic bone graft substitute for use in impaction grafting. *Bioceramics* ,14 , pp. 417-420.

76: F. A. Zacharia. (2000). Sintering and microstructure property relationships of porous hydroxyapatite. PhD. Thesis, University of Bath.

77: J. Barralet, J. C. Knowles, S. Best, W. Bonfield. (2002). Thermal decomposition of synthesised carbonate hydroxyapatite. *J. Mater. Sci. Mater. Med.* , 13, pp. 529-533.

78: J. C. Le Huec. (1995). Effects of porosity on mechanical strength of hydroxyapatite ceramics. *Biomaterials* ,16 No. 2, pp. 111-117.

79: S. H. Li, K. de Groot, P. Layrolle. (2002). Bioceramics scaffold with controlled porous

structure for bone tissue engineering. *Bioceramics* , 14 , pp. 25-30.

80: E. Landi, L. Orlandi, G. Spagna, A. Tampieri, N. Zaffaroni. (2001). Calcium phosphate ceramics as a drug delivery system for anti cancer drugs. *Bioceramics* ,13 , pp. 901-904.

8 Appendix 1

8.1 Early work: TCM Materials.

8.1.1 Description

The materials manufacturing route, as detailed by TCM, consists of four basic stages. The base materials were first wet mixed. These base materials consist of two grades of TCP and organic filler. The material was then pressed in a tablet press to produce a green body. This green material was ground to produce the required particle size; this ground material was then sintered. The sintering process caused the thermal transformation of one of the TCP grades to produce HA. The sintering process also burned out the organic filler producing the desired level of porosity. The resultant product is a granular material of HA and TCP with a high level of macroporosity.

Five variations of material were studied:

- TCM1: High TCP with no induced macroporosity.
- TCM2: High HA with no induced macroporosity.
- TCM3: HA/TCP blend with no induced macroporosity.
- TCM4: High HA material with induced macroporosity.
- TCM5: High TCP with induced macroporosity.

These materials were produced at TCM as part of the initial trials on composition and structure. Materials similar to these early samples were used in parallel animal trials.

Mixing.

Two grades of CaP powders, grade 118 and grade 130 (see section Powders for details of the powders) were mixed to produce materials with the required HA:TCP.

For the materials with induced macroporosity the CaP powders were blended with an organic filler to produce a nominal 50% porosity in the sintered material.

Each batch blend was wet mixed thoroughly in a blending drum prior to pressing.

Pressing.

The blended bulk materials were then pressed in a tablet press to produce a green body of the material.

Crushing and sieving

The green body tablets were crushed and sieved to the required granule size prior to sintering.

Sintering and transformation

Each batch was loaded into a muffle furnace and sintered for four hours time at 1150°C. The resulting sintering process is accompanied by thermal transformation of unstable phases in the grade 118 powder into βTCP.

The firing process also results in the burning out of the organic inclusions to produce a sintered material with the required degree of porosity.

8.1.2 Characterisation

SEM

Samples of the granular material were mounted and gold sputter coated for SEM examination. These granules were first cracked to expose a fracture surface for examination. In addition to the granular material from TCM samples of LubeLoc, a modified bovine xenograft material, and chips of denatured sheep bone were also mounted for SEM.

Initially the samples were mounted using adhesive pads to secure them to the conductive platters. This was found to be ineffective as the samples moved during examination. Samples were remounted using the conductive slip. This proved more effective, and samples did not move after remounting.

EDAX

During the mounting and handling of the TCM material it was observed that some of these materials had black inclusions that were suspected to be carbon residue from the incomplete burn of the organic inclusions. To verify that these inclusions were carbon EDAX analysis of these inclusions were carried out as part of the SEM work.

Optical Microscopy

Samples high TCP material with induced macroporosity (TCM5) and the non porous high HA material (TCM2) were mounted using Fastech filled resin system and allowed to set.

Mounted samples were bevelled and loaded into a carousel for planar grinding and polishing. Dummy samples were also loaded into the carousel such that even pressure was applied to all samples during grinding and polishing.

- 2 mins on 600 grit silicon carbide paper at 150 rpm, with complementary rotation at 5 lb. pressure per sample.
- 2 mins on 1200 grit silicon carbide paper at 150 rpm, with complementary rotation at 5 lb. pressure per sample.

- 2 mins on a Texmet cloth 0.05 μm at 150 rpm using Masterprep colloidal silica water based suspension. Polishing was carried out with complementary rotation at 5 lb. pressure per sample.

Samples were washed with soap and water, then distilled water and finally alcohol. Samples were then allowed to air dry. Samples were examined under a stereomicroscope to ensure an adequate level of polish had been attained.

XRD (qualitative)

Samples of materials TCM1 through TCM5 were ball milled by placing 5g of the sample material in a 100ml tumbler with 20g partially stabilised zirconia milling media. 30ml of industrial methylated spirits was then added. These tumblers were then placed on their rollers and allowed to run overnight.

The ball milling resulted in the formation of a fine slurry of material which went into suspension in the methylated spirits upon agitation. This suspension was then decanted off the milling media and filtered using funnel and filter paper. The resulting filtrate was allowed to dry before being bagged and labelled. The powder samples from the ball mill were analysed by x-ray diffraction using the philips diffractometer. Diffractometer used a copper anode producing a wavelength of 1.54Å. The data range was set $20° < 2\theta > 59.79°$ with a scan step size of 0.01°.

In addition to the samples listed above, extensive XRD analysis of the TCM material was carried out as part of a large-scale production control and materials validation exercise.

9 Appendix 2

9.1 Perl script to automate the analysis of XRD data

The following script was used to automate the analysis and plotting of the XRD data generated by the Phillips diffractometer. Thumbnails of the resulting images were then indexed on a number of html pages allowing easy browsing of large numbers of results.

```
#*************************************************************************
***

#   XRD_draw  -  Perl script to analyse and plot XRD data from Philips diffractometer
#                ------------------
#   begin            : Fri Mar  7 11:39:11 GMT 2003
#   copyright        : © 2003 by Brian P Casey
#   email            : setanta@dspsrv.com
#
*************************************************************************
**
#
#*************************************************************************
***
#
#   This program is free software; you can redistribute it and/or modify
#   it under the terms of the GNU General Public License as published by
#   the Free Software Foundation; either version 2 of the License, or
#   (at your option) any later version.
#
#
*************************************************************************
**

# This program relies heavily on gnuplot (http://www.gnuplot.info/ ) for its plotting
functionality
# and uses code based on Geoff Silver's <geoff@uslinux.net> Tigger image gallery
generator
# which can be found at http://uslinux.net/software/

#!/usr/bin/perl -w
use Cwd;
use strict;

# declare some global variables.
my $thumbsize    = "160x120";
my $pagebreak    = 12;
my $title        = "Image Gallery"; # Make this dynamically linked to filenames later.
my $CELLWIDTH    = 120;
my $footer       = "This is the footer , lots of nice HTML, date, created by etc  ";
my $per_line     = 3;


# Changes the cwd to the target directory.
sub changedir{
                print "Enter directory: ";
                my $targetdir =<STDIN>;
                chomp $targetdir;
                chdir $targetdir || die "Failed to change dir: $!";
                print "\nEntering ", cwd;
                return 0;
}
```

```
# Opens the target file for reading and lifts out the xrdcount data
# from the other data in the file.
sub dataplot {
		my $targetfile = $_[0];
		open (XRDFILE , $targetfile ) || die "Cannot open file $targetfile for reading:
		$!";
		my $entry;
		my (@holding,@counts,@xrdcounts);
		@holding=<XRDFILE>;
		@xrdcounts = grep /\s+\d+,\s+\d+,\s+\d+,.*/, @holding;
		close (XRDFILE);

# Flattens the data in the @xrdcounts array by splitting each element.
		@holding =grep s/,/\n/g, @xrdcounts;
		foreach $entry (@holding) {
				my @temp = split (/\n/,$entry);
				push @counts, @temp;
		}
#Gets rid of last point , often a "/".
		pop @counts;

#Opens a ".out2" filehandle for writing.
		my $output = $targetfile .".out2";
		open (OUTPUT, ">$output");
		my $length=@counts;
		my $i=0;
# Read in from headings of udf file
		my $stepsize= dataget("ScanStepSize",$targetfile);
		my @scanrange = split (/,/,dataget("DataAngleRange",$targetfile));
		my $startpoint = $scanrange[0];
		while ($i<$length) {
				my $xval=$i*$stepsize+$startpoint;
				print OUTPUT $xval," ",$counts[$i],"\n";
				$i++;
	}
		close OUTPUT;
		rundata($targetfile);
#Write gnuplot file.
		my $plotfile=$targetfile.".gp";
		my $gif_file=$targetfile.".gif"; # look at format other than gif
		my $thumbs=$targetfile.".gif"; # Generate thumbnail.
		`mkdir -p thumbnails`;
		open (PLOTFILE,">$plotfile") || die "Cannot open file $plotfile for writing:
		$!";;
		print PLOTFILE "set xlabel \'Two theta degrees\' \n";
		print PLOTFILE "set ylabel \'Counts\' \n";
		print PLOTFILE "set title \'Plot of $targetfile \' \n";
		print PLOTFILE "set terminal gif size 800,600\n"; # IMPORTANT change
type for later conversion to JPEG
		print PLOTFILE "set output \'$gif_file\'\n";
		print PLOTFILE "plot  \'$output\' with lines\n";
		print PLOTFILE "set terminal gif size 200,150\n";
		print PLOTFILE "set output \'thumbnails\/$thumbs\'\n";
		print PLOTFILE "replot\n";
```

```
        print PLOTFILE "set terminal X11\n";
        print PLOTFILE "quit";
        close PLOTFILE;
        my $cwd = cwd;
        system ("gnuplot \'$cwd\/$plotfile\'");
}

#Reads requested data from udf file headings
# Called by rundata and also for scan step size
# and start point in dataplot
sub dataget {

        my $pattern = $_[0];
        my $file = $_[1];
        open (READHEAD,"$file")|| die;
        my @holding=<READHEAD>;
        my @dummy= grep /$pattern/,@holding; #/
        $_=$dummy[0];
        my @item = m/,(.*),\//;
        close (READHEAD);
        return $item[0] ;
}

# Gathers default run data from the headings on the udf file.
# Out put is called in by indexnoshadow for index generation.
sub rundata {
        my $testfile= $_[0];
        my $SampleIdent = dataget("SampleIdent",$testfile);
        my $Labda = dataget ("LabdaAlpha1",$testfile);
        my $Runtime = dataget("FileDateTime",$testfile);
        my $DataRange = dataget("DataAngleRange",$testfile);
        my $ScanStep = dataget("ScanStepSize",$testfile);
# Could generate seperate HTML file with this code
#       my @a= split (/\./,$testfile);
#       my $htmldata = $a[0].".html";
#       open (DATAFILE,">$htmldata");
#       print DATAFILE "<ul>
#                               <li>Sample ID = $SampleIdent </li>
#                               <li>Wave Length = $Labda </li>
#                               <li>Run Time = $Runtime </li>
#                               <li>Scan Range= $DataRange </li>
#                               <li>Stepsize = $ScanStep </li>
#                               </ul>" ;
#       close (DATAFILE);
        my $rundata = " <font size=\"-2\">
                               <dl>
                               <dt>Sample ID = $SampleIdent </dt>
                               <dt>Wave Length = $Labda </dt>
                               <dt>Run Time = $Runtime </dt>
                               <dt>Scan Range= $DataRange </dt>
                               <dt>Stepsize = $ScanStep </dt>
                               </dl>
                               </font>" ;
        return $rundata;
```

```
}

sub fileselect {
        my $name;
        opendir (TEMPDIR, cwd) || die "Listing failed : $!";
        my @listing= grep(/\.udf$/i, readdir TEMPDIR);
        print "\nGenerating XRD traces: ";
        foreach $name (@listing){
                print "#";
                dataplot($name);
                rundata ($name);
        }
        closedir (TEMPDIR);
        return 0;
}

# Generate HTML output based on data and images produced by the above.
# Get the list of files in the directory and return an array of image files
sub getfiles {
        my @images;
        @images=''; pop(@images);
        my $allfiles = `ls -1`;
        print "\nGenerating thumbnail gallery: ";
        foreach my $possible (split(/\n/, $allfiles)) {
        print "#";
        my $result = `file $possible`;
        if ($result =~ /gif/) { push(@images, $possible); }
        }
        print "#";
        return(@images);
}

# Make thumbnails which are 160x120 (or $thumbnailsize)
# Convert does gif to gif conversion/resize
# sub thumbnail {
#       my ($thumbnailsize) = @_;
#       my $file;
#       print "\nGenerating thumbnail gallery: ";
#       `mkdir -p thumbnails`;
#       foreach $file (getfiles()) {
#       print "#";
#       `convert -geometry $thumbnailsize "$file" "thumbnails/$file"`;
#       }
#}

# Build the top of the web page
sub buildtop {
        my ($htmlfile, $forwardlink) = @_;
        my ($left,$right,$ext,$index,$backlink);
        open (F, ">$htmlfile");
        print F "<HTML><HEAD><TITLE>$title</TITLE></HEAD><BODY
BGCOLOR=WHITE>\n";
        print F "<table width=* valign=top align=center>\n";
        print F "<tr><td align=center valign=top colspan=5><font
```

```
size=+3>$title</font></td></tr>\n";
                if ($htmlfile eq "index.html") {
                print F "<tr><td align=left valign=top
width=$CELLWIDTH> </td>\n";
                } else {
                ($left, $right) = split(/-/, $htmlfile);
                ($index, $ext) = split(/\./, $right);
                $index--;
                if ($index != 0) { $backlink = "$left-$index.$ext"; }
                else { $backlink = "index.html"; }
                print F "<tr><td align=left valign=top><a href=\"$backlink\">Previous
$pagebreak</a></td>\n";
                }
                print F "<td align=center valign=top colspan=3>Click on a thumbnail to view
a larger image version</td>\n";
                if ($forwardlink) {
                if ($htmlfile eq "index.html") {
                $forwardlink = "index-1.html";
                } else {
                ($left, $right) = split(/-/, $htmlfile);
                ($index, $ext) = split(/\./, $right);
                $index++;
                $forwardlink = "$left-$index.$ext";
                }
                print F "<td align=right valign=top><a href=\"$forwardlink\">Next
$pagebreak</a></td></tr>\n";
                } else {
                print F "<td align=right valign=top
width=$CELLWIDTH> </td></tr>\n";
                }
                close(F);
}

# Build the bottom of the page & close table.
sub buildbottom {
                my ($htmlfile) = @_;
                open (F, ">>$htmlfile");
                print F "<tr><td colspan=5 align=center valign=top>$footer</td></tr>\n";
                print F "</table></BODY></HTML>\n";
                close(F);
}

sub indexnoshadow {
                my ($j, @files) = @_;
                my $targetfile = 0;
                my $trash =0;
                my @longname= split(/\./, $files[$j]);
                $targetfile=$longname[0].".udf";
        print F "<td width=$CELLWIDTH valign=top align=center><a
                                href=\"$files[$j]\" target=\"new\"><img
src=\"thumbnails/$files[$j]\"
                                border=0></a>";
                print F "<br>";
                print F rundata($targetfile);
```

```
		print F "</td>\n";
}

# Determine number of files and therefore number of pages to build.

sub pagegen {
		my ($forward,$newid,$k,$l);
		my @files = getfiles();
		if (($#files > $pagebreak-1) && ($pagebreak != 0)) {
		buildindex("index.html", 0, $pagebreak-1, 1);
		for ($k = $pagebreak; $k < $#files; $k=$k+$pagebreak) {
		$newid = $k/$pagebreak; #/ #just to get rid of incorrect highlighting.
		if ($k+$pagebreak > $#files) {
		$forward = 0;
				$l = $#files;
		} else {
				$forward=1;
				$l = $k+$pagebreak-1;
		}
		buildindex("index-$newid.html", $k, $l, $forward);
		}
		} else {
		buildindex("index.html", 0, $#files, 0);
		}
}

# Build the page of 25 (or $pagebreak) images

sub buildindex {
		my($htmlfile, $start, $end, $forward) = @_;
		my ($i,$j);
		buildtop($htmlfile,$forward);
		open(F, ">>$htmlfile");
		my @files = getfiles();
		$i=0;
		for ($j=$start; $j <= $end; $j++) {
		if ($i == 0) { print F "<tr>\n"; }
		indexnoshadow($j, @files);
		$i++;
		if ($i == $per_line) { print F "</tr>\n"; $i = 0; }
		}
		close(F);
		buildbottom($htmlfile);
}

# Main program start.
changedir(); # Change to the target directory.
fileselect (); # Select files to analyse and analyse.
# thumbnail ($thumbsize); # Create thumbnail dir and thumbnail images.
pagegen();# Generate index pages.
print "\nIndex created at ",cwd, "/index.html\n\n";
```

10 Appendix 3

10.1 Materials data sheets

This appendix contains the materials health and safety data, and technical data for the two base powders and the Dispex dispersant used in the manufacture of the ceramic slips used in this project.

Product Technical Data

TRICALCIUM PHOSPHATE 130

Code: tcp130 Version: 4 Date: 28/06/01

Tricalcium phosphate is the generic name given to a range of precipitate orthophosphates in which the calcium oxide/phosphorus pentoxide ratio can vary from 1.1 to 1.6; all contain hydroxyapatite.
ALBRITE tricalcium phosphate 130 is one such product in the range.

Tricalcium phosphate 130 complies in all respects with the requirements of the UK Miscellaneous Food Additive Regulations (as amended in 1997) and Commission Directive 96/77/EC.

If specified in the order, it can be supplied to the requirements of BP2000 or the US Food Chemicals Codex IV – First Supplement December 1997. Tricalcium phosphate 130 can also be supplied to the requirements of NF 19 for tribasic calcium phosphate.

Details of the pharmaceutical quality product CALIPHARM T are available on request.

Synonyms	EC:	tricalcium phosphate	EC No: E341(iii)
	FCC:	calcium phosphate tribasic	
	Other:	tricalcium phosphate 118	
		tricalcium diorthophosphate	
		tricalcium orthophosphate	
CN Heading		28.35	
CAS No.		12167-74-7	
EINECS No.		235-330-6	
Approximate Formula		$Ca_5OH(PO_4)_3$	
Molecular weight		502	
Taste and odour		none	

		Product Specification	Typical*
Appearance		White, fine powder.	
Assay (as $Ca_3[PO_4]_2$)	% m/m	90 min	98.5
Loss on Ignition @ 800°C	% m/m	8 max.	3.9
Fluoride	ppm	50 max	
Arsenic	ppm	3 max	<1
Lead	ppm	5 max	
Heavy Metals	ppm	10 max	<10
Mercury	ppm	1 max	<1
P_2O_5	% m/m	-	41.2
% Ca	% m/m	-	38.1
pH (1% aqueous)		-	6.8
Bulk density	g/ml	-	0.68

*Typical data does not represent a specification, but is indicative of typical analysis.
Specification is uncontrolled for ISO9002 purposes

TECHNICAL SERVICE
P.O. Box 80,
Trinity Street,
Oldbury,
West Midlands,
B69 4LN.
Telephone +44 (0)121 541 3200
Fax: +44 (0)121 541 3300

Rhodia
Specialty Phosphates

Applications

Flow conditioner for powdered materials such as icing sugar and dry bases for soups and drinks.
Dispersant in tablet manufacture.
Mineral supplement in medicinal preparations and nutrition foods.
Ceramic opacifier.

Packaging (Please contact Customer Services for further information).

25 Kg multi-ply paper sacks

Storage

SEE SAFETY DATA SHEET [Ref. 04490A]
Product should be stored in cool dry conditions. Use of warehouse racking or single stacking of pallets is also advisable.

Health and Safety Information

SEE SAFETY DATA SHEET [Ref. 04490A]

---

tcp130

TECHNICAL SERVICE
P.O. Box 60,
Trinity Street,
Oldbury,
West Midlands,
B69 4LN.
Telephone +44 (0)121 541 3280
Fax: +44 (0)121 541 3300

Product Technical Data

TRICALCIUM PHOSPHATE 118

Code: tcp118 Version: 4 Date: 27/06/01

Tricalcium phosphate is the generic name given to a range of precipitate orthophosphates in which the calcium oxide/phosphorus pentoxide ratio can vary from 1.1 to 1.6; all contain hydroxyapatite.
Ttricalcium phosphate 118 is one such product in the range.

Tricalcium phosphate 118 complies in all respects with the requirements of the UK Miscellaneous Food Additive Regulations (as amended in 1997) and Commission Directive 96/77/EC.

If specified in the order, it can be supplied to the requirements of BP2000 or the US Food Chemicals Codex IV – First Supplement December 1997.

A further grade of tricalcium phosphate is available under the name of tricalcium phosphate 130. Details of this and the pharmaceutical quality products are available on request.

Synonyms	EC:	tricalcium phosphate	EC No: E341(iii)
	FCC:	calcium phosphate tribasic	
	Other:	tricalcium phosphate 118	
		tricalcium diorthophosphate	
		tricalcium orthophosphate	
CN Heading		28.35	
CAS No.		7758-87-4	
EINECS No.		231-840-8	
Approximate Formula		$Ca_3(PO_4)_2$	
Molecular weight		310	
Taste and odour		none	

		Product Specification	Typical*
Appearance		White, fine powder.	
Assay (as $Ca_3[PO_4]_2$)	% m/m	90 min	94.5
Loss on Ignition @ 800°C	% m/m	8 max.	4.7
Fluoride	ppm	50 max	
Arsenic	ppm	3 max	<1
Lead	ppm	5 max	
Heavy Metals (as Pb)	ppm	10 max	<10
Mercury	ppm	1 max	<1
P_2O_5	% m/m	-	43
% Ca	% m/m	-	36.6
pH (1% aqueous)		-	5.3
Bulk Density	g/ml	-	0.68

*Typical data does not represent a specification, but is indicative of typical analysis.
Specification is uncontrolled for ISO9002 purposes.

TECHNICAL SERVICE
P.O. Box 80,
Trinity Street,
Oldbury,
West Midlands.
B69 4LN.
Telephone +44 (0)121 541 3280
Fax: +44 (0)121 541 3300

Rhodia
Specialty Phosphates

Applications

Flow conditioner for powdered materials such as icing sugar and dry bases for soups and drinks.
Dispersant in tablet manufacture.
Mineral supplement in medicinal preparations and nutrition foods.
Ceramic opacifier.

Packaging (Please contact Customer Services for further information).

25 Kg multi-ply paper sacks

Storage

SEE SAFETY DATA SHEET [Ref. 04400A]
Product should be stored in cool dry conditions. Use of warehouse racking or single stacking of pallets is also advisable.

Health and Safety Information

SEE SAFETY DATA SHEET [Ref. 04400A]

---

tcp118

TECHNICAL SERVICE
P.O. Box 80
Trinity Street,
Oldbury,
West Midlands.
B69 4LN.
Telephone +44 (0)121 541 3280
Fax: +44 (0)121 541 3330

SPECIFICATION

Ellis & Everard
CHEMICALS MARKETING & DISTRIBU

P060 0126 | **TRICALCIUM PHOSPHATE 130 B.P.** | OCTOBER 1997

Synonyms: Tricalcium Diorthophosphate
Tricalcium Orthophosphate
Calcium Phosphate, Tribasic
Tribasic Calcium Phosphate

CAS: 12167-74-7
UN: ---
EINECS: 231-840-8

Properties:

Formula: $Ca_5(PO_4)_3OH$

Description: White powder

M.W. 502

Specification:	
Assay (as Ca)	35.0 - 40.0%m/m
Maximum Levels of Impurities:	
Acid insoluble	0.2% m/m max
Chloride	0.15% m/m max
Sulphate	0.5% m/m max
Iron	400 ppm max
Fluoride	50 ppm max
Heavy metals, as Pb	30 ppm max
Arsenic	4 ppm max
Carbonate	passes Test
Loss on ignition (as 800°C for 30 mins)	8.0% m/m max

Meets the requirements of:

Special Notes: B.P. 1993 Addendum 1996

[redacted]

ERCO ref.- PCL 0654
Validation ref- VA-076

87

SPECIFICATION

Ellis & Everard
CHEMICALS MARKETING & DISTRIBUTI

P060 0122 **TRICALCIUM PHOSPHATE 118 B.P.** **OCTOBER 1997**

Synonyms: Tricalcium Diorthophosphate
Tricalcium Orthophosphate
Calcium Phosphate, Tribasic
Tribasic Calcium Phosphate

CAS: 12167-74-7(130)
UN: —
EINECS: 231-840-8

Properties:

Description: White powder

Formula: $Ca_3(PO_4)_2$
M.W. 310

Specification:

Assay (as Ca)	35.0 - 40.0% m/m
Maximum Levels of Impurities:	
Acid Insoluble	0.2% m/m max
Chloride	0.15% m/m max
Sulphate	0.5% m/m max
Iron	400 ppm max
Flouride	50 ppm max
Heavy metals, as Pb	30 ppm max
Arsenic	4 ppm max
Carbonate	passes test
Loss on ignition (at 800°C for 30 mins)	8.0% m/m max

Meets the requirements of: B.P. 1993 Addendum 1996

Special Notes:

[redacted]

ERCO ref:- PCL 0654
Validation ref- VA-076

88

Ciba Specialty Chemicals

Additives
Imaging and Coating Additives

Ciba

Ciba® DISPEX® R50/A40/N40 Dispersing Agent

General

DISPEX R50, DISPEX A40 and DISPEX N40 are derivatives of a family of highly effective, low viscosity dispersing agents for water-borne coating systems. The products are especially suited for the dispersion of inorganic pigments.

Chemical Nature

DISPEX R50 is a solution of an acrylic polymer in water.

DISPEX N40 is a solution of a sodium salt of an acrylic polymer in water.

DISPEX A40 is a solution of an ammonium salt of an acrylic polymer in water.

Physical Properties
(typical values)

	DISPEX R50	DISPEX N40	DISPEX A40
Appearance:	straw coloured liquid	straw coloured liquid	straw coloured liquid
pH:	3.0	7.5	8.0
Solid Content:	51 %	45 %	43 %
Active Content:	50 %	40 %	40 %
Viscosity at 25°C: (Brookfield 20 rpm)	500 mPa·s	400 mPa·s	400 mPa·s
Density at 20°C:	1.26 $g \cdot cm^{-3}$	1.30 $g \cdot cm^{-3}$	1.16 $g \cdot cm^{-3}$

Applications

DISPEX N40, DISPEX A40 and the DISPEX R50 preparation are ideal dispersing agents for a wide range of water-borne coatings.

DISPEX A40 and DISPEX N40 can be used as supplied.

The neutralising alkali used in conjunction with the acrylic polymer can significantly impact the properties of the final coating. DISPEX A40 releases ammonia during the drying process and therefore has little impact on water and alkaline resistance of the dry film while the sodium-based DISPEX N40 often contributes slightly negatively to the coating properties.

DISPEX R50 must be converted to an aqueous solution of a salt of the acrylic polymer for use. The appropriate choice of the neutralising alkali allows the user to comply with specific environmental and legal requirements.

DISPEX N40 is effective over a pH range 5-12 and up to temperatures

in excess of 100°C.

Use of DISPEX A40 should be limited to pH 5-10.5 and temperatures lower than 70°C due to potential loss of volatile ammonia.

Compared with inorganic dispersing agents, e.g. polyphosphate products, the organic polymer based DISPEX N40 and DISPEX A40 provide improved storage stability of both, the pigment dispersion and the formulated paint. There is little or no adverse reaction to high temperatures or pH changes as indicated in the graphs below, which are examples showing the accelerated effects.

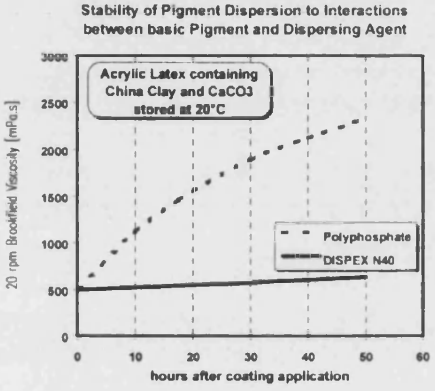

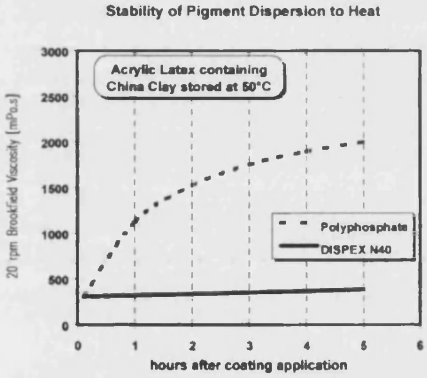

Preparation of the ready-for-use DISPEX R50 formulation
Dilute DISPEX R50 to a 10% active substance solution by adding water. Then carefully add the selected alkali with constant stirring to achieve a pH of 7.5 - 8.5. It is natural that some heat is generated during this procedure.

Incorporation of DISPEX N40, DISPEX A40 or DISPEX R50 formulation
It is recommended to add the pigment to heavily stirred water

containing the dispersing agent as opposed to addition of the dispersing agent to a pigment slurry. In general, the pH of the final preparation should be in the region of 8.5 to obtain optimum dispersing efficiency.

The optimum amount of dispersing agent required to form a stable dispersion strongly depends on the pigment's chemical nature, the particle surface and shape. The polymer base of the latex also plays a very important part in the stability equation. In general, significant overdosing may deteriorate the coatings properties (e.g. water resistance) and also generates an economic disadvantage. Likewise insufficient dispersing agent will lead to instability on storage.

In common with other dispersing agents, because of the batch-to-batch variations of the demands of a specific pigment or latex type it is recommended that the formulator uses 1.5 - 2.0 times the determined optimum level of the dispersing agent.

Example:
Rheology Curve of a Pigment Slurry System
(containing 65% pigment solids)

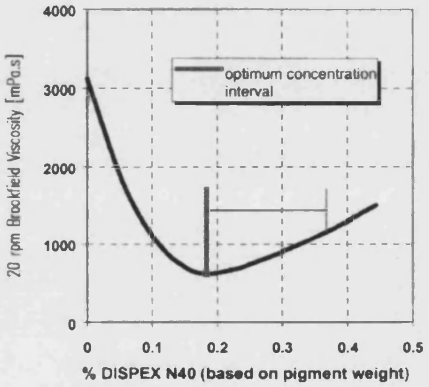

Ciba Specialty Chemicals holds a database with information on recommended dosage levels for a variety of commonly used pigments in selected latex preparations.

A more detailed explanation of dispersing agent evaluation is contained in the "Rheology Performance Brochure" which is also available from Ciba Specialty Chemicals.

Recommended concentration :

0.5 – 2.0 % DISPEX R50 formulation
(based on total pigment weight)

Ciba

or

0.5 – 2.0 % DISPEX N40 or DISPEX A40)
(based on total pigment weight)

Safety and Handling

DISPEX R50, DISPEX N40 and DISPEX A40 should be handled in accordance with good industrial practice. Detailed information is provided in the Safety Data Sheet.

Although DISPEX R50, DISPEX N40 and DISPEX A40 are freeze stable it is recommended to store the products at temperatures above 5°C to enable easy handling of the product.

Trademark

DISPEX is a registered trademark.

Important Notice

IMPORTANT: The following supersedes Buyer's documents. SELLER MAKES NO REPRESENTATION OR WARRANTY, EXPRESS OR IMPLIED, INCLUDING OF MERCHANTABILITY OR FITNESS FOR A PARTICULAR PURPOSE. No statements herein are to be construed as inducements to infringe any relevant patent. Under no circumstances shall Seller be liable for incidental, consequential or indirect damages for alleged negligence, breach of warranty, strict liability, tort or contract arising in connection with the product(s). Buyer's sole remedy and Seller's sole liability for any claims shall be Buyer's purchase price. Data and results are based on controlled or lab work and must be confirmed by Buyer by testing for its intended conditions of use. The product(s) has not been tested for, and is therefore not recommended for, uses for which prolonged contact with mucous membranes, abraded skin, or blood is intended; or for uses for which implantation within the human body is intended.

11 Appendix 4

11.1 Abstracts accepted for presentation.

The following abstracts outline work presented at the European Society for Biomaterials Annual Conference 2001 and 2002 respectively.

Production of porous bi-phasic calcium phosphate materials for use in bone graft applications

B. P. Casey[1] , I.G. Turner[1] and A.W. Miles[2]

[1]Department of Engineering and Applied Science, University of Bath, Claverton Down, Bath, BA2 7AY, U.K.
[2]Department of Mechanical Engineering, University of Bath, Claverton Down, Bath, BA2 7AY, U.K.

Introduction

The introduction of impaction grafting for revision arthoplasty has greatly increased the need to develop a synthetic bone graft material[(1)].

The physical structure and chemical composition of the graft are vital to the biological response of the body to the material. It has been shown that the optimal pore size to promote bone ingrowth is 100μm to 200μm [(2)].

Available bulk synthetic bone graft materials are primarily based on calcium phosphate ceramics. These are produced by a burnt out organic inclusion method which tends to produce non-interconnected porosity (Fig.1).

The method currently being devloped as part of this project involves impregnation of an organic foam structure with a high loading calcium phosphate slip[(3,4)]. On sintering, the organic foam is burned out to produce a porous ceramic with a highly interconnected network of pores.

Materials and Methods.

Two grades of calcium phosphate powder were used, one stable hydroxyapatite and one low crystallinity hydroxyapitite (HA) which readily transformed to β-tricalcium phosphate (TCP). These powders were blended to produce the required HA/TCP ratio in the sintered product.

The organic foam supports used were reticulated polyurathane foams of 10ppi, 20ppi and 45ppi which have an inherent open structure.

A high loading slip was produced from these powder blends by the gradual addition of powder to distilled water in a ball mill charged with ziriconia milling media. Typically 80g to 100g of powder were added to 100g of water over a period of 48 hours.

The foam support was loaded with the slip by submersion and mechanical working of the foam in the slip. Vibration of the slip improves entry into the foam support. The impregnated foam was removed from the slip and set to dry for 24 hours at 40°C.

The green body was sintered at temperatures of up to 1280°C. A slow temperature ramp during sintering allows complete burnout of the organic foam and significant densification of the material.

Scanning electron microscopy (SEM) of the fracture surfaces and polished sections were used to determine the morphology, scale and degree of the porosity in the material. Image analysis of SEM micrographs was used to quantitively assess the scale and structure of the porosity.

X-ray diffraction analysis was used to determine the chemical composition of the sintered materials.

Results.

SEM micrographs, figures 1 and 2, show the difference in the nature and scale of the porosity in materials produced via burnt out organic inclusion and those produced by the method under development.

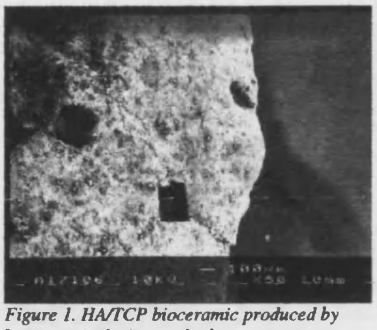

Figure 1. HA/TCP bioceramic produced by burnt out inclusion method.

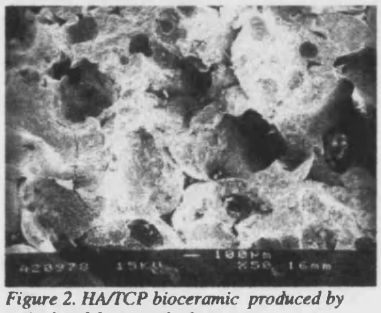

Figure 2. HA/TCP bioceramic produced by reticulated foam method.

Analysis of the micrographs shows much of the porosity in the current material to be in the size range of 100μm-200μm and to be highly interconnected. The material also contains a high degree of microporosity in the 1μm-2μm range.

X-ray analysis confirmed a specific range of HA/TCP ratios could be reliably produced in the sintered material.

Conclusions.

The new range of bioceramic materials provide a structure with interconnecting macro- and micro-porosity optimal for bone ingrowth. The material itself is robust with a high degree of structural integrity.

By adjustment of slip loading, foam density and slip composition the structure and composition of the current material can be tailored specifically for a range of applications.

Acknowledgements.

The authors are grateful for the support of the University of Bath and Stryker Howmedica Osteonics.

Refrences.

1. Galea *et al.* (1998) J. Bone Joint Surg. (Br), 80-B, No.4, pp.595-567.
2. Oonishi *et al.* (1999) J. Biomed. Mat. Res. , No. 44, pp. 31-43.
3. Binner (1997) British Ceramic Transactions, 96, No. 6, pp. 247-249.
4. Perry *et al.* (1999) *Scripta Materialia*, 41, Issue 9, pp. 1001-1007

Characterisation of biphasic calcium phosphate for use as bone substitutes

B. P. Casey[1] , I.G. Turner[1] A.W. Miles[2] and J. P. Gittings[1].

[1]Department of Engineering and Applied Science, University of Bath, Claverton Down, Bath, BA2 7AY, U.K.

[2]Department of Mechanical Engineering, University of Bath, Claverton Down, Bath, BA2 7AY, U.K.

Introduction

Development of synthetic bone graft material has become increasingly important in recent years due in part to the increasing use of impaction grafting for revision arthoplasty and the demand this useage puts on current allograft stock[(1)].

The physical structure and chemical composition of the graft are vital to the biological response of the body to the material. It has been shown that pore size and the interconnection of pores has a strong influence on the osteoinductive potential of a synthetic graft material [(2,3)]

The current method[(4)] allows the production of porous calcium phosphate ceramic components with an interconnected porosity in the required size range. This method involves impregnation of an organic foam structure with a high loading calcium phosphate slip[(5,6)], followed by burning out of the foam to leave a ceramic with an interconnected network of pores. Samples were then characterised using image analysis and compression testing.

Materials and Methods

Two grades of calcium phosphate powder were blended to produce the required HA/TCP ratio in the sintered product.Organic foams comprising of reticulated polyurethane of 30ppi, 45ppi and 65ppi were used as supports .

Slips of 400-600g of powder per litre were ball milled. Slip viscosity was controlled with a dispersant and measured using a Brookfeild viscometer using a spindle speed of 10 rpm and a No. 5 spindle.

The foam support was loaded with the slip and set to dry overnight at room temperature on tissue or on wire mesh and then further dried for 24 hours at 40°C.

The green body was sintered at temperatures of up to 1280°C. A slow temperature ramp during sintering allowed complete burnout of the organic foam and significant densification of the material.

Scanning electron microscopy (SEM) and darkfield imaging of polished sections were used to determine the morphology, scale and degree of the porosity in the material. Image analysis of SEM micrographs was used to quantitatively assess the scale and structure of the porosity and the contribution of microporosity to the overall porosity of the material.

Samples for compression testing were produced by grinding 15mm cubes from large blocks of material. These were weighed to determine density then compression tested using an 1122 Instron.

Results

Figure 1 shows the macroporosity generated by a 45ppi foam with high levels of slip impregnation, this macroporosity accounts for 6% of the materials volume. The area equivalent diameter of the pore structure was effected by the input foam with 45ppi producing an average pore size of 80µm and the 65ppi producing an average pore size of 20µm. Image analysis of high magnification SEM shows a high level of microporosity in the 1-5µm range which resulted in 18% porosity in the material. This was present in all variations of the material produced for study.

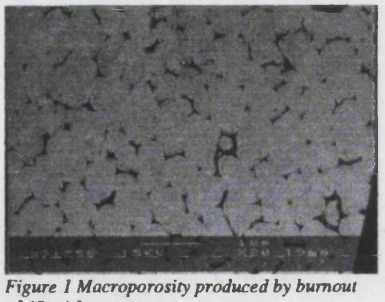

Figure 1 Macroporosity produced by burnout of 45ppi foam support.

Figure 2 shows the compression test results. The samples produced showed a degree of variation in density. The graph shows the compressive strength against density for two batches sintered at 1150°C and 1280°C .

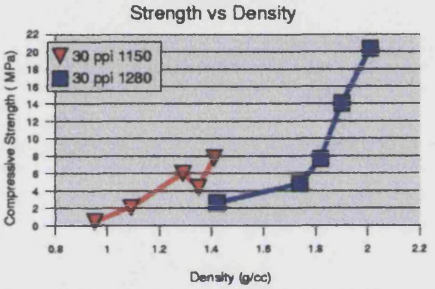

Figure 2 Strength vs. Density for 30ppi based bulk material.

Conclusions

A range of materials with different pore sizes can be produced by this method, the macropore structure being determined by the input foam.

The compressive strength shows a strong dependency on density with the well impregnated samples producing compressive strengths in the range of 14-20 MPa. Further work is nessary to optimise the bulk properties of the material.

Acknowledgements

The authors would like to thank the University of Bath and Stryker Howmedica Osteonics for their support.

Refrences.

1. Galea *et al.* (1998) J. Bone Joint Surg. (Br), 80-B, No.4, pp.595-567.
2. Oonishi *et al.* (1999) J. Biomed. Mat. Res. , No. 44, pp. 31-43.
3. Hing *et al.* (1999) J. Mat. Sci. : Mat. Med. , 10, pp. 663-670.
4. Casey *et al.* (2001) Proceedings 16th Confrence for European Society for Biomaterials, T211.
5. Binner (1997) British Ceramic Transactions, 96, No. 6, pp. 247-249.
6. Perry *et al.* (1999) *Scripta Materialia*, 41, Issue 9, pp. 1001-1007